



**Non-hematopoietic lymphoid stromal cells prime alloreactive CD4⁺
T cells during acute graft-versus-host disease**

Nicht-hämatopoetische lymphoide Stromazellen aktivieren alloreaktive CD4⁺ T-Zellen
in der Initiierung der akuten Graft-versus-Host Disease

Doctoral thesis for a doctoral degree
at the Graduate School of Life Sciences,
Julius-Maximilians-Universität Würzburg,
Section Infection and Immunity

submitted by

Muhammad Haroon Shaikh

from

Karachi, Pakistan

Würzburg 2020



Submitted on:
Office stamp

Members of the Thesis Committee

Chairperson: Prof. Dr. Georg Gasteiger

Primary Supervisor: Prof. Dr. Dr. Andreas Beilhack

Supervisor (Second): Prof. Dr. Manfred Lutz

Supervisor (Third): PD Dr. Niklas Beyersdorf

Date of Public Defence:

Date of Receipt of Certificates:

For my family

I. Table of Contents

1.	Introduction.....	5
1.1	Lymph node stromal cells	5
1.1.1	Fibroblastic reticular cells (FRCs).....	5
1.1.2	Marginal reticular cells (MRCs).....	9
1.1.3	Follicular dendritic cells (FDCs).....	9
1.1.4	Lymph endothelial cells (LECs).....	9
1.1.5	Blood endothelial cells (BECs).....	10
1.1.6	Double-negative stromal cells and pericytes	11
1.2	Acute Graft-versus-Host disease.....	11
1.2.1	Clinical relevance of GvHD	12
1.2.2	aGvHD pathophysiology and target organs.....	12
1.2.3	Target antigen recognition	13
1.2.4	Activation of T cells in aGvHD	14
1.2.5	Mouse models of GvHD.....	14
1.3	MHC class II antigen presentation by non-hematopoietic cells of lymphoid organs.....	15
1.3.1	MHCII expression by LNSCs	16
1.3.2	LNSCs in antigen specific CD4 ⁺ T cell responses	16
1.3.3	LNSCs in GvHD	16
1.4	Knowledge gap.....	17
2	Specific Aims.....	18
3	Material and Methods.....	19
3.1	Materials	19
3.1.1	Chemical reagents.....	19
3.1.2	Buffers and solutions	19
3.1.3	Antibodies and secondary reagents.....	20
3.1.4	Commercially available kits.....	21
3.1.5	Consumables	21
3.1.6	Mice	21
3.2	Methods.....	23
3.2.1	Cell culture.....	23
3.2.2	Hematopoietic cell transplantation	23
3.2.3	Diphtheria toxin mediated cell depletion	24
3.2.4	Polymerase chain reaction.....	24
3.2.5	Generation of bone marrow chimeras.....	24
3.2.6	Single cell suspension from spleen and lymph nodes	25
3.2.7	Single cell suspension of LNSCs from the lymph nodes	25
3.2.8	Isolation of T cells from the GIT	26
3.2.9	Mixed lymphocyte reaction (MLR)	26
3.2.10	Cytokine bead array (CBA)	27
3.2.11	Multicolour flow cytometry.....	27
3.2.12	Bioluminescence imaging (BLI).....	27
3.2.13	Fluorescence activated cell sorting (FACS).....	28
3.2.14	Antigen processing assay	28
3.2.15	Bulk RNA sequencing	28
3.2.16	Single cell RNA sequencing.....	29
3.2.17	Light-sheet fluorescence microscopy.....	29
3.2.18	Immunostaining for confocal microscopy.....	30
3.2.19	Mesenteric lymph node transplantation surgery	31
3.2.20	Statistical analysis.....	32
4	Results	33
4.1	LNSCs possess necessary APCs characteristics.....	33
4.1.1	LNSCs up-regulate co-stimulatory receptors after irradiation	33
4.1.2	LNSCs process exogenous antigen via MHC class II.....	36
4.2	CD4 ⁺ T cell are activated in the SLOs early after allo-HCT	37
4.2.1	Allogeneic T cell activation kinetics in the initiation phase of aGvHD	37
4.2.2	Allogeneic CD4 ⁺ T cell are activated in SLOs of mice with MHC class II deficient myeloid cells during the aGvHD initiation phase.....	39
4.3	Targeting the lymph node stroma and hematopoietic system	43
4.3.1	Deciphering LNSCs by scRNA sequencing	43
	46
4.4	Subset of LNSCs activate alloreactive CD4 ⁺ T cells in SLOs	47

4.4.1	MHCII ^{ΔVav1} mice, a suitable model for studying non-hematopoietic antigen presentation	47
4.4.2	Mesenteric lymph node transplantation in mice	51
4.4.3	Alloreactive CD4 ⁺ T cells show effector phenotype in the B6.MHCII ^Δ mice transplanted with mesenteric LNs of CD11c.DOG mice.....	56
4.5	MHC class II on reticular stromal cells.....	57
4.5.1	FRCs moderately prime CD4 ⁺ T cells in the initiation phase of aGvHD	57
4.5.2	MHC class II on FRCs plays an immune-modulatory role during the effector phase of aGvHD.....	62
4.5.3	FRCs MHC class II regulate donor Tregs during aGvHD effector phase	63
4.6	MHC class II on endothelial cells.....	71
4.6.1	Knock-out of MHC class II on endothelial cells results in improved clinical score and survival following GvHD.....	71
5	Discussion	75
5.1	LNCSs process exogenous antigen and upregulate co-stimulatory receptors under inflammatory conditions	75
5.2	Alloreactive T cells home to and are activated in secondary lymphoid organs at the initiation phase of aGvHD	75
5.3	Allo-reactive CD4 ⁺ T cells are activated within the SLOs in the absence of professional MHC class II antigen presentation.....	76
5.4	Genetic targeting of lymph node stroma and endothelium	78
5.5	Alloreactive CD4 ⁺ T cells receive activation cues from LNCSs within SLOs.....	79
5.6	MHC class II on FRCs activate alloreactive CD4 ⁺ T cells in the initiation phase of GvHD	80
5.7	MHC class II presentation on FRCs regulates Tregs in the effector phase of GvHD	81
5.8	Endothelium MHC class II antigen presentation in GvHD	82
5.9	Conclusion	83
6	References	87
7	Acknowledgements	96
8	List of publications.....	97
9	Curriculum vitae	98
10	Affidavit.....	101

II. List of Figures

Figure 1.1 Stromal cell heterogeneity and function during LN homeostasis.....	8
Figure 1.2 The initiation and maintenance of acute graft-versus-host disease (aGvHD) have been conceptualized into four phases with positive feedback loops that perpetuate the process.....	13
Figure 1.3 Vascular endothelial cells and lymph node stromal cells can express MHC class II molecules.....	15
Figure 2.1 Research questions of this thesis project.....	18
Figure 3.1 Principle of Cre-LoxP mouse.....	22
Figure 4.1 Immortalized fibroblastic reticular cells (iFRCs) up-regulate co-stimulatory molecules after irradiation.....	33
Figure 4.2 LNSCs upregulate CD80 and CD86 co-stimulatory receptors while down-regulating MHC class II after irradiation due to the depletion of dendritic cells.....	35
Figure 4.3 LNSCs can process exogenous antigen under homeostatic conditions.....	36
Figure 4.4 Naïve alloreactive T cells migrate to and are activated in secondary lymphoid organs during aGvHD initiation.....	38
Figure 4.5 Alloreactive CD4 ⁺ T cells are activated in SLOs even in absence of antigen presentation from CD11c-expressing myeloid cells during the aGvHD initiation phase.....	41
Figure 4.6 Alloreactive CD4 ⁺ T cells are activated in SLOs of MHC class II deficient BM chimeras during aGvHD initiation. phase.....	42
Figure 4.7 Single cell RNA sequencing experimental strategy.....	44
Figure 4.8 Single cell RNA sequencing of steady-state LNSCs.....	46
Figure 4.9 Characterization of endothelial cells in LNSCs scRNA dataset.....	46
Figure 4.10 Phenotyping of MHCII ^{ΔVav1} mice.....	47
Figure 4.11 LNSCs endogenous MHCII process exogenous antigen under homeostatic conditions.....	48
Figure 4.12 B6.MHCII ^{ΔVav1} mice are susceptible to aGvHD.....	49
Figure 4.13 Non-hematopoietic cells of lymph nodes activate alloreactive CD4 ⁺ T cells in mixed lymphocyte reactions.....	50
Figure 4.14 Procedure of mesenteric lymph node transplantation.....	51
Figure 4.15 Donor mLNs were engrafted in the recipient mice after lymph node transplantation.....	52
Figure 4.16 Donor mLNs lymph vessels conjoin with recipient's intestinal lymphatic vasculature after LN transplantation.....	53
Figure 4.17 Donor mLNs are populated with recipient hematopoietic cells after surgically transplantation.....	54
Figure 4.18 Alloreactive CD4 ⁺ T cells are robustly activated and proliferate in the transplanted mLNs in aGvHD after allo-HCT.....	55
Figure 4.19 Alloreactive CD4 ⁺ T cells activate in MHCII ^Δ mouse transplanted with mLNs of CD11c.DOG mouse.....	56
Figure 4.20 LNSCs upregulate MHC class II upon treatment with IFN γ	57
Figure 4.21 Alloreactive CD4 ⁺ T cells are activated by allogeneic FRCs in a mixed lymphocyte reaction.....	58
Figure 4.22 Alloreactive CD4 ⁺ T cells proliferation is slightly decreased in MHCII ^{ΔCcl19} mice during aGvHD initiation.....	60
Figure 4.23 Naïve OT-II T cells do not proliferate in the SLOs of iFABP-tOVA mouse.....	61
Figure 4.24 RNA sequencing revealed genes involved in mitosis were enriched whereas glucose pathways were down-regulated in MHCII ^{ΔCcl19} mice at the effector phase of allo-HCT.....	64
Figure 4.25 Alloreactive CD4 ⁺ T cells upregulate effector molecules whereas FoxP3 ⁺ CD4 ⁺ Tregs are reduced during the GvHD effector phase in MHCII ^{ΔCcl19} recipient mice.....	65
Figure 4.26 Exacerbated aGvHD in MHCII ^{ΔCcl19} mice displaying enhanced effector molecule expression and poor survival.....	66
Figure 4.27 Tregs fail to protect MHCII ^{ΔCcl19} mice against GvHD.....	67
Figure 4.28 Alloreactive CD4 ⁺ T cells express higher levels of effector molecules in MHCII ^{ΔCcl19} recipients that had been co-transplanted with Tregs in comparison to WT littermate controls.....	68
Figure 4.29 MHCII on FRCs supports the proliferation of pre-activated OT-II Tregs and moderately of Tcons in aGvHD like inflammatory conditions in iFABP-tOVA transgenic mice.....	69
Figure 4.30 Ccl19.iDTR mice develop severe aGvHD.....	70
Figure 4.31 Alloreactive CD4 ⁺ T cell proliferation is moderately decreased in MHCII ^{ΔVE-Cadherin} mouse in the initiation phase of aGvHD.....	72
Figure 4.32 MHCII ^{ΔVE-Cadherin} mice trend toward improved survival subsequent to GvHD.....	73
Figure 4.33 Allogeneic CD4 ⁺ are not activated by the LNSCs of MHCII ^{ΔVav1ΔVE-Cadherin} mice in a mixed lymphocyte reaction.....	74
Figure 5.1 Alloreactive naïve CD4 ⁺ T cells home to SLOs and not to the target organs during the initiation phase of aGvHD.....	85
Figure 5.2 MHC class II on lymph node stromal cells modulate allogeneic CD4 ⁺ T cells in graft-versus-host-disease.....	86
Figure 5.2 MHC class II on lymph node stromal cells modulate allogeneic CD4 ⁺ T cells in graft-versus-host-disease.....	86

III. List of Tables

Table 1.1 Lymph node FRC subset	6
Table 1.2 Lymph node LEC subsets.....	9
Table 3.1 Murine antibodies used for flow cytometry staining and fluorescence microscopy.....	20
Table 3.2 Mice	22
Table 3.3 Cell culture medium	23
Table 3.4 Clinical score to assess GvHD severity	23
Table 3.5 Criteria to define the humane endpoint.....	24
Table 3.6 PCR primers	24

IV. List of Abbreviations

α MEM	minimum essential medium
ACKR	atypical chemokine receptor
AF	Alexa Fluor
aGvHD	acute Graft-versus-Host Disease
allo-HCT	allogeneic-hematopoietic cell transplantation
APCs	antigen presenting cells
B6	C57BL/6
BABB	benzyl-alcohol/ benzyl benzoate
BAFF	B-cell activating factor
BECs	blood endothelial cells
BM	bone marrow
CCL	C-C motif chemokine ligand
CCR	C-C motif chemokine receptor
CD	cluster of differentiation
CDH5	Cadherin-5
CXCR3	C-X-C Motif Chemokine Receptor 3
Cy	cyanine
DMEM	Dulbecco's modified eagle medium
DOG	diphtheria toxin-OVA-GFP
DTx	diphtheria toxin
EDTA	ethylenediaminetetraacetic acid
FACS	fluorescence-activated cell sorting
FCS	fetal calf serum
FDCs	follicular dendritic cells
FITC	fluorescein isothiocyanate
FRCs	fibroblastic reticular cells
GIT	gastrointestinal tract
GvHD	Graft-versus-Host Disease
Gvl	Graft-versus-Leukemia
Gy	gray
HBSS	Hank's buffered salt solution
HEVs	high endothelial venules
IAPs	integrin α 7 pericytes
IL	Interleukin
IFN	interferon
iFABP-tOVA	intestinal fatty acid binding protein – truncated ovalbumin
IU	international units
LP	lamina propria
LECs	lymph endothelial cells
LNSts	lymph node stromal cells
LNs	lymph nodes
Luc	luciferase
MACS	magnetic activated cell sorting
MAdCAM	mucosal-associated cell adhesion molecule
MLR	mixed lymphocyte reaction
MHC	major histocompatibility complex
mHAs	minor histocompatibility antigens
MRCs	marginal reticular cells
OVA	ovalbumin
PBS	phosphate-buffered saline
PD-L1	programmed cell death-ligand 1
PD-1	programmed cell death protein 1
PECAM1	platelet endothelial cell adhesion molecule 1

PerCP	peridinin-chlorophyll-protein complex
PPs	Peyer's patches
PTAs	peripheral tissue antigens
RPMI	Roswell Park Memorial Institute
scRNA seq	Single cell RNA sequencing
SLOs	secondary lymphoid organs
Syn-HCT	syngeneic-hematopoietic cell transplantation
TBI	Total body irradiation
TCR	T cell receptor
Th1	T helper cell type 1
Th2	T helper cell type 2
Th17	T helper cell type 17
Tregs	regulatory T cells
TNF	tumor necrosis factor
XCL	C-motif chemokine ligand

V. Summary

In the initiation phase of acute graft-versus-host disease (aGvHD), CD4⁺ T cells are activated by hematopoietic antigen presenting cells in secondary lymphoid organs whereas in effector phase by non-hematopoietic cells in the small intestine. We hypothesized that alloreactive CD4⁺ T cells primarily home to the secondary lymphoid organs subsequent to allogeneic hematopoietic cell transplantation in the initiation phase of aGvHD and are activated by the non-hematopoietic lymph node stromal cells via MHC class II. To test this hypothesis, we employed CD4⁺ T cell-dependent major mismatch aGvHD mouse model to study this correlation.

Upon analyzing the early events following allo-HCT with bioluminescence imaging, flow cytometry and whole-mount light sheet fluorescence microscopy, we found that allogeneic T cells exclusively home to the spleen, lymph nodes and the Peyer's patches and not to the intestinal *lamina propria* in the initiation phase of aGvHD. Utilizing mice devoid of partial or complete hematopoietic antigen presentation we could show allogeneic CD4⁺ T cells activation in the lymphoid organs of MHCII^{ΔCD11c} and MHCII^Δ BM chimeric mice early after allo-HCT. MHCII^Δ BM chimeras failure of thymic negative selection and developing tissue wasting disease upon syn-HCT deemed them unsuitable to study non-hematopoietic antigen presentation in aGvHD. To overcome this challenge, we generated MHCII^{ΔVav1} mice that lack MHC class II expression on all hematopoietic cells. MHCII^{ΔVav1} mice were susceptible to aGvHD and LNSCs from these animals activated allogeneic CD4⁺ T cells in mixed lymphocyte reaction. Likewise, mesenteric lymph nodes from CD11c.DTR mice surgically transplanted into a MHCII^Δ mouse could activate CD4⁺ T cells *in vivo*, clearly demonstrating LNSCs as non-hematopoietic APCs of the lymphoid organs.

We specifically target lymph node stromal cell subsets via the Cre/loxP system, we employed single cell RNA sequencing and selected *Ccl19* and *VE-Cadherin* to specifically target the fibroblastic reticular cells and endothelial cells of the lymph nodes respectively. In MHCII^{ΔCcl19} mice, alloreactive CD4⁺ T cells activation was discreetly reduced in the initiation phase of aGvHD whereas absence of MHCII on fibroblastic reticular cells resulted in hyper-activation of allogeneic CD4⁺ T cells leading to poor survival. This phenotype was modulated by the regulatory T cells that were able to rescue *H2-Ab1*^{fl} mice but not the MHCII^{ΔCcl19} subsequent to GvHD.

Knock-out of MHCII on endothelial cells MHCII^{ΔVE Cadherin}, resulted only in modest reduction of CD4⁺ T cells activation in the initiation phase of GvHD, conversely MHCII^{ΔVE Cadherin} mice showed a protective phenotype compared against littermates *H2-Ab1*^{fl} mice in long-term survival. Furthermore, to pin-point endothelial cells MHCII antigen presentation we generated MHCII^{ΔVE Cadherin ΔVav1} animals devoid of antigen presentation in both endothelial and

hematopoietic compartments. LNSCs from $MHCII^{\Delta VE} \text{ Cadherin } \Delta Vav1$ were unable to activate alloreactive $CD4^+$ T cells in mixed lymphocyte reaction.

Altogether, we demonstrate for the first time that MHC class II on the lymph node stromal cells plays a crucial role in the modulation of allogeneic $CD4^+$ T cells in the initiation and later in the effector phase of graft-*versus*-host-disease.

I. Zusammenfassung

In der Initiationsphase der akuten Graft-versus-Host Erkrankung (GvHD) werden CD4⁺ T-Zellen in den lymphatischen Organen durch hämatopoetische Antigen-präsentierende Zellen aktiviert. Im Gegensatz dazu, werden in der Effektorphase CD4⁺ T-Zellen von nicht-hämatopoetischen Zellen im Dünndarm aktiviert. Wir stellten die Hypothese auf, dass alloreaktive CD4⁺ T-Zellen nach allogener hämatopoetischer Zelltransplantation, welche in der Initiationsphase der aGvHD vorwiegend in die sekundären lymphatischen Organe migrieren, dort durch nicht-hämatopoetische Lymphknoten-Stromazellen über die Erkennung von MHC-Klasse II aktiviert werden. Um diese Hypothese zu testen, setzten wir ein von allogenen CD4⁺ T-Zellen-abhängiges MHC Major Mismatch aGvHD Mausmodell ein, um diese Zusammenhänge näher zu erforschen.

Mittels Biolumineszenz-Bildgebung und dreidimensionale Lichtblattmikroskopie und Durchflusszytometrie-Analysen von früheren Zeitpunkten nach einer alloHCT bzw. im Anfangsstadium der aGvHD konnten wir zeigen, dass allogene T-Zellen exklusiv in die Milz, Lymphknoten und die Peyerschen Plaques migrieren und nicht in die intestinale *Lamina propria*. Indem wir transgene Mauslinien verwendeten, die keine oder eine nur partielle komplette hämatopoetische Antigenpräsentation aufwiesen, konnten wir eine sehr früh auf die alloHCT folgende allogene CD4⁺ T-Zellaktivierung in den lymphoiden Organen von MHCII^{ΔCD11c} and MHCII^Δ Knochenmark-Chimären nachweisen. Aufgrund des, bei den MHCII^Δ Knochenmarks-Chimären auftretenden Versagens der negativen Thymusselektion und die daraus resultierende autoreaktive Immunreaktionen nach einer syngenen HCST stellte sich heraus, dass dies ein ungeeignetes Modell für die Untersuchung der Präsentation nicht-hämatopoetischer Antigene bei GvHD ist. Um diese Herausforderung zu bewältigen, generierten wir MHCII^{ΔVav1} Mäuse bei denen die MHC-Klasse-II-Expression auf allen hämatopoetischen Zellen fehlt. MHCII^{ΔVav1} Mäuse entwickelten eine aGvHD, wobei die Lymphknoten-Stromazellen dieser Tiere allogene CD4⁺ T-Zellen in gemischten Lymphozytenreaktionen aktivieren konnten. Ebenso konnten mesenteriale Lymphknoten von CD11c.DTR-Mäusen, die zuvor in eine MHCII^Δ Maus transplantiert wurden, CD4⁺ T-Zellen *in vivo* aktivieren, wodurch die Lymphknoten-Stromazellen eindeutig als nicht-hämatopoetische Antigen-präsentierende Zellen der lymphoiden Organe nachgewiesen werden konnten.

Über das Cre/loxP-System konnten wir Knockout-Mäuse mit fehlender MHCII-Expression in Subpopulationen von Lymphknoten-Stromazellen generieren und verwendeten dann Einzelzell-RNA-Sequenzierung. Hier wählten wir *Ccl19* und *VE-Cadherin* aus, um unsere Analyse spezifisch auf die fibroblastischen retikulären Zellen bzw. Endothelzellen der Lymphknoten zu konzentrieren. Bei MHCII^{ΔCcl19} Mäusen war die Aktivierung alloreaktiver CD4⁺ T-Zellen in der Initiationsphase der aGvHD mäßig reduziert, während das Fehlen von MHCII

auf den fibroblastischen retikulären Zellen zu einer Hyperaktivierung allogener CD4⁺ T-Zellen führte, was wiederum eine schlechtere Überlebensrate der Mäuse zur Folge hatte. Dieser Phänotyp wurde durch regulatorische T-Zellen moduliert, die in der Lage waren, *H2-Ab1*^{fl} Mäuse von den Folgen von GvHD zu retten, jedoch nicht die MHCII^{ΔCcl19}.

Ein Knock-out von MHCII auf Endothelzellen von MHCII^{ΔVE-Cadherin} Mäusen, führte in der Initiationsphase der GvHD nur zu einer mäßig reduzierten Aktivierung von CD4⁺ T-Zellen. Umgekehrt zeigten MHCII^{ΔVE-Cadherin} Mäuse im Langzeitüberleben jedoch einen protektiven Phänotyp verglichen mit wurfgeschwister *H2-Ab1*^{fl} Mäusen. Um die Bedeutung der MHCII-Antigenpräsentation der Endothelzellen zu untersuchen, generierten wir außerdem MHCII^{ΔVE-CadherinΔVav1} Mäuse, bei welchen eine Antigenpräsentation, weder im endothelialen noch im hämatopoetischen Kompartiment möglich war. Lymphknoten-Stromazellen von MHCII^{ΔVE-CadherinΔVav1} Mäusen waren nicht in der Lage, alloreaktive CD4⁺ T-Zellen in einer gemischten Lymphozytenreaktion zu aktivieren.

Insgesamt konnten wir zum ersten Mal beweisen, dass die MHC-Klasse II auf den Lymphknoten-Stromazellen eine entscheidende Rolle bei der Modulation allogener CD4⁺ T-Zellen in der Initiations- und schließlich in der Effektorphase der Graft-versus-Host-Disease spielt.

1. Introduction

1.1 Lymph node stromal cells

Lymph nodes are the most prevalent secondary lymphoid organs (SLO) in humans and mice. In mice there are 22 LNs that always develop in the same distinct body sites [1-3]. They range in size and enlarge significantly under certain conditions involving immune activation i.e., infection, autoimmunity or cancer [4, 5]. Lymph nodes are structurally organized into cortex, paracortex and medulla [6]. The cortex is located beneath the capsule and subcapsular sinus with follicular dendritic cells (FDCs) and B cells contained within the follicle present in the cortical region [7]. Under the cortex lies the paracortex where T cells home and interact with antigen presenting cells [7]. The innermost part of the lymph nodes is the medulla consisting of macrophage and B cells within the medullary cords that allow the movement of lymph from the cortex to the efferent lymphatic vessels [7].

The microenvironment of the lymph node is crucial for immune function and consists of endothelial cells lining the blood and lymphatic vessels and fibroblastic reticular cells which create the reticular structure of the lymphoid tissues [8]. Structural components of the lymph nodes have been broadly appreciated as primary regulators of the adaptive immune response [9-22]. These structural components of the lymph nodes are termed as lymph node stromal cells (LNSCs) and are functionally and phenotypically distinct from each other and can be characterized by the surface expression of glycoproteins CD31 (PECAM-1) and podoplanin (gp38) and absence of CD45 (PTPRC) [12]. These include fibroblastic reticular cells (FRCs), lymph endothelial cells (LECs), blood endothelial cells (BECs), integrin $\alpha 7$ pericytes (IAPs) and follicular dendritic cells (FDCs) [12, 19, 23]. These stromal and endothelial cells play variety of functions in lymph node homeostasis, as they interact with lymphocytes to create an optimal niche for cell activation and migration.

1.1.1 Fibroblastic reticular cells (FRCs)

FRCs are of myofibroblastic origin that have evolved to create a specialized microenvironment within the lymph nodes. FRCs are quite heterogeneous and exist in different niches within the lymph nodes, fulfilling unique structural and immunomodulatory roles [23] (Table 1.1).

Table 1.1 Lymph node FRC subset

FRC subtype	Characteristics	Phenotype	Function	References
T cell zone reticular cells (TRCs)	Secretion of CCL19, CCL21, and IL-7 within paracortex.	PDPN+, desmin+, MAdCAM-, CCL19+, CCL21+.	Maintains T cell homeostasis, forming a conduit network, allowing lymphocyte to migrate and infect efficiently in the 3D meshwork.	[12, 19, 24-28]
Marginal reticular cells (MRCs)	Located in the subcapsular sinus.	PDPN+, desmin+, MAdCAM+, IL-7 ^{Hi} , CXCL13+, RANKL ^{Hi} .	Produce high levels of IL-7. Precursors of FDCs within lymph nodes.	[29-31]
Follicular dendritic cells (FDCs)	In lymph nodes, FRCs derive from FDCs, but are highly distinct from other FRCs types. Located in B cell follicles. Secretion of CXCL13.	CD21+, CD35+, CXCL13+, ICAM1+, VCAM1+, BAFF+, MFGE8+.	Maintains germinal center integrity, facilitates the production of high-affinity antibodies.	[31, 32]
B cell zone reticular cells (BRCs)	Located in (resident) or near (inducible) B cell follicles, they secrete BAFF and are induced to secrete CXCL13 during inflammation.	Resident cells: PDPN+, CCL19+, BAFF+. Inducible cells: PDPN+, CXCL13+.	Supporting B cell survival and follicle boundary integrity.	[21, 33-35]
Pericytic FRCs	Supports HEVs, PDPN signals to CLEC-2 on platelets to maintain endothelial integrity.	PDPN+.	Prevents bleeding from HEVs into lymph nodes.	[36]
Medullary FRCs	Associated with plasma cells and macrophages.	PDPN+.	Poorly studied.	[7]

FRCs plays a crucial role in secreting extracellular matrix components (collagens, laminins, decorin, biglycan, fibromodulin and vitronectin) and forming a cellular meshwork to give lymph node structure, strength and flexibility [12, 19, 26, 37, 38]. TRCs facilitate lymphocyte migration and priming by supporting and secreting a 3D conduit network to maintain lymph node microenvironment [12, 26, 37, 39, 40]. FRCs also enclose high endothelial venules (HEVs) where they maintain the lymph-blood barrier [36]. In response to inflammation and infection, FRCs dynamically regulate lymph node contraction and expansion through the podoplanin–CLEC-2 axis, expressed on DCs during inflammation [38, 41].

TRCs release chemotactic factors: chemokine CCL19 and CCL21, which signals to CCR7 expressed on naïve T cells, leading to their migration through the lymph node and interaction with antigen presenting cells (APCs) [9, 37, 42, 43] allowing them to initiate an immune response [9, 12, 25, 42]. TRCs have also been shown to promote the survival and turnover of naïve T cells via the secretion of IL-7 [12]. IL-17 is critical for the proliferation of lymph node and splenic stromal cells, particularly under inflammatory conditions. Without IL-17, FRCs go into nutrient stress, cell cycle arrest and apoptosis [44].

Moreover, FRCs have been shown to robustly suppress CD8⁺ T cell proliferation early after their activation [17, 18]. Activated T cells secrete inflammatory cytokines such as interferon gamma (IFN γ) and tumor necrosis factor alpha (TNF α), which stimulate FRCs to upregulate nitric oxide synthase 2 (NOS2) and secrete nitric oxide (NO). NO acts in a paracrine manner on T cells curbing their proliferation. Accordingly, NOS2^A FRCs are unable to mediate T cells suppressive function [17, 18]. In contrast to NO pathway that only comes into play during strong T cell responses, COX2/PGE₂ pathway is active during both strong and weak T cell responses [45, 46]. Murine FRCs produce prostaglandin E₂ (PGE₂) in a cyclooxygenase-2 (COX2)-dependent and inflammation-independent manner. LNSCs can also induce tolerance in CD4⁺ T cells through expression of MHC class II and associated pathways [19, 20, 22]. LNSCs also express and present peripheral tissue antigen (PTA) which are regulated by Aire like protein DEAF-1 [16, 47]. Contrary to self-antigen presentation, depletion of FRCs or knock-out of molecules on FRCs have been shown to significantly attenuate cell-mediated immunity against viral infections [21, 33, 48, 49].

FRCs residing in the B cell follicles produce B cell-activating factor (BAFF) [33], a cytokine which drives the proliferation and maturation of B cells [50]. FRCs in the perifollicular region have been shown to produce CXCL13 during infection, enabling the B cells follicles to expand and provide favorable niche for B cell activation and maturation [34, 51]. Furthermore, it was shown that loss of FRCs was detrimental for humoral immune response against influenza A infection [33].

FRCs not only interact with T and B lymphocytes but have also shown to promote DCs motility into and inside the lymph node via the interaction between FRCs and LECs bearing podoplanin and activated DCs expressing Clec-2 [52].

Several studies have also shown that FRCs can directly detect lymph-borne infection or inflammatory signals via toll-like receptors (TLRs) 3 and 4 [16, 19]. Furthermore, FRCs upregulate innate immune response chemoattractants and regulatory factors (CXCL1, CXCL10, CCL2, CCL7, IL-33, IL-34, CSF1, CCL5 and CXCL9) as well as type I and II interferon receptors [19].

There are differences between the differentiation trajectories and types of FRCs from the lymph node and spleen, however addressing them individually is beyond the scope of this

1.1.2 Marginal reticular cells (MRCs)

These cells populate the outer regions of the cortex of lymph nodes [29]. They are located deep on the floor of the subcapsular sinus (SCS) and are phenotypically distinct from TRCs and FDCs by their hallmark expression of MAdCAM-1, CXCL13 and RANKL, whereas they lack the expression of CCL21 and CR1/CD35 [29, 30]. MRCs are considered as direct descendants of lymphoid tissue organizer (LTo) cells [30]. In addition to their role in embryonic development MRCs have been shown to give rise to FDCs [31, 53]. In adult mice, MRCs express CXCL13 to attract CXCR5⁺ innate lymphoid cells type 3 (ILC3), which drive LNs repair and regeneration after damage [54, 55]. Since CXCL13 is a B cell chemoattractant, it has been hypothesized that MRCs might be involved in the transport of antigens from SCS into the B cell follicles [29].

1.1.3 Follicular dendritic cells (FDCs)

FDCs are contained in the B cells follicles and play an important role in the capture storage and presentation of incoming antigen to B cells [56]. They express B cell survival factor BAFF and IL-6 [32, 57, 58]. FDCs play a critical role in the formation of the germinal center and efficient hypermutation and production of high-affinity antibodies [58, 59]. FDCs also express high levels of CXCL13, which directs B cells and helper T cells leading to the border of the follicle enhancing B cell activation [42, 51].

1.1.4 Lymph endothelial cells (LECs)

LECs create afferent and efferent lymphatic vessels, that primarily allow the entry of antigen-presenting dendritic cells and soluble antigens into the paracortex [60, 61], and the egress of lymphocytes from the medulla [62]. Based on the anatomical location, LECs are classified into 3 different types having differential expression of key surface markers (Table 1.2).

Table 1.2 Lymph node LEC subsets

Cell type	Surface markers	Reference
Subcapsular LECs - Floor LECs (fLECs)	PD-L1 ^{hi} , ICAM-1 ^{hi} , MAdCAM-1 ⁺ , and LTBR ^{lo}	[61, 63]
Medullary LECs -Ceiling LECs (cLECs)	PD-L1 ^{hi} , ICAM-1 ^{hi} , MAdCAM-1 ^{neg} and LTBR ⁺	[61, 63]
Cortical LECs	PD-L1 ^{int} , ICAM-1 ^{int} , MAdCAM-1 ^{neg} and LTBR ⁺	[63]

Similar to FRCs, LECs secrete IL-7 essential for T cell homeostasis and survival [64] as well as express podoplanin and drive DCs migration toward and within lymph nodes through signalling to CLEC-2 [52]. They actively secrete CCL21 [19] as well as regulate the availability of CCL19, CCL21 and other chemokines in the subcapsular sinus and local parenchymal tissue through the expression of scavenging receptors ACKR2 and ACKR4 [19].

LECs are capable of suppressing proliferation of newly activated CD4⁺ and CD8⁺ T cells via production of NO, in a similar mechanism to FRCs [18]. LECs upregulate MHC class II under certain inflammatory conditions, and thus may contribute to increased antigen presentation [19]. This mechanism is IFN γ dependent, that has been shown to promote apoptosis of CD4⁺ T cells in an antigen-specific manner. LECs are also able to transiently acquire MHC class II from DCs [22]. LECs have also been showed to cause T cell exhaustion under prolonged inflammation via upregulation of PD-L1 [63, 65].

Similar to FRCs, LECs also express PTAs, utilizing the transcriptional factor DEAF-1. PTAs expression by tolerance inducing LECs is pivotal to delete autoreactive T cells. [15]

1.1.5 Blood endothelial cells (BECs)

BECs facilitates the migration of naïve lymphocytes into lymph nodes by forming specialized postcapillary venules know as high endothelial venules (HEVs) [6]. They allow entry of lymphocytes in the SLOs through the process known as diapedesis, trans-endothelial migration or lymphocyte extravasation. The process of slowing down and breaching the endothelial barrier involves well-characterized interaction including leukocyte rolling, activation, adhesion and intraluminal crawling [66], which involves receptor ligand interaction between T cells and the endothelium [67]. CD62L (L-Selectin) on the surface of T cells serves as primary mediator of rolling and loose attachment to HEVs via peripheral node addressin (PNAd) on HEVs BECs [68]. Next, T cells go into integrin-mediated arrest involving LFA-1, binding to endothelial ICAM-1 [69]. ICAM-1 downstream signalling prepares endothelial cells for trans-endothelial cell migration. CD31 (PECAM-1) and CD99 (MIC-2) expressed by both lymphocytes and endothelial cell with homophylic affinity, arrest the lymphocytes at the junction of adjacent endothelial cells [66]. In the last step of trans-endothelial migration adherens junctions joining endothelial cells are disassembled through phosphorylation of VE-Cadherin [66]. HEVs serve as gatekeepers of lymph nodes by creating pockets holding newly arrived lymphocytes until the space in the parenchyma becomes available [24].

BECs plays an important role in the lymph node vascular integrity, homeostasis as well as assisting FRCs and LECs in maintaining network remodelling [36, 70-72]. BECs numbers have shown to increase under inflammatory conditions, which are regulated by vascular endothelial growth factor (VEGF) primarily produced by FRCs [68]. DCs also play a role in the regulation

of HEV phenotype and functionally, which that is partially modulated by IL-1 β resulting in proliferation of endothelial cells [73]. T and B cells are dispensable for initial endothelial proliferation, however, BECs play a major role in subsequent maintenance and expansion of the lymph node [68].

1.1.6 Double-negative stromal cells and pericytes

These cells are characterized as the population that does not express GP38 and CD31, they constitute approximately 10 - 20% of non-hematopoietic LNSCs [12, 16, 74]. Until recently the lineage, location, and function of these cells were undescribed. Malhotra and colleagues [19] with the help of RNA sequencing identified the phenotype of DN cells. These cells and FRCs, share similarities in chemokine, cytokine, and growth factor expression. A notable difference between FRCs and DN cells is that they lack the expression of IL-7, whereas they express high levels of genes responsible for the structure and contractile functions including actin subtypes of myosin chains, which usually control smooth muscle contraction [19].

Accordingly, 50% of DN cells were identified as a special subset of myofibroblast pericytes, characterized by the expression of calponin-1 and integrin $\alpha 7$ [19]. The function of integrin $\alpha 7$ pericytes is yet to be identified, however, they share the expression of many immunological relevant molecules with FRCs. The other 50% of cells comprising the DN cell population are undescribed.

1.2 Acute Graft-versus-Host disease

Acute Graft-versus-Host Disease (aGvHD) occurs as a complication in 30-80% of all patients undergoing allogeneic hematopoietic stem cell transplantation (allo-HCT) [75, 76]. Second to disease relapse, aGvHD is the major cause of morbidity and mortality after allo-HCT. To date allo-HCT is considered as the most successful curative therapy against blood-borne diseases such as leukaemia and/ or inherited disorders of immune cells. Initial clinical symptoms of aGvHD are characterized by the inflammation of skin (rashes), GIT (heavy diarrhea), lung (obstruction and fibrosis) and liver (bilirubinemia, fibrosis) [77]. In contrast to chronic GvHD, aGvHD typically occurs early after transplantation, which in a clinical setting means first 100 days after allogeneic hematopoietic stem cell transplantation. GvHD is a T cell driven (Th1 and Th17) disease and is characterized by alloreactive T cell infiltration to the target organs. On the contrary, the therapeutic benefit of allo-HCT know as Graft-versus-Leukaemia (GvL) is also immunological in nature and mediate by donor T cells and natural killer cells recognizing leukaemia-specific antigens [78].

1.2.1 Clinical relevance of GvHD

20-30% of patients with hematopoietic malignancies, who undergo hematopoietic cell transplantation die due to GvHD-related complications [75]. Without immunosuppressive treatment, 100% of allogeneic transplant patients would develop GvHD. The severity of GvHD is graded into four categories, however differences exist between different scoring criteria [79, 80]. According to Glucksberg criteria, mild grade I GvHD includes only the skin. Moderate grade II GvHD includes moderate skin and mild to moderate intestinal and liver damage. Grade III GvHD is characterized by severe damage to all target organs and grade IV is very severe GvHD. Intestinal GvHD is scored clinically by assessing the volume of diarrhea and pathological evaluation of crypt- and epithelial cell apoptosis, immune cell infiltrates and villus blunting [81]. The first line treatment against GvHD is the use of steroids, however around 50% of patients develop steroid-refractory GvHD [82] and require alternate treatments like calcineurin- and rapamycin inhibitors. To date, steroid-refractory aGvHD remains difficult to treat and can result in mortality rates of up to 70-80%. [83, 84].

In summary, GvHD frequently complicates allo-HCT. GvHD poses a major hindrance to therapy success and causes severe morbidity and mortality. Because a high number of patients become resistant to conventional therapy, it is important to develop new strategies to more effectively modulate immune response for patients to benefit from allo-HCT.

1.2.2 aGvHD pathophysiology and target organs

aGvHD pathophysiology is classified into three distinct stages: tissue damage due to the conditioning (chemotherapy and/or radiation) regimen (phase I), activation of hematopoietic and non-hematopoietic antigen presenting cells leading to subsequent alloreactive T cell activation and expansion (phase II) and finally target tissue destruction and cytokine storm (phase III). [77]. Despite allo-antigen expression on all host tissues, not all host tissues are targeted by the activated allo-reactive T cells in aGvHD. The intestine, skin, liver and the lung are the target organs whereas other organs are not affected in GvHD. Factors that may contribute to allo-immune response in these organs are their high cellular turnover, which leads to more extensive damage than in organs with a high percentage of non-dividing cells. This affects the extent of tissue damage in phase I. Secondly, intestine, skin, lung and liver are exposed to a variety of microbiota and fungi via the mucosa [85, 86] and portal vein, which make them rich in immunostimulatory molecules recognized by the innate immune system. These influence the activation of antigen-presenting cells in phase II. Third, intestine, skin and liver are organs rich in resident immune cell population, which transiently survive the conditioning regimen and therefore provide a large reservoir for cells producing large amounts of inflammatory cytokines (phase III).

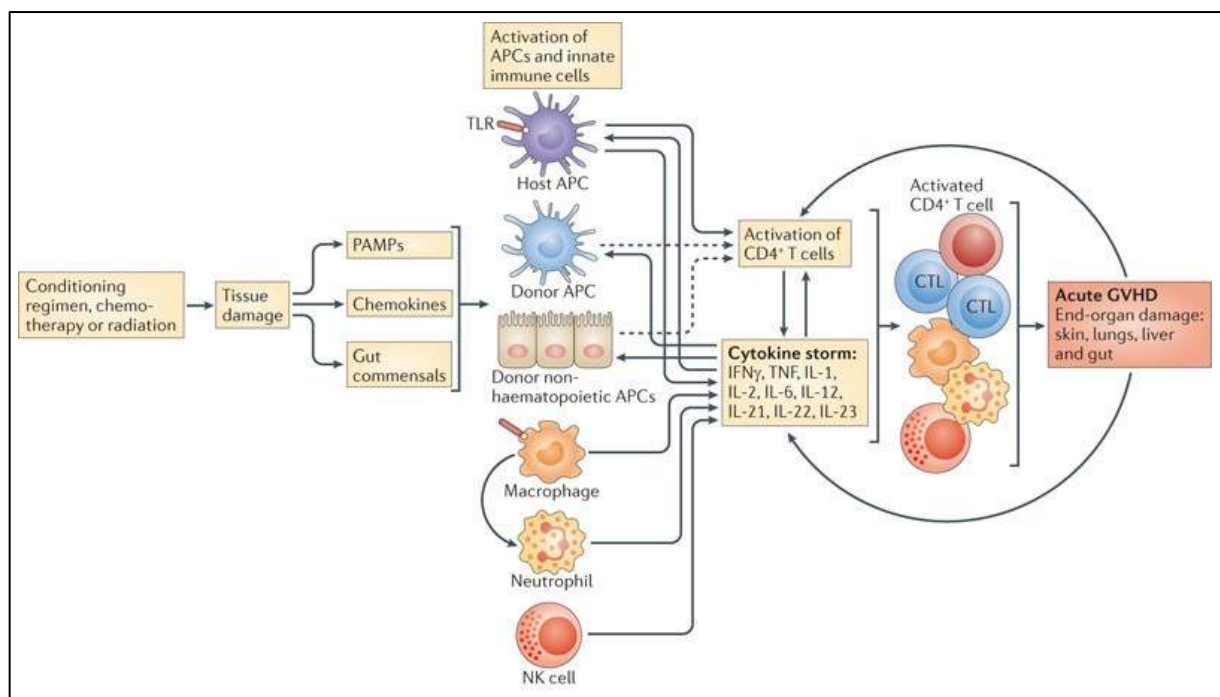


Figure 1.2 The initiation and maintenance of acute graft-versus-host disease (aGvHD) have been conceptualized into four phases with positive feedback loops that perpetuate the process.

Although the conditioning phase is not absolutely necessary for the induction of aGvHD, in many of the model's chemotherapy/myeloablative irradiation activates antigen-presenting cells (APCs), via tissue destruction, and increases APC function. Through the release of pathogen-associated molecular patterns (PAMPs), gut bacteria and chemokines, the conditioning phase can also lead to the activation of innate immune cells that participate in direct tissue damage and contribute to the cytokine storm. Host hematopoietic APCs probably have the most important role in the initiation of GvHD, but this may depend on the model; the potential role of donor APCs and host non-hematopoietic APCs should not be ignored. Following the presentation of antigens to donor T cells, a strong cytokine response is initiated. These cytokines additionally promote antigen presentation and the recruitment of effector T cells and innate immune cells, which further augment the pro-inflammatory cytokine milieu. Finally, the natural killer (NK) cells, effector T cells, macrophages and pro-inflammatory cytokines (such as tumor necrosis factor (TNF) result in end-organ damage, which is clinically recognized as aGvHD in lung, liver, skin and lung. The resulting tissue damage, if not treated, will further amplify the process to more severe stages of GvHD pathology, which are extremely difficult to control. CTL, cytotoxic T lymphocyte; IFN γ , interferon- γ ; TNF, tumor necrosis factor; TLR, Toll-like receptor. Adapted from Blazar B et al., 2012. The figure reprint permission has been granted by Springer Nature and Copyright Clearance Center under the licenses 4915850743868 and the terms and conditions provided accepted.

1.2.3 Target antigen recognition

The targets in GvHD are MHCs and peptides presented therein (in MHC-mismatched donors and recipients) and/or minor histocompatibility (mHAs) in both MHC-mismatched and MHC-matched donor-recipient pairs. mHAs such as (HA-1 or y-chromosomal proteins) are peptides generated by the polymorphic genes that differ between donor and recipient and can, in turn be presented in MHCs [87]. GvHD can be conceptualized as MHC class I and/or MHC class II dependent i.e., CD8⁺ and CD4⁺ T cells, respectively.

Allo-antigens presented in MHC class II are predominantly exogenous in origin, however, endogenous antigens can also be presented directly within MHC class II in stress conditions such as autophagy. Another 'semi-direct' pathway of antigen presentation has also been recently described, in which donor cells can acquire recipient cell-derived membrane receptors including MHC class I and MHC class II via either exosome uptake or trogocytosis [88, 89]. This type of antigen presentation can contribute to T cell activation or suppression [22, 90].

1.2.4 Activation of T cells in aGvHD

Secondary lymphoid organs (SLOs), such as spleen, lymph nodes or Peyer's patches enable interactions between activated APCs and allo-reactive T cells that, upon contact, get activated proliferate and differentiate into effector T cells that migrate to the target organs. Host hematopoietic APCs are key drivers of aGvHD initiation. Subsequently many studies have attempted to pinpoint the critical APC subsets involved, predicted on the notion that their depletion may prevent aGvHD. Longstanding dogma has been held believing that recipient DCs as initiators of aGvHD, based on their ability to initiate disease when transferred into MHC-deficient recipient [91] and their transient persistence after total body irradiation (TBI) [92]. However, generation of a new transgenic mice revealed that recipient DCs are not required to initiate MHC-class II-dependent aGvHD and may actually regulate the disease by inducing T cell apoptosis in SLOs [93-95]. Furthermore, other studies showed that B cells, macrophages, plasmacytoid DCs and Langerhans cells are redundant for the initiation of lethal aGvHD and capable of regulating disease [93, 94, 96-99].

Furthermore, several studies revealed that recipient non-hematopoietic APCs, once activated by chemoradiotherapy, can efficiently initiate MHC class II-dependent GvHD [93, 100]. Fibroblasts [101-103] have been shown to be capable of inducing cytotoxic T cell response. Also, epithelial cells express MHC class II upon inflammation particularly IFN γ [104-106]. Recently, Koyama and colleagues reported that MHC class II expressing intestinal epithelial cells (IECs) can initiate lethal gut GvHD, which in turn is influenced by microbiota and regulated by IL-12 – IFN γ cytokine axis [107]. In an exclusive MHC class II dependent setting, both hematopoietic and non-hematopoietic APCs can initiate lethal aGvHD, and non-hematopoietic APCs appear dominant.

1.2.5 Mouse models of GvHD

Immune cells function in steady-state and inflammation have been extensively studied under *in vitro* cell culture conditions. However, there are certain biological processes that are too complex to recapitulate fully *in vitro*, that is why it is imperative to study these processes in pre-clinical animal models.

There are various well-established mouse models for GvHD [108]. In our study, we employed an FVB/N to C57BL/6 allo-HCT model, in which bone marrow cells and T cells from FVB/N (H-2K^q) donors are transplanted into fully MHC-mismatched myeloablatively conditioned C57BL/6 recipients (H-2K^b). Both CD4⁺ and CD8⁺ T cells contribute to GvHD pathology [109, 110]. In our study, we used this model to study allo-reactive CD4⁺ T cell activation and expansion early after allo-HCT. This model was very useful because the time course of T cell infiltration, activation and migration to the target organs had been well established previously [109, 110].

Furthermore, most of the transgenic mouse strains employed in this study were available in C57BL/6 genetic background and FVB/N (CD45.1 and CD90.1) providing a congenic marker to differentiate between the host and the donor hematopoietic cells making the model suitable to study MHC class II-dependent antigen presentation.

1.3 MHC class II antigen presentation by non-hematopoietic cells of lymphoid organs

MHC class II-restricted antigen presentation is crucial for CD4⁺ T cell-dependent immune responses. As previously hypothesized, antigen presentation is not exclusively restricted to hematopoietic cells. Recent work has demonstrated that LNSCs not only provide a scaffold for lymphocyte interaction but also exhibit active immunomodulatory roles that are critical to mounting and resolving effective immune responses. LNSCs express endogenously MHC II and alternately can acquire MHCII molecules. They possess the machinery to present antigens and establish antigen-specific interactions with T cells [19, 20, 111]. Antigen retention is a way of modulating antigen availability in an immune response and LNSCs have been shown to retain pathogenic antigen in various experimental models [112, 113].

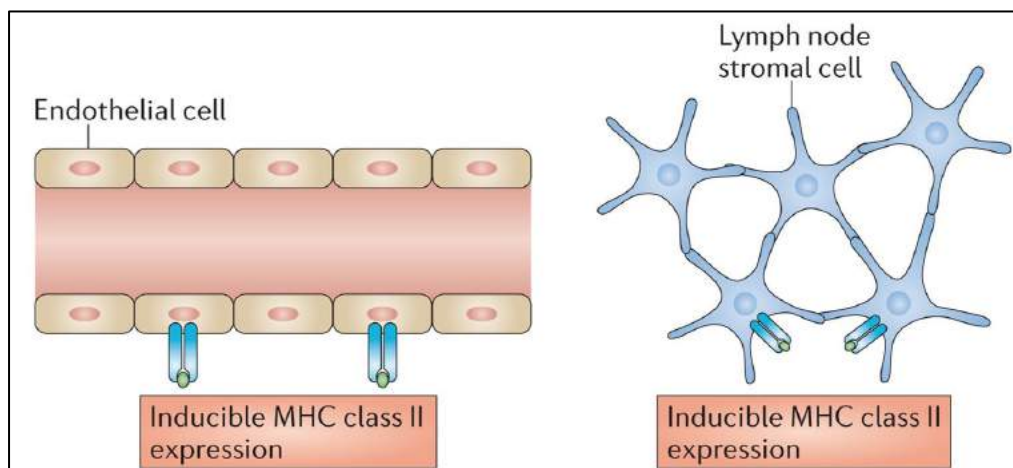


Figure 1.3 Vascular endothelial cells and lymph node stromal cells can express MHC class II molecules.

Although these cells have been shown to activate CD4⁺ T cells *in vitro*, their expression of MHC class II molecules *in vivo* is thought to be more relevant for the induction and maintenance of immune tolerance. Adapted from Kambayashi T et al., 2014. The figure reprint permission has been granted by Springer Nature and Copyright Clearance Center under the licenses 4915850596895 and the terms and conditions provided accepted.

1.3.1 MHCII expression by LNSCs

LNSCs constitute non-professional APCs that express MHCII. Unlike MHC class I molecules, however, MHCII expression is highly regulated. The class II transactivator (CIITA) is the master transcriptional factor that regulates the expression of MHC class II. CIITA itself is regulated by cell-specific promoters: pI, pIII and pIV. Amongst them, pIV is essential for constitutive expression of MHCII on thymic epithelial cells whereas on endothelial cell, epithelial cell and fibroblasts, the pIV driven MHCII expression is mediated by IFN γ [114]. Recently it has been reported that LNs FRCs, LECs and BECs express MHCII under steady-state condition [19, 20, 71, 115] as well as being capable of acquiring MHCII from DCs [22].

1.3.2 LNSCs in antigen specific CD4⁺ T cell responses

Between LNSCs and APCs, transfer of antigens and peptide:MHCII complexes seems to play an important role in MHCII restricted antigen presentation. Exosomal transfer appears to represent a major route of MHCII transfer from professional APCs to LNSCs.

FDCs does not express endogenous MHCII [116] nor phagocytose antigens [117], however, they retain exogenous MHCII expression and interact with CD4⁺ T cells [118].

The transfer of peptide: MHCII complexes from DCs, but not macrophages or B cells, maintains steady-state levels of MHCII on FRCs, LECs and BECs. Antigen transfer between LECs and DCs is nevertheless, bi-directional [111]. As LECs have shown to transfer LEC-specific PTA to hematopoietic cells. However, neither the membrane-bound nor cytoplasmic expressed PTAs failed to prime antigen-specific CD4⁺ T cells [111]. On the same line, human LN-derived LECs failed to induce allogeneic CD4⁺ T cell proliferation even after IFN γ stimulation [115]. This can be attributed to LECs' lower expression of H2-M compared to professional APCs, which is essential to free the MHCII groove for peptide binding. On the other hand, FRCs and BECs express H2-M under steady-state and under inflammatory conditions [19, 20] and immortalized FRC cell line has been shown to induce CD4⁺ T cell proliferation *in vitro* [119]. Furthermore, MHCII on LNSCs has been shown to maintain antigen-specific regulatory T cells (Tregs) under steady-state conditions [20, 120, 121].

1.3.3 LNSCs in GvHD

LNSCs have been studied in GvHD, particularly in pre-clinical models of CD8⁺ T cell-mediated aGvHD. Alloreactive CD8⁺ T cells cause severe and irreversible damage through the loss of CD157⁺ FRCs and HEVs via Fas-FasL pathway resulting in humoral immunodeficiency and susceptibility to infections even in the presence of peripheral B and T cells [122]. However, a recent study showed FRC loss resulting from CD4⁺ T cell-mediated or CD8⁺ T cell-mediated alloreactivity in polyclonal GvHD models. They showed that before profound loss of FRCs in

GvHD, FRCs tends to decrease the expression of *Deaf1*, encoding a transcriptional factor regulating expression of PTAs, thus resulting in loss of peripheral tolerance and promoting autoimmunity [123].

Furthermore, naïve T cells require notch signaling for priming and attaining effector functions. Chung and colleagues showed Ccl19 expressing cells of the SLOs deliver notch signals (DLL1/4) to incoming T cells within 2 days of allo-HCT, whereas both donor and host hematopoietic cells are dispensable as a source of Notch ligands driving aGvHD [124].

1.4 Knowledge gap

MHC class II is a crucial molecule of the adaptive immune system and its proper function is critical for fight against infections [125] as well as cancers [126]. However, polymorphism [127] and dysregulation [128] in MHCII results in T cell autoreactivity and autoimmunity [127]. In aGvHD allogeneic CD4⁺ T cells are activated into effector T cells when an antigen presenting cells present an allo-antigen via MHCII to T cells, and these are recognized by their TC receptor (TCR). The cell source that provides this MHCII signal has been debated over the last years, as dendritic cells were shown to be dispensable [93, 94, 100]. Others have shown *in vitro* and *in vivo* that liver endothelial cells [100] and gut epithelial cells [107] can activate allogeneic CD4⁺ T cells, however, an understanding is still lacking about the potential non-hematopoietic APC that reside in the secondary lymphoid organs, where naïve alloreactive CD4⁺ T cells expressing CD62L and CCR7 home subsequent to allo-HCT.

In this thesis, we elucidate the MHC class II antigen expression and presentation by non-hematopoietic structural cells of lymphoid organs that essentially provide integrity to the SLOs. Studying MHCII antigen presentation of non-hematopoietic lymph node stromal and endothelial cells of the secondary lymphoid organs will provide a better understanding of aGvHD initiation that has not yet been studied before to the best of our knowledge.

Elucidating this mechanism will potentially provide us insights of targeting these MHCII-TCR interactions in the SLOs to minimize the incidence of GvH without altering the GvL arm of hematopoietic stem cell transplantation.

2 Specific Aims

The overall aim of this thesis was to determine whether MHC class II expressing lymph node stromal cells enhance or limit alloreactive CD4⁺ T cells priming and function in aGvHD. The specific aims of this thesis were to:

1. Investigate the primary sites for CD4⁺ T cell activation in the initiation phase of aGvHD (lymphoid organs and/ or target organs).
2. To pinpoint non-hematopoietic antigen presenting cell(s) of the lymphoid organs that can promote or inhibit CD4⁺ T cell driven aGvHD.

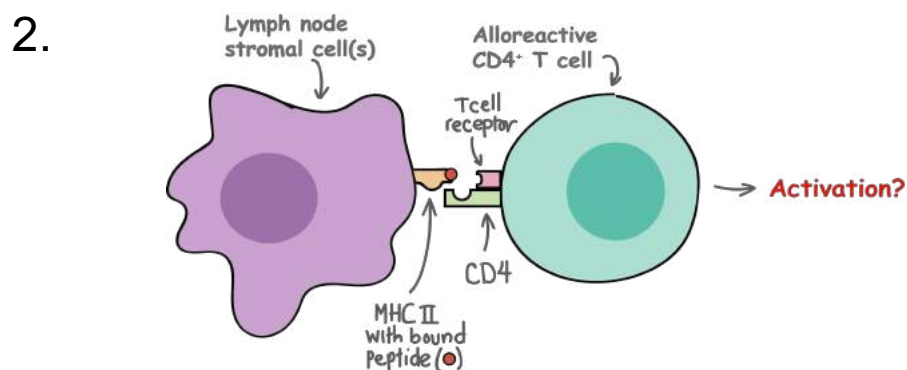
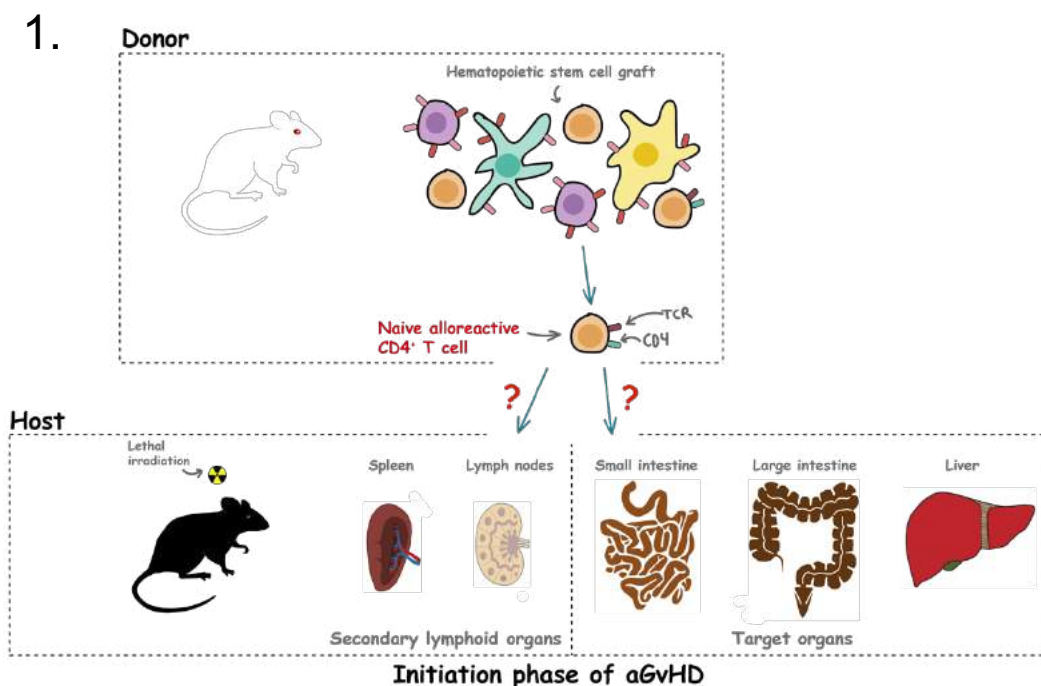


Figure 2.1 Research questions of this thesis project.

- (1) Are anatomical sites outside of SLOs priming sites for naïve alloreactive CD4⁺ T cells during aGvHD initiation?
- (2) Can defined LNSCs activate or inhibit alloreactive CD4⁺ T cell driven aGvHD after allo-HCT in pre-clinical animal models?

3 Material and Methods

3.1 Materials

3.1.1 Chemical reagents

Acetone	Sigma (Deisenhofen, Germany)
Baytril	Bayer (Leverkusen, Germany)
Benzyl alcohol	Sigma (Deisenhofen, Germany)
Benzyl benzoat	Sigma (Deisenhofen, Germany)
D-Luciferin	Biosynth (Staad, Switzerland)
Entellan	Merck (Darmstadt, Germany)
Ethanol	Sigma (Deisenhofen, Germany)
Fetal calf serum (FCS)	Invitrogen (Darmstadt, Germany)
Hexane	Sigma (Deisenhofen, Germany)
Hydrogen peroxide 30%	Sigma (Deisenhofen, Germany)
Ketamine	Pfizer (Berlin, Germany)
Methanol	Sigma (Deisenhofen, Germany)
Normal rat serum (NRS)	Invitrogen (Darmstadt, Germany)
O.C.T	Sakura (Staufen, Germany)
Paraformaldehyde	Roth (Karlsruhe, Germany)
Triton X-100	Roth (Karlsruhe, Germany)
Trypan blue	Sigma (Deisenhofen, Germany)
Xylazine 2%	CP-Pharma (Burgdorf, Germany)

3.1.2 Buffers and solutions

- RBC lysis buffer (10x): NH_4Cl (89.9 g), KHCO_3 (10 g), EDTA (0.37 g) in 1000 ml distilled water, sterile filtered
- PBS (10x): NaCl (80 g), $\text{Na}_2\text{HPO}_4 \cdot 2\text{H}_2\text{O}$ (14.2 g), KCl (2 g), KH_2PO_4 (2 g) in 1000 ml distilled water, pH: 6.8
- MACS buffer: BSA (0.5 g), EDTA 0.5 M (0.2 ml) in 500 ml (1x) PBS
- PFA (4%): 4 g PFA in 100 ml (1x) PBS, dissolved at 65°C, pH: 7.4
- Anesthetics: 8 ml Ketamine (25 mg/ml, Ketanest, Pfizer Pharma, Berlin, Germany). 2 ml Xylazine (2%) (Rompun, CP-Pharma, Burgdorf, Germany), 15 ml (1x) PBS

3.1.3 Antibodies and secondary reagents

Table 3.1 Murine antibodies used for flow cytometry staining and fluorescence microscopy

Antibody	Clone	Conjugation	Isotype	Vendor
CD11c	N418	AF647	Armenian Hamster IgG	Biolegend
CD24	M1/69	PerCP/Cy5.5	Rat IgG2b, κ	Biolegend
CD104	346-11A	PE	Rat IgG2a, κ	Biolegend
CD25	PC61	APC	Rat IgG1, λ	Biolegend
CD25	PC61	PE-Cy7	Rat IgG1, λ	Biolegend
CD274 (PD-L1)	10F.9G2	PE-Cy7	Rat IgG2b, κ	Biolegend
CD279 (PD-1)	29F.1A12	PE-Cy7	Rat IgG2a, κ	Biolegend
CD31	MEC13.3	PE-Cy7	Rat IgG2a, κ	Biolegend
CD31	390	AF488	Rat IgG2a, κ	Biolegend
CD31	390	Biotin	Rat IgG2a, κ	Biolegend
CD4	RM4-5	PerCP/Cy5.5	Rat IgG2a, κ	Biolegend
CD4	RM4-5	PE	Rat IgG2a, κ	Biolegend
CD8 α	53-6.7	PerCP/Cy5.5	Rat IgG2a, κ	Biolegend
CD40	3/23	PE-Cy7	Rat IgG2a, κ	Biolegend
CD44	IM7	PE	Rat IgG2b, κ	Biolegend
CD45	30-F11	APC-Cy7	Rat IgG2b, κ	Biolegend
CD45	30-F11	PerCP/Cy5.5	Rat IgG2b, κ	Biolegend
CD45.1	A20	APC-Cy7	Mouse (A.SW) IgG2a, κ	Biolegend
CD45.1	A20	AF647	Mouse (A.SW) IgG2a, κ	Biolegend
CD45.2	104	AF488	Mouse (SJL) IgG2a, κ	Biolegend
CD62L (L-Selectin)	MEL-14	PE-Cy7	Rat IgG2a, κ	eBioscience
CD62L (L-Selectin)	MEL-14	FITC	Rat IgG2a, κ	Biolegend
CD64 (FcyRI)	X54-5/7.1	PE-Cy7	Mouse IgG1, κ	Biolegend
CD74 (CLIP)	In1/CD74	AF488	Rat IgG2b, κ	Biolegend
CD80	16-10A1	PerCP/Cy5.5	Armenian Hamster IgG	Biolegend
CD86	GL1	APC-Cy7	Rat IgG2a, κ	Biolegend
CD90.1 (Thy 1.1)	HIS51	APC-eF780	Mouse IgG2a, κ	eBioscience
α 4 β 7 (LPAM-1)	APC	DATK32	Rat IgG2a, κ	Biolegend
α 4 β 7 (LPAM-1)	PE	DATK32	Rat IgG2a, κ	Biolegend
F4/80	BM8	AF488	Rat IgG2a, κ	Biolegend
FoxP3	FJK-16s	AF488	Mouse IgG2a, κ	eBioscience
I-Ab (MHCII)	M5/114.15.2	PE	Mouse (BALB/c) IgG2a, κ	Biolegend
IFN- γ	XMG1.2	AF488	Rat IgG1, κ	eBioscience
Ki67	16A8	AF647	Rat IgG2a, κ	Biolegend
Podoplanin (gp38)	8.1.1	APC	Syrian Hamster IgG	Biolegend
Ter-119	Ter-119	APC-Cy7	Rat IgG2b, κ	Biolegend
TNF α	MP6-XT22	PE	Rat IgG1, κ	Biolegend
CD127 (IL-7R α)	A7R34	PE-Cy7	Rat IgG2a, κ	Biolegend
CD223 (Lag3)	C9B7W	PE	Rat IgG1, κ	Biolegend
Streptavidin	-	Alexa 750	-	Invitrogen
CXCR3	CXCR-173	APC	Armenian Hamster IgG	Biolegend
CXCR3	CXCR-173	PerCP/Cy5.5	Armenian Hamster IgG	Biolegend
H2-Kd	SF1-1.1.1	APC-eFluor 780	Mouse IgG2a, κ	Invitrogen
H2-Kd	SF1-1.1.1	PE	Mouse IgG2a, κ	Biolegend

3.1.4 Commercially available kits

- CFSE cell proliferation kit Invitrogen (Darmstadt, Germany)
- DQ™ Ovalbumin kit Invitrogen (Darmstadt, Germany)
- Avidin-Biotin blocking kit Vector laboratories (Burlingame, CA, USA)
- Vectorshield mounting media Vector laboratories (Burlingame, CA, USA)
- Dynabeads Magnetic beads Invitrogen (Darmstadt, Germany)
- Cytometry Bead Array Biolegend (Koblenz, Germany)

3.1.5 Consumables

6 well flat bottom plates	Greiner Bio-One (Frickenhausen, Germany) or Sarstedt (Newton, USA)
96 well flat bottom culture plates	Sarstedt (Newton, USA)
96 well U bottom culture plates	Sarstedt (Newton, USA)
96 well V bottom culture plates	Sarstedt (Newton, USA)
5,12- and 25-ml single use pipettes	Greiner Bio-One (Frickenhausen, Germany)
10 µl tips	Sarstedt (Newton, USA)
200 µl tips	Sarstedt (Newton, USA)
1000 µl tips	Sarstedt (Newton, USA)
15 ml and 50 ml centrifuge tubes	Greiner Bio-One (Frickenhausen, Germany)
Cell strainer 70 µM	Greiner Bio-One (Frickenhausen, Germany)
Cell strainer 100 µM	Miltenyl Biotech (Gladbach, Germany)
Cryomolds	Sakura (Staufen, Germany)
Superfrost microscope slides	R. Langenbrinck (Emmendingen, Germany)
U-100 Insulin syringes	BD Bioscience (Heidelberg, Germany)
5,12- and 25-ml syringes	BD Bioscience (Heidelberg, Germany)

3.1.6 Mice

C57BL/6 (B6), BALB/c and FVB/N mice between the age of 8 and 12 weeks were purchased from Charles River laboratories (Sulzfeld, Germany) or Janvier Laboratories (Le Genest-Saint-Isle, France). Following, transgenic mice used in the study were bred in our own mouse colony at the Centre for Experimental Molecular Medicine (ZEMM) Würzburg or purchased from Jackson Laboratories (Bar Harbor, ME, United States).

Table 3.2 Mice

Scientific name	Transgene and phenotype	Short name
FVB/N-L2G85	Ubiquitous luciferase expression (β -Actin promoter)	FVB.L2G85
B6.Tg(Itgax-DTR/OVA/EGFP)1Garbi	DTR-OVA-GFP on CD11c cells	B6a.CD11c.DOG
B6.129S2-H2 ^{dAb1-Ea} /J	<i>H2-Ab1</i> ^{-/-} (ubiquitous knock out)	B6.MHCII ^A
B6.129X1-H2-Ab1 ^{tm1Koni} /J.Tg(Itgax-cre)1-1Reiz/J	Cre specific <i>H2-Ab1</i> ^{-/-} (CD11c)	B6.MHCII ^A CD11c
B6.129X1-H2-Ab1 ^{tm1Koni} /J.Tg(Cdh5-cre)7Mlia/J	Cre specific <i>H2-Ab1</i> ^{-/-} (VE Cad)	B6.MHCII ^A VE-Cadherin
B6.129X1-H2-Ab1 ^{tm1Koni} /J.Commd10 ^{Tg(Vav1-icre)A2Kio} /J	Cre specific <i>H2-Ab1</i> ^{-/-} (Vav1)	B6.MHCII ^A Vav1
B6.129X1-H2-Ab1 ^{tm1Koni} /J.Tg(Ccl19-cre)489Biat	Cre specific <i>H2-Ab1</i> ^{-/-} (Ccl19)	B6.MHCII ^A Ccl19
B6-Gt(ROSA)26Sor ^{tm1(HBEGF)Awai} /J.Tg(Ccl19-cre)489Biat	DTR expression on Ccl19 cells	B6.Ccl19.iDTR
B6.Cg- B6.Cg-Tg(TcraTcrb)425Cbn	<i>Rag1</i> ^{-/-} , OVA specific	B6a.Rag ^A .OTII.L2G85.CD45.1
Rag1tm1Mom Tg(CAG-luc,-GFP)L2G85Chco Ptrca ^{Zemm}	TCR on CD4 ⁺ T cells	
STOCK Tg(IFABP-GH)15Bir/J	OVA expression on enteric cells and on FRCs	B6a.iFABP-tOVA
B6.Cg-Tg(CAG-DsRed*MST)1Nagy/J	Widespread DsRed expression	B6.DsRed
B6.SJL-Ptrca Pepcb/BoyJ	CD45.1 congenic	B6.CD45.1
B6.129X1-H2-Ab1 ^{tm1Koni} /J.Tg(Cdh5-cre)7Mlia/J. Commd10 ^{Tg(Vav1-icre)A2Kio} /J	Cre specific <i>H2-Ab1</i> ^{-/-} (Vav1 and VE Cad)	B6.MHCII ^A VE-Cadherin Δ Vav1

FVB/L2G85 (H-2^a, CD90.1, CD45.1) expressing firefly luciferase (luciferase⁺) were generated previously [109, 129]. B6.CD11c.DOG (H-2^b, CD90.2, CD45.2) transgenic mice, were kindly provided by Günter J. Hämmerling (German Cancer Research Center, Heidelberg, Germany). B6.Ccl19-Cre (H-2^b, CD90.2, CD45.2) mice were kindly provided by Burkhard Ludewig (Konstanzspital St. Gallen, Switzerland). B6.MHCII^A, B6.*H2-Ab1*^{fl}, B6.CD11c-Cre, B6.VE-Cadherin-Cre, B6.Vav1-iCre and B6.R26-stop-iDTR (H-2^b, CD90.2, CD45.2) were purchased from The Jackson Laboratories (St. Bar Harbor, ME, USA).

Before each experiment, all transgenic mice were genotyped with PCR using KAPA HotStart Mouse Genotyping Kit (Sigma-Aldrich, Hamburg, Germany) or phenotyped by flow cytometry. When using transgenic animals Cre negative littermates from the same litter were used as control and are designated as *H2-Ab1*^{fl}. Mice were maintained in pathogen-free conditions in individually ventilated cages (IVCs) at the Centre for Experimental Molecular Medicine (ZEMM), Würzburg. All animal experiments were approved by local authorities (Regierung von Unterfranken) and complied with German animal protection laws under TVA RUF 55.2-2532-2-692-17 and RUF 55.2.2-2532-2-1038-9.

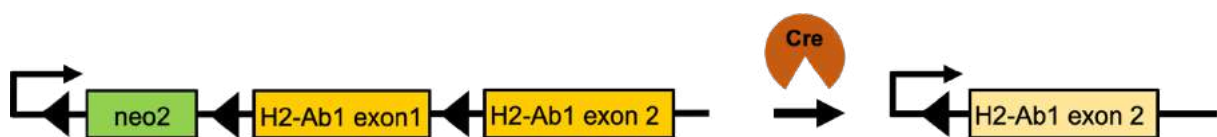


Figure 3.1 Principle of Cre-LoxP mouse.

Cre recombinase recognizes the *loxP* sites of specific 34 bp DNA sequences. Generally, one mouse must have a tissue-specific driven cre gene and another mouse have *loxP* flanked (floxed) alleles of interest gene (here *H2-Ab1*). Expression of Cre recombinase excises floxed loci and inactivates the gene *H2-Ab1* on Cre specific cells.

3.2 Methods

3.2.1 Cell culture

All the cell used in the study were incubated in humidified cell culture incubator supplied with 5% CO₂ at 37°C. Following cell culture medium composition was used for culturing:

Table 3.3 Cell culture medium

Cell type	Medium	Supplements
Enriched T cells	RPMI 1640	1% Pen/Strep, 1% L-Glutamine, 10% FCS
iFRCs	DMEM	1% Pen/Strep, 1% ITS, 10% FCS
LNSCs	αMEM	1% Pen/Strep, 10% FCS

3.2.2 Hematopoietic cell transplantation

Sex matched 8 to 12 weeks old recipient mice received myeloablative total body irradiation (TBI) of 9Gy using a Faxitron CP-160 X-ray irradiation system (Faxitron X-Ray, Lincolnshire, IL, USA). Within 4 h after TBI, mice were i.v. injected (retro-orbitally) with 5x10⁶ FVB/N TCD BM cells for hematopoietic reconstitution. T cells from the BM were depleted (TCD BM) using CD90.1 MicroBeads (Miltenyl Biotech, Gladbach, Germany) following manufacturer's instructions. In order to induce acute GvHD, allogeneic enriched T cells were co-injected intravenously. The specific numbers of transferred T cells are stated for each experiment in the figure legends. T cells were purified from the spleen using Dynabeads™ Untouched™ Mouse T Cells Kit or Dynabeads™ Untouched™ Mouse CD4⁺ Cells Kit (Invitrogen, Darmstadt, Germany) according to manufacturer's instructions. Cell purify was accessed by flow cytometry (>95%).

Table 3.4 Clinical score to assess GvHD severity

	Score 0	Score 1	Score 2
Weight loss	<10%	>10% <20%	Score 2+: >20% longer than 2 days
Posture	normal	Hunchback at rest	Hunchback limits mobility
Behaviour	normal	Reduced slight to moderately	Absent, only after provocation
Ruffled fur	normal	Slightly to moderately	Strong, no grooming
Skin	normal	Dandruff on paws and tail	Strong fur defects
Eyes	normal	Conjunctivitis of one eye or slightly of both eyes	Strong conjunctivitis of both eyes
Licking and scratching of inflamed skin	normal	<1x/min	>1x/min
Stool	normal	Slightly diarrhea, anus swollen	Strong diarrhea, melena
Anemia	normal	Paleness visible on skin without fur	Paleness visible on whole body

Table 3.5 Criteria to define the humane endpoint

	Intestinal aGvHD	Skin aGvHD	Anemia
Weight loss	1-2+	0-1	1-2+
Posture	2	0-1	2
Behaviour	1-2	0	1-2
Ruffled fur	1-2	2	0-1
Skin	0	2	0
Eyes	0-1	1-2	0-1
Licking and scratching of inflamed skin	0	2	0
Stool	1-2	0	0
Anemia	0	0	1-2
Score sum	6-11	7-10	5-10
Humane endpoint		≥8	

3.2.3 Diphtheria toxin mediated cell depletion

For DCs depletion in B6a.CD11c.DOG recipient mice were injected intraperitoneally (i.p.) with diphtheria toxin (Sigma-Aldrich, Hamburg, Germany) at doses of 20 ng/g body weight on day -2, -1, +1 and +2 of allo-HCT. For depletion of FRCs in B6.Ccl19-Cre.iDTR mice received diphtheria toxin (Sigma-Aldrich, Hamburg, Germany) i.p. at dose of 8 ng/g body weight on day -5 and -3 of allo-HCT.

3.2.4 Polymerase chain reaction

Semi-quantitative reverse transcription polymerase chain reaction (RT-PCR) was performed as below. Isolated RNA was reverse transcribed using RevertAid first strand cDNA synthesis kit (Thermo Fischer, Darmstadt, Germany) and PCR was performed using KAPA HotStart Mouse Genotyping Kit (Sigma-Aldrich, Hamburg, Germany) with the primers as listed in (Table 3.6).

Table 3.6 PCR primers

Primer	Sequence (5' to 3')
GAPDH forward	AGTATGACTCCACTCACGGC
GAPDH reverse	ATGTTAGTGGGGTCTCGCTC
OVA forward	GCTGCAGATCAAGCCAGAGAGC
OVA reverse	ATTGATTTCTGCATGTGCTGC

3.2.5 Generation of bone marrow chimeras

B6 and B6.MHCII^A recipient mice were pre-treated with acid water (pH 2-3) containing 1 mg/ml gentamycin sulphate solution (Carl Roth, Karlsruhe, Germany) 1 week prior to irradiation (9 Gy), followed by retro-orbital injection of 1×10^7 TCD BM in 200 μ l PBS from either B6 (B6→B6)

or MHCII^A (B6.MHCII^A →B6) for hematopoietic reconstitution. The T cells from the BM were depleted using DynabeadTM Mouse Pan T (Thy1.2) kit (Invitrogen, Darmstadt, Germany). Eight to ten weeks after bone marrow reconstitution, mice were accessed for successful chimerism via flow cytometry and used for further experiments.

3.2.6 Single cell suspension from spleen and lymph nodes

Mice were euthanized, and organs were isolated from the mice, cut into pieces and homogenized by gently smashing through with a 5 ml syringe plunger on a 70 µm cell strainer. The cell strainer was rinsed with 8 ml of RBC lysis buffer into a 50 ml centrifuge tube. RBCs were lysed by incubating the cell suspension in RBC lysis buffer for 2 minutes (min) at room temperature and reaction was stopped by adding of 10 ml PBS. The cells were centrifuged at 400 g for 5 min at 4°C, resuspended in appropriate volume and counted.

3.2.7 Single cell suspension of LNSCs from the lymph nodes

Axillary, brachial, cervical, inguinal LNs (pLNs) and mesenteric LNs (mLNs) were dissected. While the peripheral LNs were pooled, mesenteric LNs were processed separately. All lymph nodes were pierced with a syringe needle 2-3 time and directly transferred into a centrifuge tube containing 2 ml RPMI-1640 medium on ice for further processing.

The RPMI medium was replaced with 2 ml freshly prepared enzyme mix 0.8 mg/ml Dispase II (Roche, Mannheim, Germany), 0.3 mg/ml Collagenase P (Roche, Mannheim, Germany) and DNase I (Sigma, Hamburg, Germany).

Tubes were incubated at 37°C in a water bath for 20 min and gently inverted several times at 5 min intervals. To carefully disrupt the capsule after the first incubation step, the cell suspension was gently resuspended with a 1 ml pipette. LNs pieces were allowed to settle down for 1 min and subsequently, release leukocytes in the cell suspension were transferred into a new tube containing 20 ml FACS-buffer (2 mM EDTA, 2% FCS in PBS) stored on ice. 2 ml of fresh enzyme-mix was added to the remaining LNs pieces and mixed with a 1 ml pipette and again incubated for 10 min in a water bath at 37°C. After incubation, the cell suspension was again gently resuspended and released cells were transferred to previous supernatant into ice-cold FACS-buffer. For a last time, 2 ml of digestion-solution was added to the residual LNs fragments and this time vigorously mixed every 5 min using a 1 ml pipette until all fragments were digested. Collected supernatants, that have been stored on ice were pooled and centrifuged at 400 g, 4°C for 5 min and counted.

3.2.8 Isolation of T cells from the GIT

Mice were anesthetized and euthanized, small intestine from the stomach to caecum were excised out. Fat and mesenteric tissue was cleared from the intestine and the intestine was washed with PBS. After removal of all fecal material, intestine pieces were transferred to a 50 ml centrifuge tube containing 20 ml medium 2 - HBSS medium (Ca-/Mg-, 2 mM EDTA, 5% FCS) and incubated for 20 min at 37°C with gentle rotation (100 RPM).

After incubation, gut pieces were passed through a 70 µm cell strainer over a new 50 ml centrifuge tube. The flow-through, containing the intraepithelial cells were stored on ice. Remaining gut pieces were transferred back into the tube containing medium 2 and again incubated for 20 min in a thermal incubator at 37°C with gentle rotation (100 RPM). This step disrupted the remaining intraepithelial fraction from the underlying mucosa. After incubation, gut pieces were again passed through a 70 µm cell strainer and pooled with the first fraction. This cell fraction contained the gut intraepithelial lymphocytes (IELs). IELs fraction was centrifuged at 400 g for 5 min at 4°C, resuspended in appropriated volume and counted.

To further process *lamina propria*, the remaining intestine pieces on the cell strainer were transferred on to a plastic trough and reduced to pulp using fine dissection scissors. The gut-pulp was transferred to a new 50 ml centrifuge tube containing 10 ml of digestion solution (Pre-warmed HBSS Ca+/Mg+, 2%FCS, 5 mg/ml DNase I (Sigma, Hamburg, Germany), 10 mg/ml Collagenase P (Sigma, Hamburg, Germany) and incubated at 37°C for 20 min under vigorous rotation (200 RPM). Followed incubate, cell suspension was vortexed for 30 secs and passed through a 100 µm cell strainer (Miltenyl Biotech, Gladbach, Germany). The cell strainer was rinsed with 30 ml of ice-cold Ca+/Mg+ HBSS containing 10% FCS as washing-buffer and centrifuged at 500g for 10 min at 20°C. Cell pellet was resuspended in 10 ml PBS for counting.

3.2.9 Mixed lymphocyte reaction (MLR)

MLRs were performed with responder enriched splenic CD4⁺ T cells isolated from BALB/c mouse with CD45 cells magnetically depleted (Biolegend, Koblenz, Germany), enzymatically digested pooled LNs, from the allogeneic stimulators: C57BL/6 or syngeneic stimulators: BALB/c at ratio of 1:3.

Furthermore, to assess CD4⁺ T cell activation and proliferation MLRs were also performed with FACS sorted different subsets of LNSCs (stimulators) with enriched splenic CD4⁺ T cells isolated from BALB/c mouse (responders) at ratio of 1:1.

3.2.10 Cytokine bead array (CBA)

Serum and tissues were collected for cytokine analysis. Serum was obtained by centrifugation of 200 μ l of blood during centrifugation at 4°C. Spleen, LNs, liver, lung and small intestine (2 cm) were homogenized (2x 30 sec each) at 65000 RPM (Percellys, Peqlab, Erlangen, Germany) and supernatant was stored at -80°C for cytokine analysis. Cytokine concentrations were determined using LEGENDplex™ Multi-Analyte Flow Assay Kit, according to manufacturer's protocol. Data was analyzed with LEGENDplex™ data analysis software.

3.2.11 Multicolour flow cytometry

Flow cytometry was performed on single-cell suspension using a BD FACS Canto II flow cytometer (Becton Dickinson, BD, Heidelberg, Germany) or Attune NXT flow cytometer (Thermo Fischer Scientific, Darmstadt, Germany).

For analysis of *in vitro* cultured and primary mouse cells the single cell suspension was transferred to a 96-well plate or FACS tubes. To block the unspecific binding to Fc receptors, cells were incubated with NRS (1:20) for 5 min at 4°C. The cells were stained with fluorochrome labelled antibodies for 30 min at 4°C. To exclude dead cells from the analysis, cells were co-stained with LIVE/DEAD™ Fixable Violet Dead Cell Stain Kit (Invitrogen, Darmstadt, Germany) or Zombie Aqua Fixable Viability kit (Biolegend, Koblenz, Germany). For staining of intracellular antigens, the cells were fixed for 30 min at 4°C with mouse regulatory T cell staining kit (eBioscience/ Thermo Fischer, Darmstadt, Germany) and stained intracellularly for 30 min to overnight at 4°C in permeabilizing buffer. To compensate for the spillover in the emission spectrums for each fluorochrome, UltraComp eBeads™ Compensation Beads (Invitrogen, Darmstadt, Germany) were individually stained with single fluorochrome labelled antibody also used in the multiple staining. This compensation procedure [130] allowed calculating and subtracting the appropriate overlap to yield the specific signal intensity for each fluorochrome. To set the gates in multicolour stained samples the fluorescence minus one (FMO) method [131] was performed. In this gating control strategy, the samples were stained with all fluorochrome, but one fluorochrome at a time. All antibodies were titrated for optimal performance before their application. Used antibodies are listed (Table 3.1). Acquired cytometry data was analyzed on FlowJo version 10 software (Tree Star, Ashland, OR, USA).

3.2.12 Bioluminescence imaging (BLI)

In vivo bioluminescence imaging was performed using IVIS Spectrum CCD-imaging system (PerkinElmer, Waltham, MA, USA). Mice were anesthetized with an i.p. injected mixture of Ketamine (50 μ g/g body weight) and Xylazine (5 μ g/g body weight) in PBS in a total volume of

10 µl/g body weight. D-Luciferin was injected in a concentration of 300 mg/kg of body weight and images were taken 10 min after the injection and allowed the identification of T cell proliferation and migration. Alternatively, mice were i.p. injected with 300 mg/kg of D-Luciferin and anesthetized with 2% isoflurane in O₂. After 10 min the bioluminescence signal was acquired with an IVIS Spectrum (PerkinElmer, Waltham, MA, USA).

To perform *ex vivo* imaging mice were injected with the same mixture of anesthetic and Luciferin, 10 min after injection, mice were euthanized, and organs were removed within 4 min. *ex vivo* images provided higher resolution of selective organ signal distribution. Samples were processed for flow cytometric analyses or stored in PFA or TissueTec (O.C.T) for further analysis. Imaging data was analyzed on Living image ® 4.5.5 (PerkinElmer, Waltham, MA, USA) software.

3.2.13 Fluorescence activated cell sorting (FACS)

Cells isolated from mouse tissue were antibody stained and sorted on FACS Aria™ III (Becton Dickinson, BD, Heidelberg, Germany). T cells, DCs and LN_{SC}s subsets were all sorted with 100 µm nozzle into ice-cold cell culture medium or lysis buffer depending on downstream application.

3.2.14 Antigen processing assay

FACS sorted cells were incubated with 10 µg/ml DQ-OVA (Invitrogen, Darmstadt, Germany) in cell culture medium at 4°C and 37°C for 3 h followed by processed DQ-OVA analysis on Attune NxT flow cytometer (Thermo Fischer Scientific, Darmstadt, Germany) under the blue laser (488 nm), BL-1.

3.2.15 Bulk RNA sequencing

H2-Ab1^{fl} and MHCII^{ΔCcl19} mice were transplanted with 5x10⁶ TCD BM and 6x10⁵ CD4⁺ T cells from FVB/N. On day +30, spleens were processed and magnetically enriched for CD4⁺ T cells using Dynabeads™ Untouched™ Mouse CD4⁺ Cells Kit (Invitrogen, Darmstadt, Germany) according to manufacturer's instructions. Enriched cells were stained with LIVE/DEAD™ Fixable Violet Dead Cell Stain Kit (Invitrogen, Darmstadt, Germany) for dead cells and CD90.1⁺CD4⁺ staining of donor alloreactive CD4⁺ T cells. Total viable, CD90.1⁺CD4⁺ cells were sorted using a 100 µm nozzle in 150 µl of lysis buffer and stored on dry ice for further processing.

FRCs were isolated from pooled lymph nodes on day +30 of allo-HCT, dissociated and stained with LIVE/DEAD™ Fixable Violet Dead Cell Stain Kit (Invitrogen, Darmstadt, Germany) for

dead cells and CD45⁺CD24⁺ staining of hematopoietic cells was used as a dump channel. Total viable, non-hematopoietic cells expressing gp38⁺CD31⁻ cells were sorted using a 100 µm nozzle in 150 µl of lysis buffer and stored on dry ice for further processing.

RNA was isolated PicoPure™ RNA isolation kit (Thermo Fischer, Darmstadt, Germany) following manufacturer protocol. Isolated RNA was quantified on 2100 Bioanalyzer instrument (Aligent, CA, United States). cDNA synthesis and subsequent library preparation was performed by 1 ng of RNA using a NEBNext® Single Cell/ Low Input RNA Library Prep kit for Illumina® following manufacturer protocol. Libraries were sequenced on Illumina NextSeq500 system (Illumina, CA, United States) as single end sequencing and 75 bp read length.

3.2.16 Single cell RNA sequencing

In order to analyze LNSCs mesenteric lymph nodes were dissociated and stained with LIVE/DEAD™ Fixable Violet Dead Cell Stain Kit (Invitrogen, Darmstadt, Germany) for dead cells and CD45⁺CD24⁺ staining of hematopoietic cells was used as a dump channel. Total viable, non-hematopoietic cells expressing gp38⁺CD31⁺ were sorted using a 100µm nozzle in PBS-0.4% BSA using a FACS Aria III (BD Biosciences) and immediately processed for Single-cell RNA-seq.

Single cells were encapsulated in droplets using 10X Genomics GemCode Technology (10x Genomics, CA, USA) and processed following manufacturer's specifications. Briefly, every cell and every transcript were uniquely barcoded using a unique molecular identifier (UMI) and cDNA ready for sequencing on Illumina platforms was generated using the Single Cell 3' Reagent Kits v2 (10X Genomics). Libraries were sequenced on a HiSeq 2500 System (Illumina, CA, United States).

Single cell RNA-Seq reads from the library was counted using Cell Ranger, the result was processed and analyzed with Loupe browser (10x Genomics, CA, USA).

3.2.17 Light-sheet fluorescence microscopy

Mice were intracardially perfused with 40 ml of ice-cold PBS to remove all the red blood cells and subsequently with 40 ml of ice-cold 4% paraformaldehyde in PBS to fix the tissues. The tissues were excised and fixed for 2 h at 4°C in 4% paraformaldehyde. After three washing steps in PBS at 4°C the tissues were blocked and permeabilized in 2% FCS and 0.01% Triton X-100 in PBS at 4°C overnight. All following incubations were carried out at 4°C. The primary antibodies were added in 800 µl of PBS at a dilution of 1:100. The samples were incubated in flat-bottom glass containers on an orbital shaker for 24 h and after three 30 min washing steps in PBS, secondary antibody incubation was performed for another 24 h on a shaker. After three more washing steps in PBS, the samples were dehydrated in ascending concentrations of

ethanol in water (30%, 50%, 70%, 80%, 90%) for 1.5 h at room temperature and incubated in 100% ethanol overnight at 4°C. Final dehydration with n-hexane was performed for 2 h at room temperature, which was afterwards gradually replaced with the clearing solution BABB (2 parts benzyl alcohol: 1-part benzyl benzoate). This solution has a refractive index of 1.56, which matches that of soft tissues. Because this abolishes light scattering at water/ tissue interfaces with different refractive indices inside the tissue, it makes them transparent. Clearing solution was added three times for 30 min and air contact of the samples was strictly avoided to prevent a tissue-darkening reaction. The images were acquired in a home-build light sheet microscope equipped with a 5x and 20x objective [132]. The whole-mount sample is optically sectioned, and slices are afterwards reconstructed to a three-dimensional image.

3.2.18 Immunostaining for confocal microscopy

Organs were isolated and embedded in O.C.T (Cat. # 4583, Sakura, Zoeterwoude, Netherlands) in cryomolds (Cat. # 4728, Sakura, Zoeterwoude, Netherlands) within 10 minutes and directly frozen on dry ice. Tissue samples were stored at -20°C for cryopreservation. Frozen sections were cut in 7 µm thickness using Leica CM1950 Cryostat (Leica, Wetzlar, Germany) at -22°C and mounted onto SuperFrost® Plus Microscope Slides (Cat. # 03-0060, R. Langenbrinck, Emmendingen, Germany).

Before staining, slides were thawed for 5 minutes at RT and subsequently fixed with acetone or 100 % Ethanol at -20°C. Sections were then clipped into coverslips, instantly rehydrated with (1 x) PBS and washed twice, before blocking for 15 minutes without light exposure followed. Depending on antibodies, that were used, blocking reagents contained goat or donkey serum (5% in PBS with 2% FCS), PBS with 2% FCS, PBS (2% FCS) with Avidin/Biotin Blocking Kit (Cat. # ZD0913D, Vector, Linaris GmbH) 4 drops/ml or combinations.

Blocked sections were washed three times with (1x) PBS, then incubated with primary antibodies for 1 hour in the dark at RT. Again, three washing steps followed, before secondary antibodies were added onto samples in coverslips. Secondary antibodies incubated for 30 minutes at RT, without light exposure. All primary and secondary antibodies are listed (Table 3.1).

Sections were washed 3 times with (1 x) PBS and once with deionized distilled water.

To stain cell nuclei, slides were then incubated with 100 µl DAPI (1:3000) and incubated for 15 minutes at RT in the dark.

5 more washing steps with (1 x) PBS followed, then slides were carefully removed from coverslips and tissue samples were mounted with Fluoroshield (Cat. # F6182-20ML, Sigma, Deisenhofen, Germany) and covered with microscope cover glasses to prevent photo bleaching.

Fluorescence microscope images were obtained with a Zeiss Imager Z1m fluorescent microscope (Carl Zeiss, Jena, Germany) equipped with a AxioCam MRm camera or ZEISS LSM 780 (Carl Zeiss, Jena, Germany) and processed and analyzed using Axio Vision 4.8 (Zeiss, Jena, Germany) or Image J software (US National Institutes of Health, Maryland, USA). Standard magnification was 200 x using 20 x Plan-Apochromat with a 0.8 numerical aperture [NA].

3.2.19 Mesenteric lymph node transplantation surgery

Mice were anesthetized with an i.p. injected mixture of Ketamine (80 mg/kg body weight) and Xylazine (16 mg/kg body weight) and Acepromazine (2 mg/kg) [133] dissolved in PBS (200 – 250 μ l) and placed on a sterile, heated OP towel for preparation. The animals were given subcutaneous (s.c) injection of the perioperative analgesic Carprofen (5 mg/kg) to relieve pain 30 min before opening the abdominal cavity and every 12 h up to third day after the surgery. Eyes were protected from dehydration by applying eye ointment - Bepanthen® - Augen- und Nasensalbe (Bayer Vital GmbH, Leverkusen, Deutschland). The ventral fur was wetted with 70% ethanol using a dissection swab and shaved; the skin was disinfected with Braunol® (B. Braun, Melsungen, Germany) in an outward circling motion.

After 10 min, anesthetic depth was ensured to be stadium III.2 (surgical tolerance) by pinching the hind paw (planter reflex). The dosage of the anesthetic used is usually very well tolerated and leads to a reliable depth of anesthesia up to stage III.2 (stage of surgical tolerance).

If in exceptional cases by checking the planter reflex, anesthesia depth up to stage of III.2 is not achieved, an intraperitoneal (i.p.) additional dose of the anesthetic is provided (20% of the original dose). The volumes can easily be applied accurately using an Insulin syringe. For a more precise dosage of the amount of anesthesia, the anesthetic was additionally diluted 1:1 in PBS so that the injection volumes double.

The prepared animal was transferred onto a fresh sterile and heated OP towel and the prepared OP-cover was applied. A 1-1.5 cm midline incision was made in the skin and in the peritoneum on the linea alba, no bleeding should be visible. The wound was covered with the prepared gauze swab, the slit overlaid on the incision. The swab was soaked with PBS to prevent drying of externalized intestinal tissue. Next, two cotton swabs were soaked with PBS and used to handle the intestinal contents. The swabs were inserted into the peritoneum to localize and gently exteriorize the caecum, which is located left cranio-lateral to the incision. The intestinal tissue was handled with great care to prevent postoperative ileus. First, the caecum was placed on the gauze swab left lateral to the incision, and the intestinal tissue was kept moist at all times by dripping PBS on it using a Pasteur pipette. The large intestine was then gently pulled out, starting from the caecum, until the mesenteric lymph node appeared

attached to mesenteric tissue. The part of small intestine adjacent to the caecum was also gently pulled out to have visible access to all the lobes of mesenteric lymph nodes.

With the help of fine surgical scissors, the mesenteric lymph nodes of the recipient mice were excised out with minimal fat tissue. Extra care was taken to avoid injuring the superior mesenteric artery lying behind the mesenteric lymph nodes. Minor bleeding was stopped by holding the Setpack dissecting swabs (Megro, Wesel, Germany) to the bleeder. The donor lymph node was joined to the mesenteric tissue using fibrin glue: TISSEEL (Baxter, Höchststadt, Germany). 20 μ l of fibronectin (component to fibrin glue) was pipetted to the area from where the recipient mesenteric lymph node was excised out. The donor mesenteric lymph nodes (isolated with the same procedure as recipient mice) were dipped in Thrombin solution (component to fibrin glue) and placed on the wound in the same orientation as removed recipient lymph node: from distal (from the caecum) to the proximal region (towards the ileum). The glue was allowed to adhere for 3-5 min and the small, large intestine along with the caecum were carefully placed back into the peritoneum. Correct organization of intestinal loops was important to prevent a postoperative ileus. The peritoneum was closed with three non-consecutive stiches with coated VICRYL® (polyglactin 910) suture (Ethicon, Dülmen, Germany). Subsequently, the skin was closed with four stiches. Bepanthen® Wund- und Heilsalbe (Bayer Vital GmbH, 51368 Leverkusen, Deutschland) was applied on the closed surgical wound. The overall operation procedure took 15-25 min per animal. The mice were placed into a clean cage and held warm with and infrared lamp until recovered from anesthesia. The local temperature around the animal was monitored not to rise above 30°C to avoid overheating. When conscious, the animals were transferred back into their group cages. The mice were rested for 5-10 weeks to allow the angiogenesis of blood vessels and connection of lymphatics to the donor mesenteric lymph node.

3.2.20 Statistical analysis

Data is shown as mean \pm standard deviation (SD). Different groups were compared by two-tailed unpaired student's t-tests or unpaired non-parametric Mann-Whitney test using GraphPad Prism 8 software (La Jolla, CA, USA). Level of significance was set at $P < 0.05$. Survival experiments/ Kaplan-Meier curves were analysed by Log-Rank test (Mantel-Cox test).

4 Results

4.1 LNSCs possess necessary APCs characteristics

4.1.1 LNSCs up-regulate co-stimulatory receptors after irradiation

The aim of this thesis was to investigate whether LNSCs acquire phenotype of APCs under inflammatory milieu caused by the conditioning regimen (irradiation and/or chemotherapy) prior to allo-HCT. Professional hematopoietic APCs tend to up-regulate MHC class II and co-stimulatory receptors (CD40, CD80 and CD86) under inflammatory conditions triggered by infection, injury or stress. Henceforth in our experiments we analyzed whether LNSCs upregulate MHC class II and co-stimulatory molecules after lethal total body irradiation (TBI).

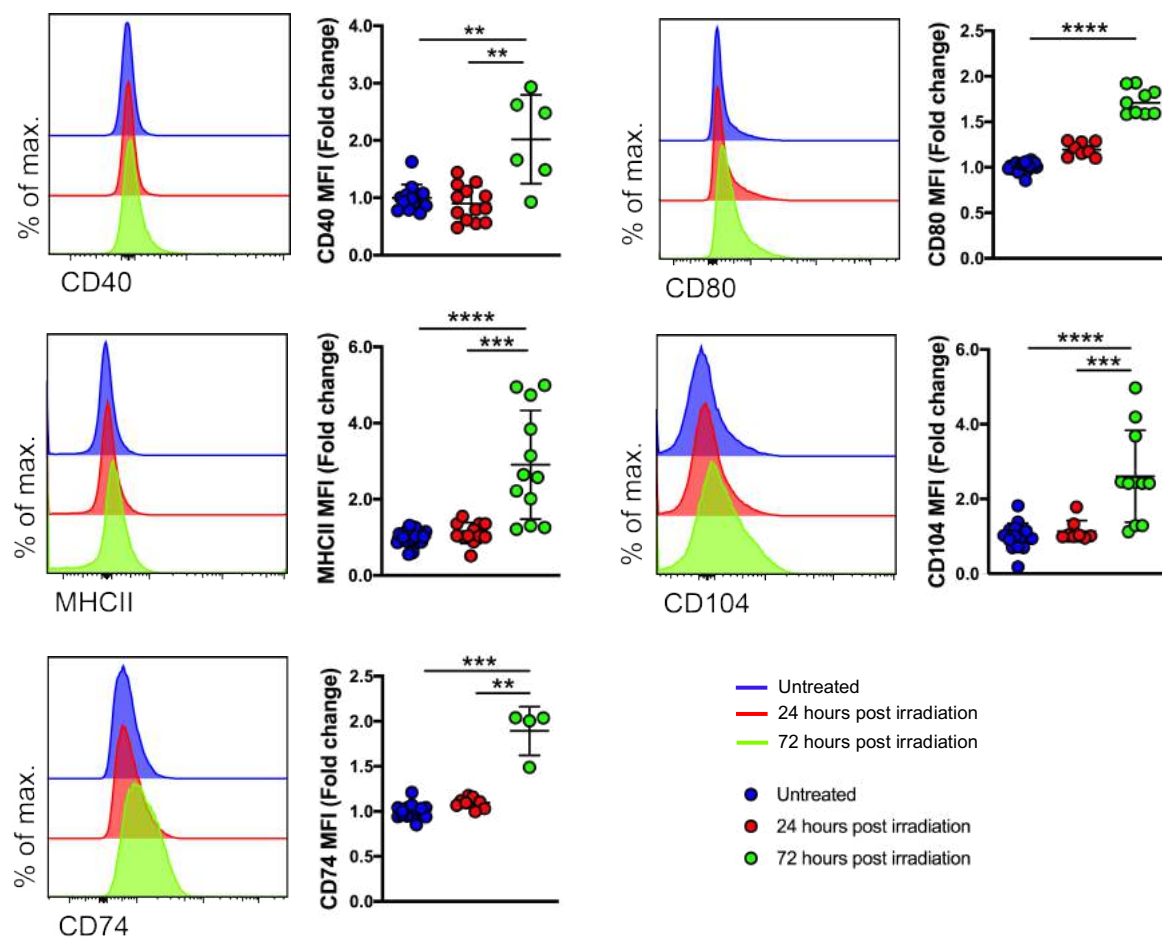


Figure 4.1 Immortalized fibroblastic reticular cells (iFRCs) up-regulate co-stimulatory molecules after irradiation.

Cultured iFRCs were irradiated and after 24- and 72-hours incubation, cells were analyzed for antigen presentation and co-stimulatory molecules expression with flow cytometry. One data point represents one technical replicate analyzed in three experiments. Statistics are according to unpaired non-parametric Mann-Whitney test, (Mean± SD); *p < 0.05, **p < 0.01, ***p < 0.001, and ****p < 0.001.

First, to dissect the co-stimulatory molecule expression patterns on FRCs, we irradiated the immortalized fibroblastic reticular cells (iFRCs) and examined the expression of CD104 (integrin β 4), CD40 (TNFRSF5), CD80 (B7-1), CD74 (HLA-DR), MHC class II (I-Ab), 24 h and 72 h post-irradiation versus the steady state. iFRCs upregulated CD40 and CD80 co-stimulatory receptors within 24 h of irradiation and displayed an even more pronounced CD40 and CD80 expression post 72 h. Likewise iFRCs upregulated crucial antigen presentation receptors molecules: MHC class II and its invariant chain CD74 24- and 72-h post conditioning (**Figure 4.1**). To recapitulate these findings *in vivo*, we myeloablatively irradiated B6 mice. Flow cytometry analysis revealed that all subsets of LNSCs (FRCs, LECs, BECs, integrin α 7+ pericytes - DNCs) upregulated co-stimulatory molecules (CD80 and CD86) within 24 h post-conditioning. However, MHC class II was noticeably downregulated on all LNSC subsets (**Figure 4.2a, b**). Others have shown that LNSCs acquire MHC class II from DCs via endocytosis [22]. To elucidate the loss of MHCII expression on LNSCs and its correlation with DCs in the SLOs (**Figure 4.2c**), we irradiated B6 mice and detected that absolute numbers of DCs dramatically decreased in spleen and the mLNs (**Figure 4.2d**). This indicates that the loss of MHCII on LNSCs post-conditioning occurs due to rapid depletion of DCs in SLOs. Taken together, these results suggest that LNSCs and particularly FRCs have the potential to serve as non-hematopoietic APCs in the aGvHD inflammatory milieu.

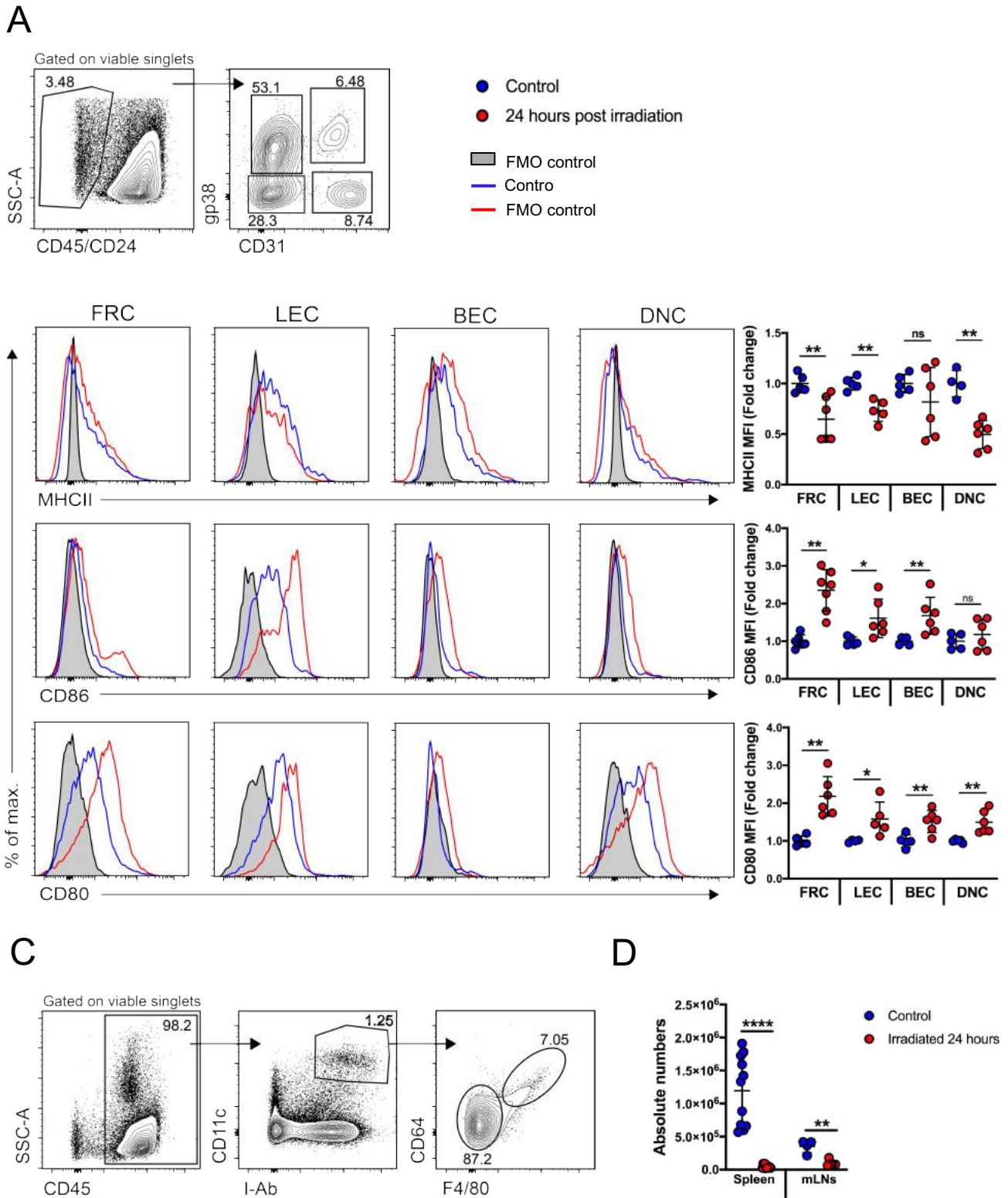


Figure 4.2 LNSCs upregulate CD80 and CD86 co-stimulatory receptors while down-regulating MHC class II after irradiation due to the depletion of dendritic cells.

(A) Gating strategy for the analysis of LNSCs from SLOs. (B) Flow cytometry analysis of cell surface molecules shown in histograms on LNSCs subsets at steady-state and 24 h post irradiation and quantification. (C) Gating strategy for the analysis of myeloid cells (DCs: I-Ab⁺CD11c⁺CD64⁻F480⁻) and (Mφ: I-Ab⁺CD11c⁺CD64⁺F480⁺). (D) Absolute numbers of DCs in spleen and mLNs. One data point represents one mouse analyzed in two experiments. Statistics are according to unpaired non-parametric Mann-Whitney test, (Mean± SD); *p < 0.05, **p < 0.01 and ****p < 0.001.

4.1.2 LNSCs process exogenous antigen via MHC class II

As we had observed LNSCs to up-regulated co-stimulatory molecules post conditioning, we further probed whether LNSCs degrade and process exogenous antigen under homeostatic, non-inflammatory conditions. To this end, we employed ovalbumin (OVA) as a model antigen molecule. Culturing FACS sorted LNs derived FRCs, LECs and BECs at 37°C with DQ-Ovalbumin (a self-quenched conjugate of ovalbumin that exhibits bright green fluorescence Ex/Em of digestion product: 505/515 nm upon antigen processing) resulted in processing of DQ-OVA in an MHC class II-dependent manner. FACS sorted splenic DCs (CD45⁺CD11c⁺MHCII⁺F4/80⁻) served as positive hematopoietic professional antigen presenting cell controls in these experiments. These findings suggested that LNSCs subsets (FRCs, LECs and BECs) have the ability to acquire and process/ degrade exogenous antigens (Figure 4.3).

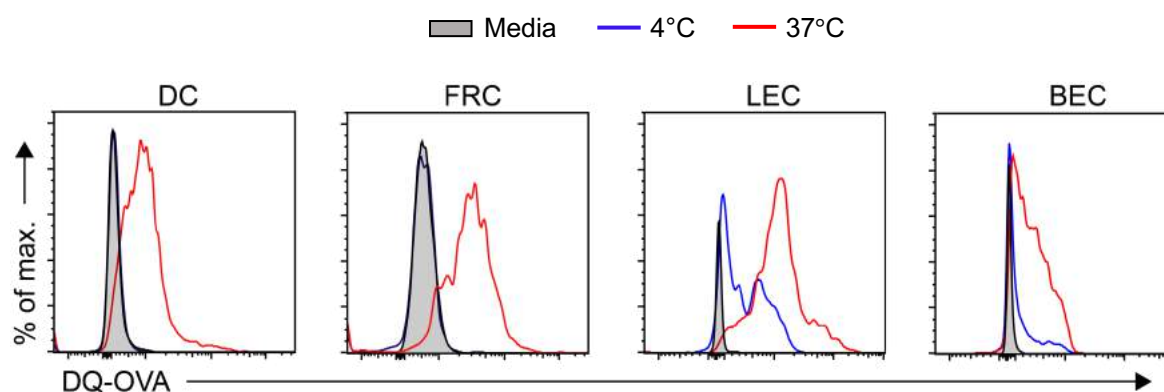


Figure 4.3 LNSCs can process exogenous antigen under homeostatic conditions.

DQ-OVA incubated with FACS sorted splenic DC (positive control) or LNs-derived FRC, LEC and BEC from a wild-type mouse for 3 h at 4°C (as negative control) and 37°C, followed by analysis of processed DQ-OVA with blue laser light excitation at 488 nm (BL-1 channel).

4.2 CD4⁺ T cell are activated in the SLOs early after allo-HCT

4.2.1 Allogeneic T cell activation kinetics in the initiation phase of aGvHD

To study whether donor alloreactive T cells are exclusively activated in the secondary lymphoid organs (spleen, lymph nodes and Peyer's patches) or in part in the aGvHD target organs (e.g., in the mucosa of the GIT) during the aGvHD initiation phase, we myeloablatively irradiated C57BL/6 mice and transplanted CFSE labeled allogeneic T cells together with BM cells from FVB.L2G85 and FVB/N mice, respectively (**Figure 4.4a**). *Ex vivo* bioluminescence imaging during the initiation phase of aGvHD revealed infiltration of luciferase⁺ donor T cells into the SLOs on day 3 after allo-HCT. The spleen, mesenteric lymph nodes, Peyer's patches and some colonic cryptopatches showed signal of day 2.5 (not shown), which increased up to day 3 due to cell proliferation. On day 4, first T cells entered the small intestine commencing the effector phase of aGvHD (not shown).

Flow cytometric evaluation of donor T cells in the SLOs revealed proliferation in the SLOs (**Figure 4.4b**). In contrast, in the small intestine's *lamina propria* (LP) we found only donor T cells that had already highly/completely diluted CFSE, indicating that donor T cells present in the LP likely had migrated from the SLOs after activation and had not actively proliferated in the *lamina propria* during aGvHD initiation (**Figure 4.4b**).

To spatially assess the localization of recently activated donor T cells within the SLOs and the small intestine LP, we co-stained donor T cells (CD45.1) around the Peyer's patches with CD31, a marker for blood vasculature and employed LSM. The analysis revealed that the T cells were located inside and at the border of Peyer's patches with few scattered T cells in the LP (**Figure 4.4c**). These findings confirmed that the T cells during the initiation phase of aGvHD localize and proliferate primarily in SLOs.

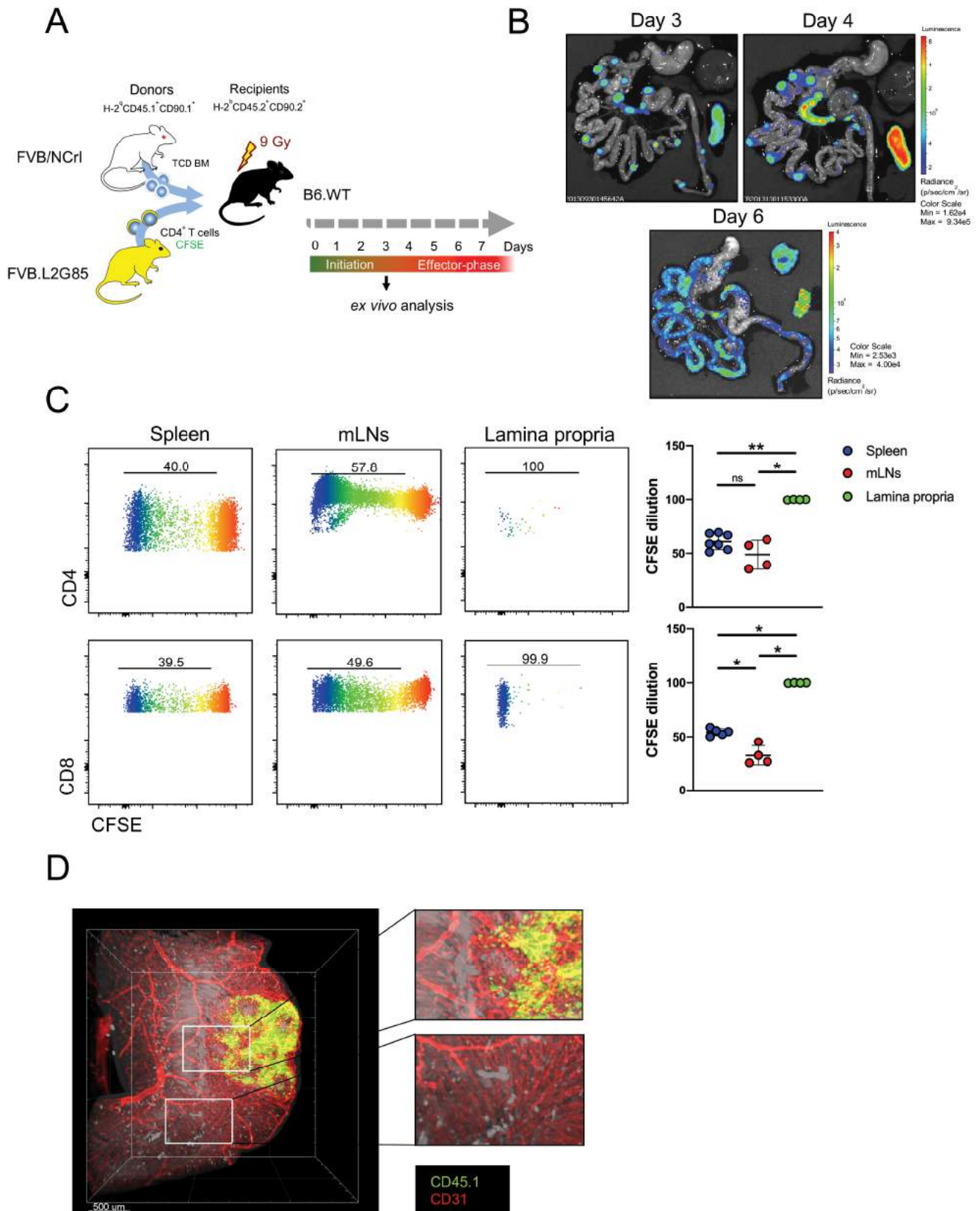


Figure 4.4 Naïve alloreactive T cells migrate to and are activated in secondary lymphoid organs during aGvHD initiation. (A) Experimental strategy: B6.WT recipient mice were myeloablatively irradiated with 9 Gy and i.v. transplanted with 5×10^6 BM and 5×10^8 CFSE labelled luc⁺ T cells from FVB/N mice and FVB.L2G85 mice respectively. (B) Ex vivo bioluminescence imaging of GIT and spleen on days +3, +4 and +6 after allo-HCT. (C) Flow cytometry analysis of donor T cells (CD45.1⁺ and CD4⁺ or CD8⁺ for CFSE dilution and quantification). (D) LSFM Z-stack of the small intestines: Blood vessels were *in vivo* stained with primary CD31 biotin and subsequently with streptavidin AF750 and donor T cells with CD45.1 with AF647. Each data point represents one analyzed mouse in two independent experiments. Unpaired non-parametric Mann-Whitney test, (Mean ± SD); * $p < 0.05$, ** $p < 0.01$.

4.2.2 Allogeneic CD4⁺ T cell are activated in SLOs of mice with MHC class II deficient myeloid cells during the aGvHD initiation phase

To study alloreactive CD4⁺ T cells activation in the lymphoid organs and in the absence of myeloid cell antigen presentation we generated MHCII^{ΔCD11c} mice. The CD11c-intrinsic deletion of MHC class II on all *CD11c* expressing DCs, macrophages and other CD11c expressing cells was achieved by crossing mice with the floxed *H2-Ab1* gene (*H2-Ab1^{fl}*) and a mouse expressing Cre recombinase under the control of *CD11c* promoter (*CD11c^{Cre}*) (**Figure 3.1**). Additionally, we used CD11c.DOG mice in which we could deplete *CD11c*⁺ cells pre allo-HCT via administration of diphtheria toxin (DTx) in these experiments (**Figure 3.1**). Additionally, we used CD11c.DOG mice in which we could deplete *CD11c*⁺ cells pre allo-HCT via administration of diphtheria toxin (DTx) in these experiments [134] (**Figure 4.5a**). *Ex vivo* bioluminescence imaging on day 3 after allo-HCT revealed reduced donor T cell derived bioluminescence signals in MHCII^{ΔCD11c} recipient mice when compared to the control *H2-Ab1^{fl}* littermate recipients and in contrast to increased bioluminescence signals in CD11c.DOG recipients after CD11c cell depletion (**Figure 4.5b**). Flow cytometric analysis of T cell activation (CD44 and CD25) and proliferation (CFSE dilution) showed reduced CD4⁺ T cell activation in MHCII^{ΔCD11c} mice compared to the *H2-Ab1^{fl}* control mice, however alloreactive donor T cells were still activated within 3 days of allo-HCT in the spleen (**Figure 4.5c, d**) In contrast, alloreactive donor T cells in CD11c.DOG mice showed a hyper-activated phenotype as shown by others in another model [93]. Furthermore, MHCII^{ΔCD11c} mice showed late aGvHD onset, with 80% survival and moderate clinical score compared to the *H2-Ab1^{fl}* mice, which developed full-blown aGvHD with only 20% overall survival. CD11c cell depleted CD11c.DOG mice developed hyper-acute GvHD with 0% overall survival (**Figure 4.5e**).

As the knock-out model in MHCII^{ΔCD11c} mice cannot target all hematopoietic cells we next employed MHCII^Δ BM chimeras, generated by syngeneic HCT of TCD BM cells from the MHCII^Δ mice into myeloablatively irradiated WT mice. After immune reconstitution, these (MHCII^Δ BM → WT) chimeras lacked expression of MHC class II on all BM derived hematopoietic cells and, subsequently, were further used as the recipient for allogeneic HCT experiments (**Figure 4.6a**). Unexpectedly within few weeks, these syngeneically-transplanted BM chimeras developed a tissue wasting disease resembling the development of lethal autoimmune disease (**Figure 4.6b**). This observation can be ascribed to a failure of thymic negative selection in MHCII^Δ BM → WT chimeras (see chapter 5 Discussion) [135]. However, considering humane endpoints to address our scientific questions, we performed short-term experiments with the MHCII^Δ BM → WT chimeras. We observed, that also in these mice alloreactive CD4⁺ T cells conventionally homed to SLOs (spleen, LNs and Peyer's patches) early after allo-HCT (**Figure 4.6c**) as measured with *ex vivo* bioluminescence imaging and were activated and proliferated at these sites. However, the level of activation and proliferation

state were significantly diminished compared to the WT → WT chimeras (**Figure 4.6d, e**), suggesting that alloreactive CD4⁺ are indeed modulated by non-hematopoietic cells of the LNs in aGvHD in these chimeras.

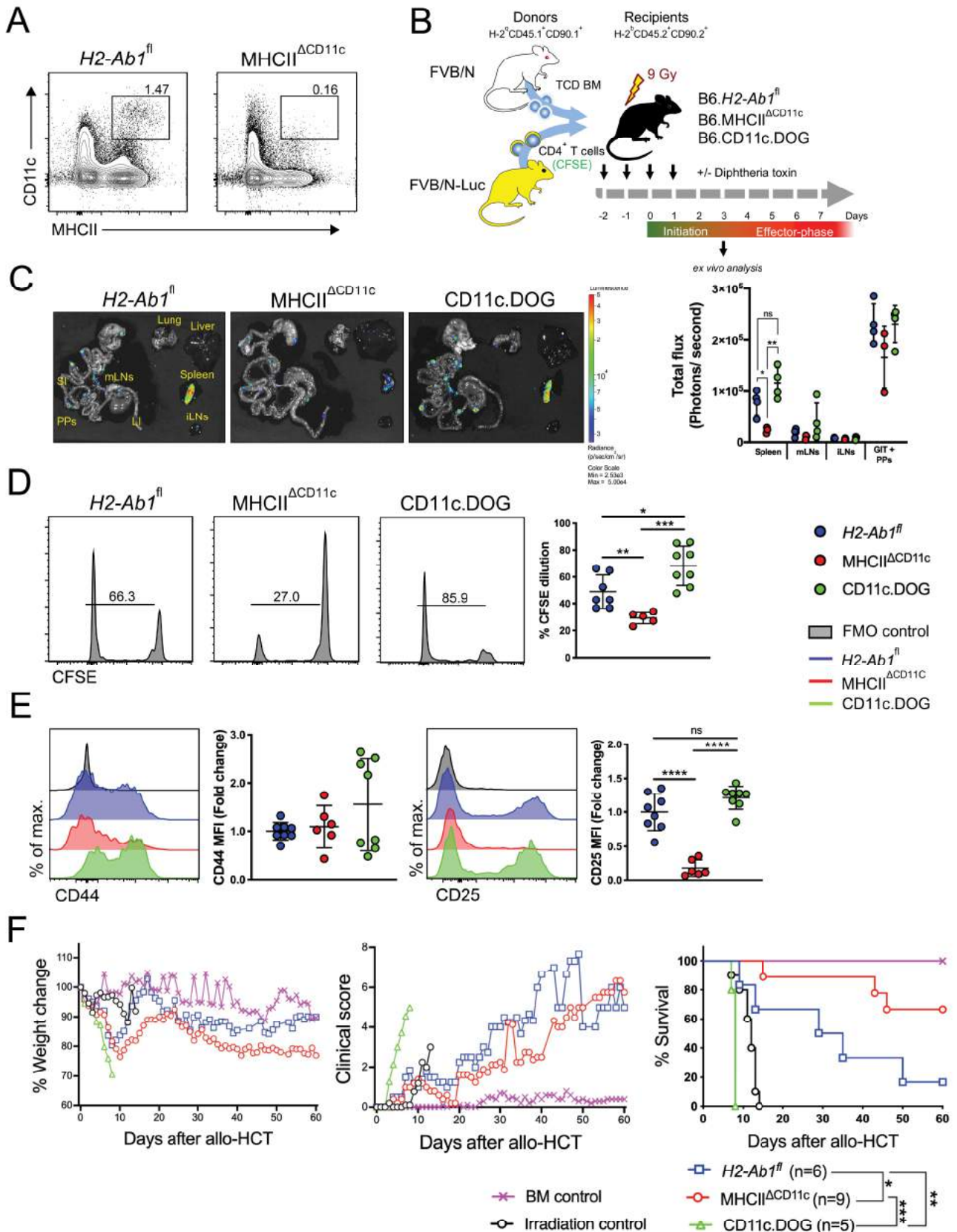


Figure 4.5 Alloreactive CD4⁺ T cells are activated in SLOs even in absence of antigen presentation from CD11c-expressing myeloid cells during the aGvHD initiation phase.

(A) Myeloid cells (CD45⁺CD11c⁺MHCII⁺) profile in *H2-Ab1^{fl}* and *MHCII^{ΔCD11c}* mice from spleen. (B) Experimental strategy: B6.*H2-Ab1^{fl}*, B6.*MHCII^{ΔCD11c}* and B6.*CD11c.DOG* recipients were myeloablatively irradiated with 9 Gy and i.v. transplanted with 5x10⁶ T cell-depleted (TCD) BM and 5x10⁶ CFSE labelled CD4⁺ T cells from FVB/N and FVB.L2G85 mice respectively and analyzed on day +3 after allo-HCT. B6.*CD11c.DOG* recipients were i.p. injected with diphtheria toxin (20 ng/gram body weight) day -2 until day +2 after allo-HCT to deplete recipient CD11c cells. (C) *Ex vivo* bioluminescence images and quantification on day +3 after allo-HCT. (D and E) CFSE dilution flow cytometry analysis and expression of CD44 and CD25 on donor T cells (CD90.1⁺ and

CD4⁺) on day +3 after allo-HCT. One data point represents one mouse analyzed in two experiments. Unpaired parametric, 2-tailed Student's t test, (Mean±SD); **p* < 0.05, ***p* < 0.01 and ****p* < 0.001. (F) Survival, clinical score and weight of myeloablatively irradiated (9 Gy) B6.H2-Ab1^f, B6.MHCII^{ΔCD11c} and B6.CD11c.DOG recipient mice transplanted with 5x10⁶ allogeneic T cell-depleted (TCD) BM and 0.6x10⁶ enriched CD4⁺ T cells from FVB/N donor mice (n = 6-9 per group).

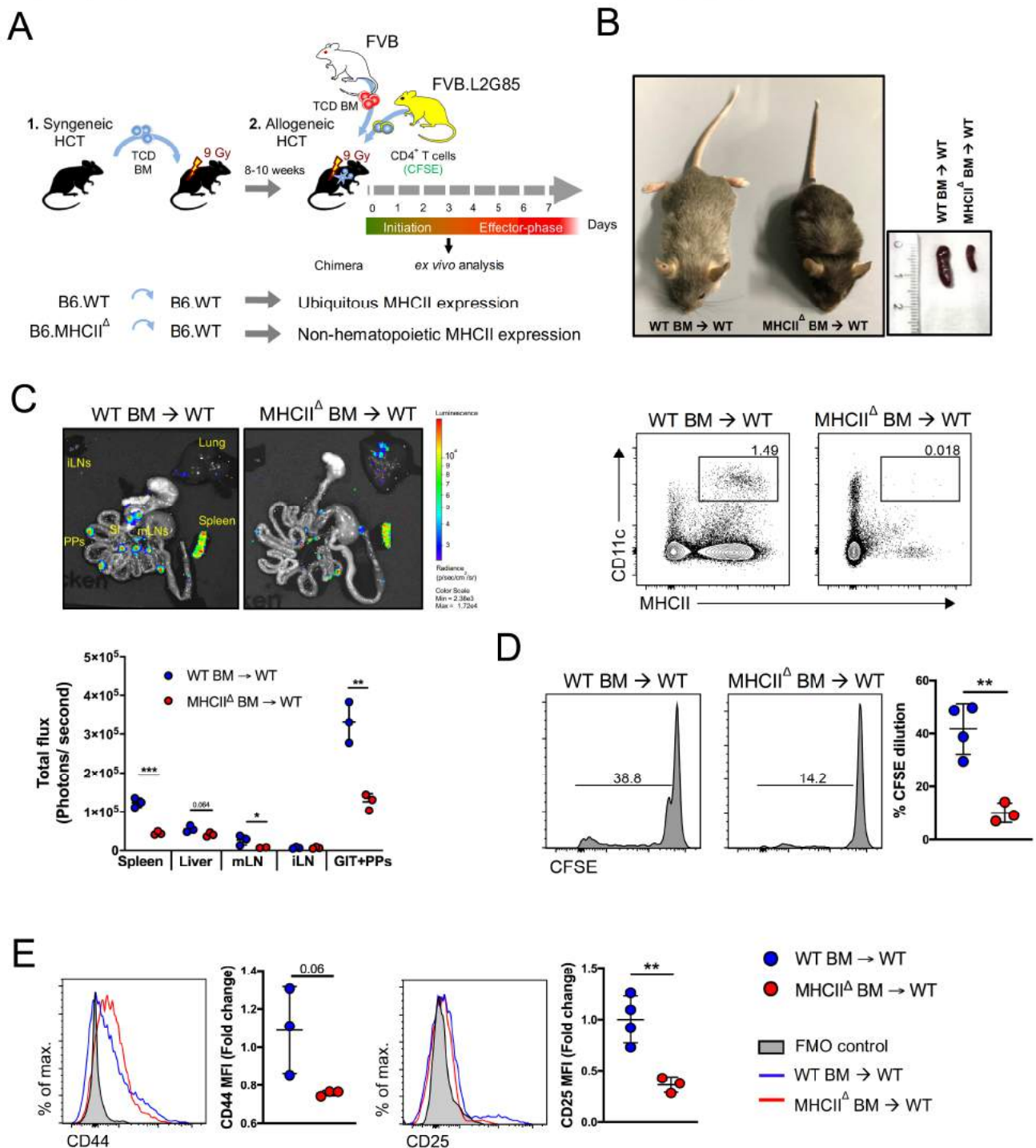


Figure 4.6 Alloreactive CD4⁺ T cells are activated in SLOs of MHC class II deficient BM chimeras during aGvHD initiation. (A) Experimental strategy: For the generation of MHCII^Δ BM chimeras: TCD BM from the B6.WT or B6.MHCII^Δ mice was syngeneically transplanted into myeloablatively irradiated (9 Gy) B6.WT mice. 8-10 weeks after HCT and successful BM engraftment, mice were again myeloablatively irradiated (9 Gy) and allogeneically transplanted with 5x10⁶ TCD BM cells from FVB/N mice and 5x10⁶ CD4⁺ T cells from FVB.L2G85 mice and analyzed day +3 after allo-HCT. (B) Phenotype of WT BM chimeras versus MHCII^Δ BM chimeras. (C) *Ex vivo* bioluminescence images and quantification on day +3 after allo-HCT. (D and E) CFSE dilution flow cytometry analysis and expression of CD44 and CD25 on donor T cells (CD90.1⁺ and CD4⁺) on day +3 after allo-HCT in mLNs. Unpaired parametric, 2-tailed Student's t test, (Mean±SD); **p* < 0.05 and ***p* < 0.01.

These experiments in the MHCII^{ΔCD11c} mice and MHCII^Δ BM chimeras let us conclude that even in the absence of host hematopoietic APCs, alloreactive donor CD4⁺ T cells are activated in the SLOs early after allo-HCT leading to lethal aGvHD. However, these results have to be cautiously interpreted as both of the employed models had some technical and physiological shortcomings.

4.3 Targeting the lymph node stroma and hematopoietic system

4.3.1 Deciphering LNSCs by scRNA sequencing

Lymph node stroma and endothelium are characterized into 4 distinct CD45⁻ cell populations based on their expression of surface molecules: podoplanin (Pdpn) and CD31. However, recent findings have further identified heterogeneity and niche specific cell lineages of stroma of LNs and spleen [136], [137], as well as of lymph [138] and vascular [139] endothelium utilizing single cell RNA sequencing (scRNA seq). Here we utilized scRNA sequencing to identify cell-specific molecules for specific targeting of LNSCs sub-population for further targeting with Cre/lox mouse models. FACS-sorted CD45⁻CD24⁻ cells from C57BL/6 mLNs, processed using 10x Genomics pipeline (**Figure 4.7**) and by unsupervised clustering with Loupe browser (10x Genomics, San Francisco, CA, USA) we identified 9 distinct population on (t-distributed stochastic neighbor embedding) t-SNE distribution expressing a distinct transcriptome that has been previously identified by Pezoldt J and colleagues (**Figure 4.8a, b**) [140]. We identified differentially expressed genes (DEGs) for each cluster calculated as the difference between the average expression by cells in the cluster and the average expression by cells not in the cluster. At first glance, we could recognize the known major LNSCs subpopulations, including BECs (Pdpn⁻ Pecam1⁺), LECs (Pdpn⁺ Pecam1⁺) and non-endothelial cells stromal cells as Pdpn⁺ Pecam1⁻ Akr4⁻ cells.

Perivascular cells (PvCs) - DNCs could be distinguished by high expression of Acta2⁺. We used Ccl21⁺ Ccl19⁺ Pdpn⁺ to target T cell zone reticular cells (TRCs), however these molecules were insufficient to underpin TRCs and other LNSCs subsets in our analysis. We could further identify a large proportion of CD34⁺ LNSCs, which are known to predominantly be located at the LNs capsule and around large vessels [140], [141]. These CD34⁺ LNSCs could be further subdivided into distinct subsets based on the expression of CD34⁺(Aldh1a2⁺), CD34⁺(Akr3⁺), CD34⁺(Gdf10⁺) and CD34⁺(CD248⁺) SCs, each bearing distinct transcriptional profiles. Considering that CD4⁺ T cells are predominantly localized in the T cell zone of the LNs, we could employ *Ccl19*-Cre [48] or *Ccl21*-Cre transgene to target the TRCs (**Figure 4c**). However, endothelial cells are difficult to target as certain genes are shared by hematopoietic and endothelial cell precursors during development stages. In our scRNA analysis we could clearly distinguish cluster 9 accumulating LECs and BECs (**Figure 4.9**). Here we used Pecam1⁺

Lyve1⁺ Prox1⁺ Ackr4⁺ and Pdpn⁺ to pinpoint LECs, whereas we identified BECs by their expression profile of Esm1 and Igta1. Tie2 has been successfully used by others to target the hematopoietic and endothelial cells, however, to exclusively target endothelial cells, *Cdh5*-Cre [142] is a suitable option as it is not expressed on hematopoietic cells as well as on cells of stromal lineages. Moreover, to overcome the biological difficulty and ensuing experimental bias of using MHCII BM chimeras to study MHCII mediated non-hematopoietic antigen presentation, *Vav1*-iCre mice [143] could be used to target all hematopoietic cells. In fact, we could not detect *Vav1* expression in our scRNA seq data sets confirming its exclusive expression in hematopoietic cells (**Figure 4.8b**).

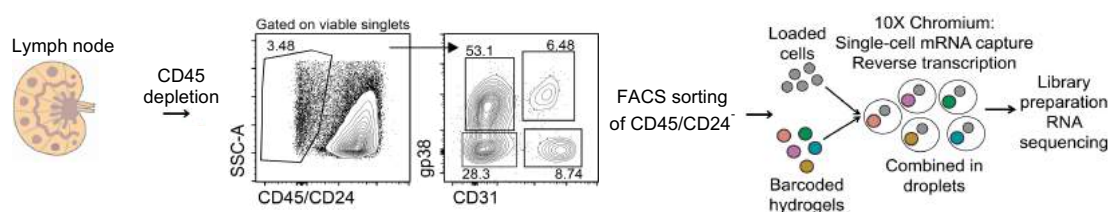
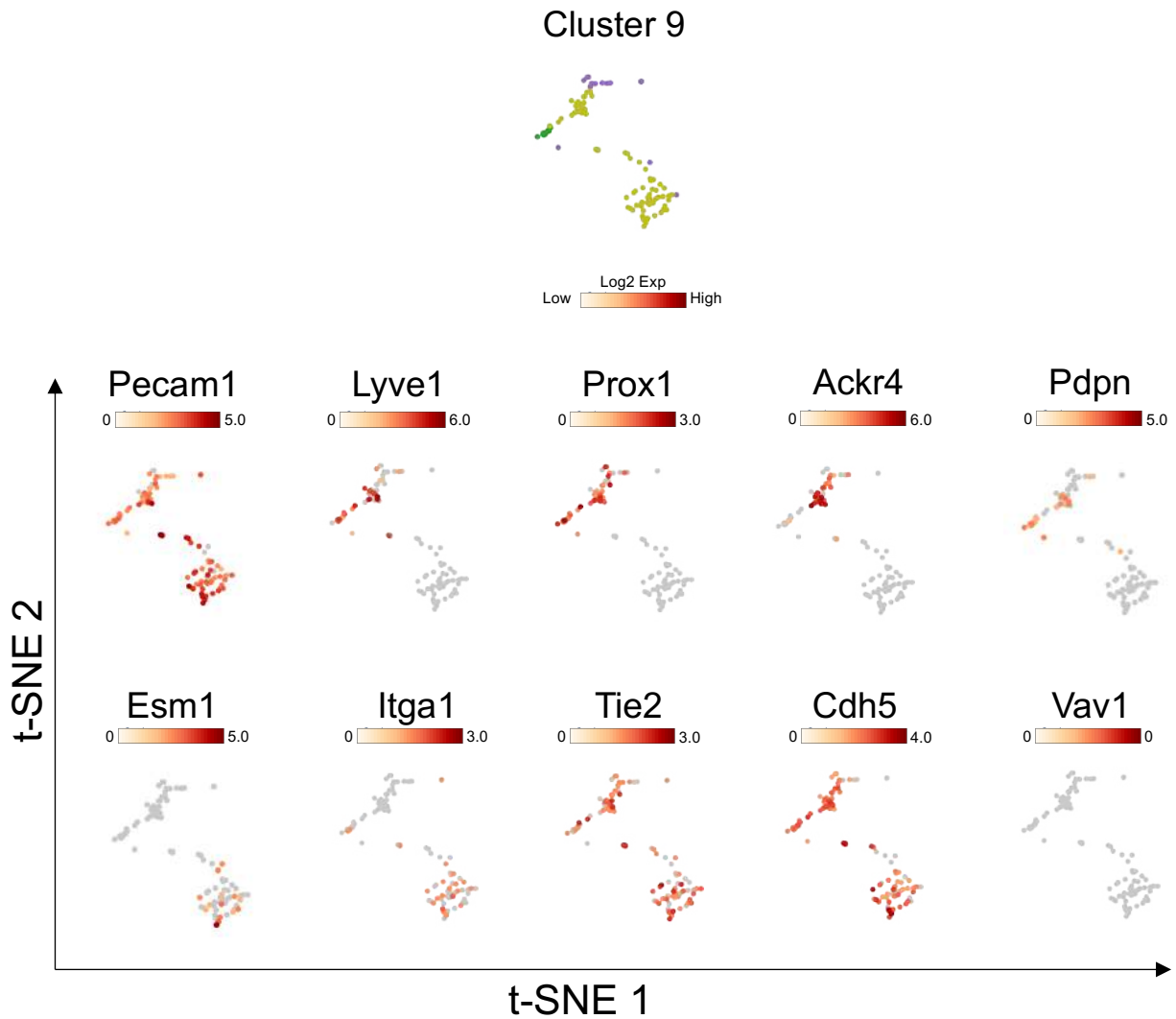


Figure 4.7 Single cell RNA sequencing experimental strategy.

Enzymatically digested mLNs from B6 mice were magnetically depleted of CD45⁺ cells and subsequently FACS sorted according to the displayed gating strategy of viable singlets that were negative for CD45 and CD24 followed by 10x Chromium single cell RNA capture, reverse transcription of combined in droplets followed by library preparation and RNA sequencing.

Figure 4.8 Single cell RNA sequencing of steady-state LNSCs.

(A) Heat-map of highly upregulated and downregulated genes in t-SNE differentiated clusters (log2 expression). (B) t-SNE clustering of LNSCs performed on Loupe software. (C) Log2 expression on t-SNE plot of genes for characterization of non-endothelial LNSCs.

**Figure 4.9 Characterization of endothelial cells in LNSCs scRNA dataset.**

Focused analysis of cluster 9 for the identification of LEC and BEC specific gene signature.

4.4 Subset of LNSCs activate alloreactive CD4⁺ T cells in SLOs

4.4.1 MHCII^{ΔVav1} mice, a suitable model for studying non-hematopoietic antigen presentation

The ability of non-hematopoietic APCs to induce CD4⁺ T cell mediated GvHD has not been addressed in depth due to technical difficulties such as using MHCII^Δ BM chimeras that developing autoimmunity and wasting disease even without an allo-HCT setting (see section 4.2.2). To circumvent this technical hurdle, we generated MHCII^{ΔVav1} mice with Vav1-intrinsic deletion of MHC class II on all *Vav1*-expressing hematopoietic lineage cells by crossing mice with floxed *H2-Ab1* gene (*H2-Ab1*^{fl}) with a mouse expressing Cre recombinase under the control of *Vav1* promoter (*Vav1*^{iCre}).

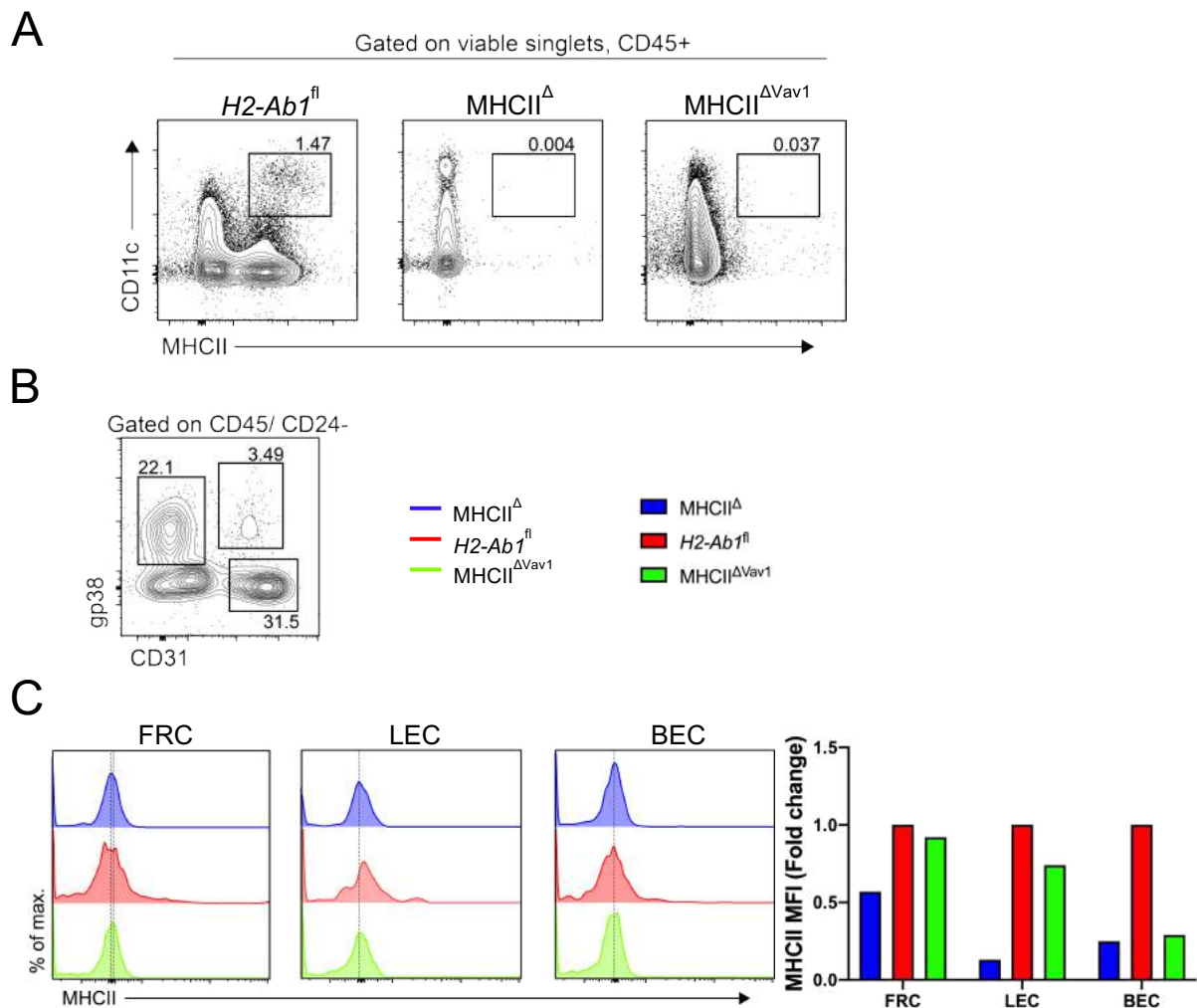


Figure 4.10 Phenotyping of MHCII^{ΔVav1} mice.

(A) MHC class II expression on CD45⁺ hematopoietic cells from *H2-Ab1*^{fl} wild-type littermates against MHCII^Δ and MHCII^{ΔVav1} mice. (B) Gating of lymph node LNSCs (C) Expression and quantification of MHCII on FRC, LEC and BEC from MHCII^Δ, *H2-Ab1*^{fl}, and MHCII^{ΔVav1} mice.

MHCII^{ΔVav1} mice are viable and breed normally, however we observed that older mice (males ≥ females) were susceptible to developing a rectal prolapse. MHCII^{ΔVav1} mice lacked expression of MHCII on all hematopoietic cells, which we analyzed in SLOs (**Figure: 4.10a**) and shared the MHCII negative profile in CD11c⁺ cells with MHCII^Δ mice. Moreover, MHCII expression of FRCs, LECs and BECs in these mice was comparatively lower to that in WT mice, due to the lack of MHCII transfer from DCs (**Figure: 4.10b, c**).

LNSCs being able to endogenously express MHC class II and their capacity to acquire MHC class II from DCs led us to further evaluate MHC class II antigen processing in mice lacking MHCII on DCs: MHCII^{ΔVav1} mice. Indeed, all subsets of LNSCs in MHCII^{ΔVav1} mice (**Figure: 4.11**) processed DQ-OVA demonstrating that the inherently expressed MHC class II molecules can functionally process antigens on LNSCs.

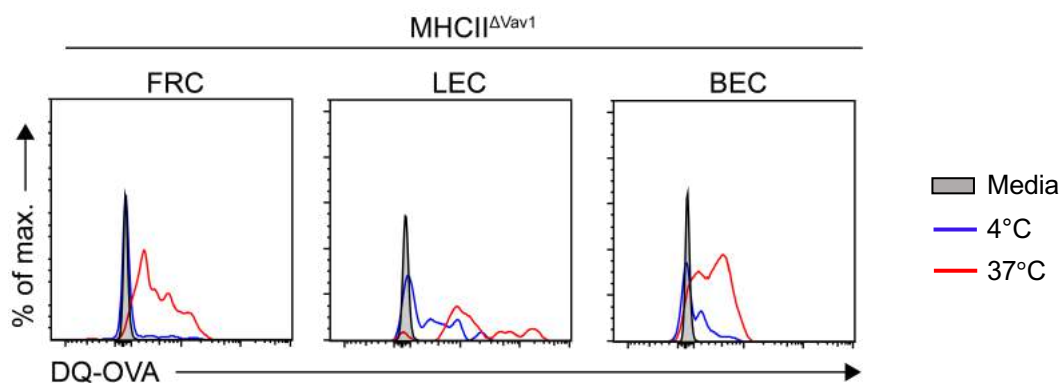


Figure 4.11 LNSCs endogenous MHCII process exogenous antigen under homeostatic conditions.

Antigen processing assay with DQ-OVA on FACS sorted LNs derived FRC, LEC and BEC from MHCII^{ΔVav1} mouse; for 3 h at 4°C and 37°C, followed by analysis of processed DQ-OVA with blue laser light excitation at 488 nm (BL-1 channel).

Allogeneic transplantation of FVB/N CD4⁺ T cells and TCD BM into MHCII^{ΔVav1} resulted in induction of lethal aGvHD that was comparable to WT littermates: *H2-Ab1^{fl}* according to survival and clinical score date (**Figure: 4.12**).

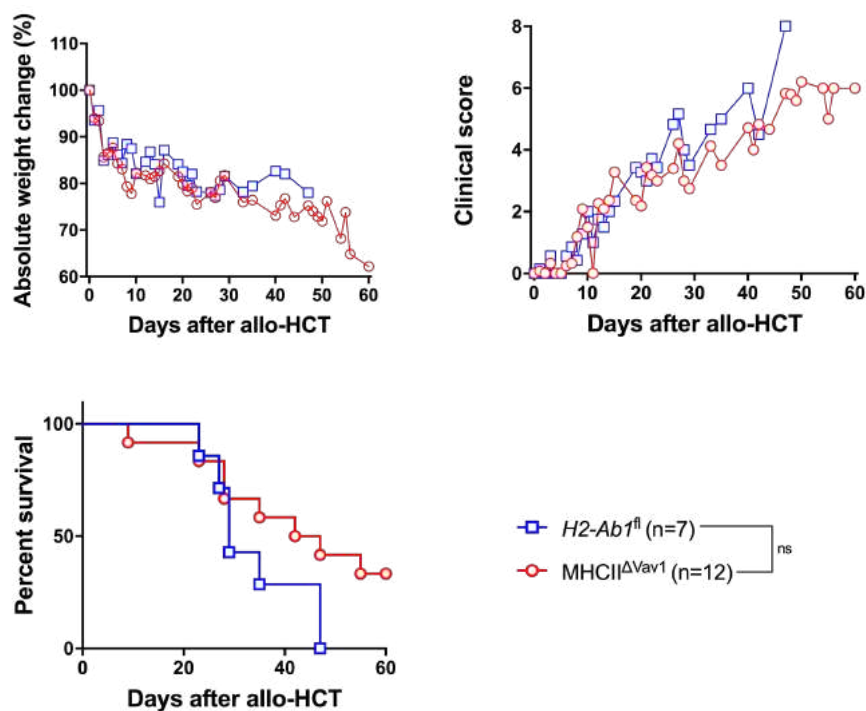
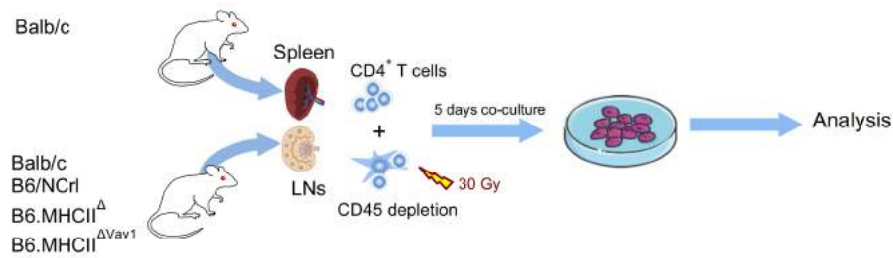


Figure 4.12 B6.MHCII^{ΔVav1} mice are susceptible to aGvHD.

Survival, clinical score and absolute weight change of myeloablatively irradiated (9 Gy) B6.*H2-Ab1^{fl}* and B6.MHCII^{ΔVav1} mice transplanted with 5×10^6 TCD BM and 0.6×10^6 enriched CD4⁺ T cells from FVB/N mice.

Polyclonal mixed lymphocyte reaction (MLR) of enriched CD4⁺ T cells from BALB/c with irradiated cells from the enzymatically digested whole mLNs from: BALB/c (syngeneic control), B6 (allogeneic control), B6.MHCII^Δ, and B6.MHCII^{ΔVav1} mice (**Figure: 4.13a**), showed significant upregulation of T cell activation molecules CD44, CD25 and CXCR3 on CD4⁺ T cells cultured with LNs cells from B6.MHCII^{ΔVav1} compared to cells from B6.MHCII^Δ mice. Also, the ratios of the effector to naïve T cells as well as of Ki67⁺ T cells increased, indicating non-hematopoietic LNSCs in MHCII^{ΔVav1} can induce MHCII-driven activation and proliferation of alloreactive CD4⁺ T cells and proliferation in contrast to B6.MHCII^Δ and syngeneic BALB/c control LNSCs (**Figure: 4.13b**).

A



B

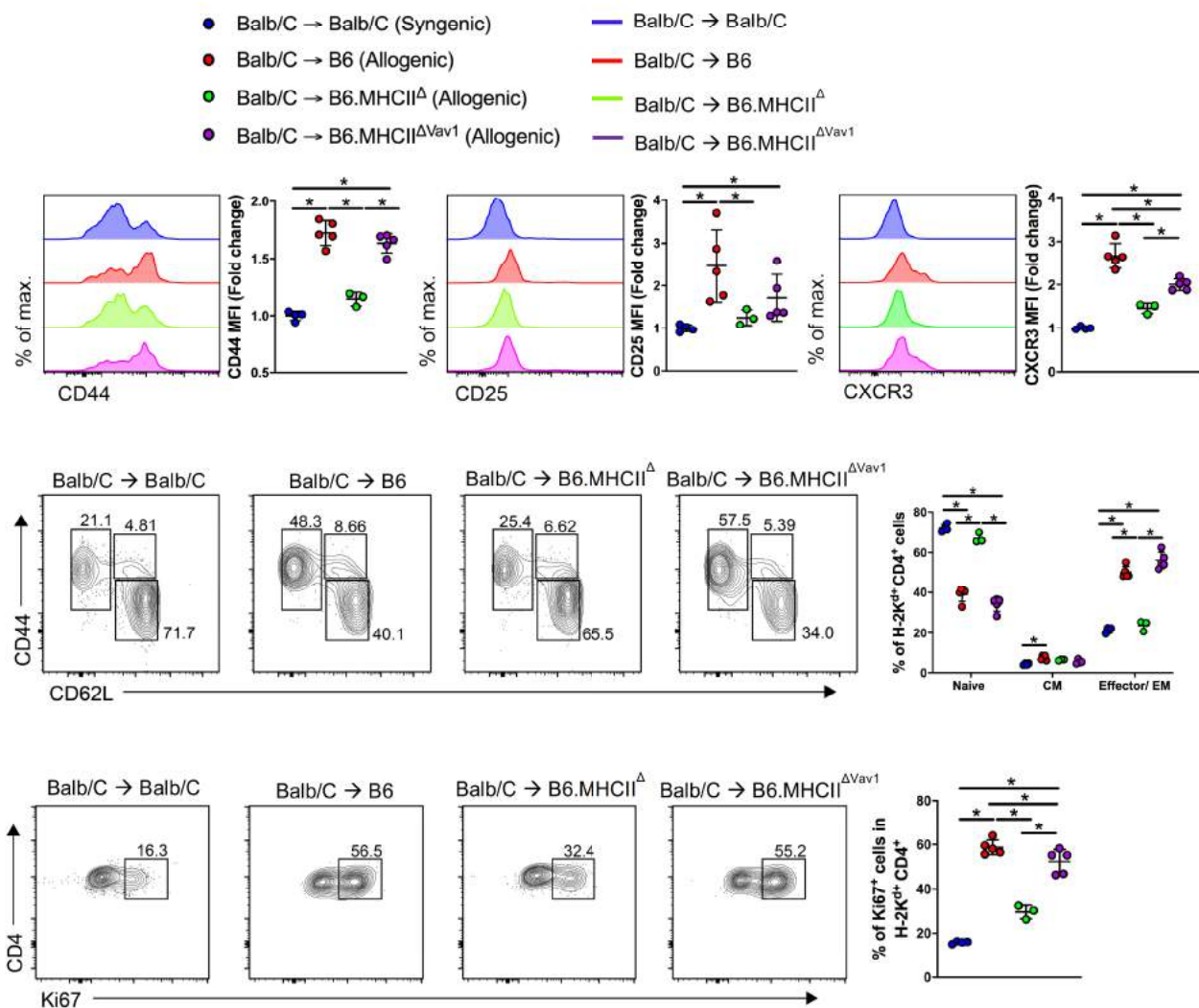


Figure 4.13 Non-hematopoietic cells of lymph nodes activate alloreactive CD4⁺ T cells in mixed lymphocyte reactions.

(A) Experimental strategy: Magnetically enriched CD4⁺ T cells (H-2^d) from BALB/c mice were cultured with the enzymatically digested BALB/c, B6 WT, B6.MHCII^Δ or MHCII^{ΔVav1} irradiated LNSCs derived from pooled CD45 cell depleted lymph nodes for 5 days at 37°C. (B) Flow cytometry analysis of alloreactive CD4⁺ T cells gated on CD4⁺ and H-2k^d population for T cell activation and proliferation. Unpaired non-parametric Mann-Whitney test, (Mean± SD); **p* < 0.05.

4.4.2 Mesenteric lymph node transplantation in mice

In the previous sections, we could show that SLOs are the alloreactive T cell priming and activation sites under the inflammatory conditions during the initiation phase of aGvHD. Mesenteric lymph nodes (mLNs) are the sentinel sites of gut immunosurveillance and gastrointestinal tract (GIT) homeostasis. As the GIT represents one of the target organs in aGvHD, we employed a sophisticated technique of lymph node transplantation to further delineate MHCII mediated non-hematopoietic antigen presentation in aGvHD. (**Figure: 4.14a, b, c**)

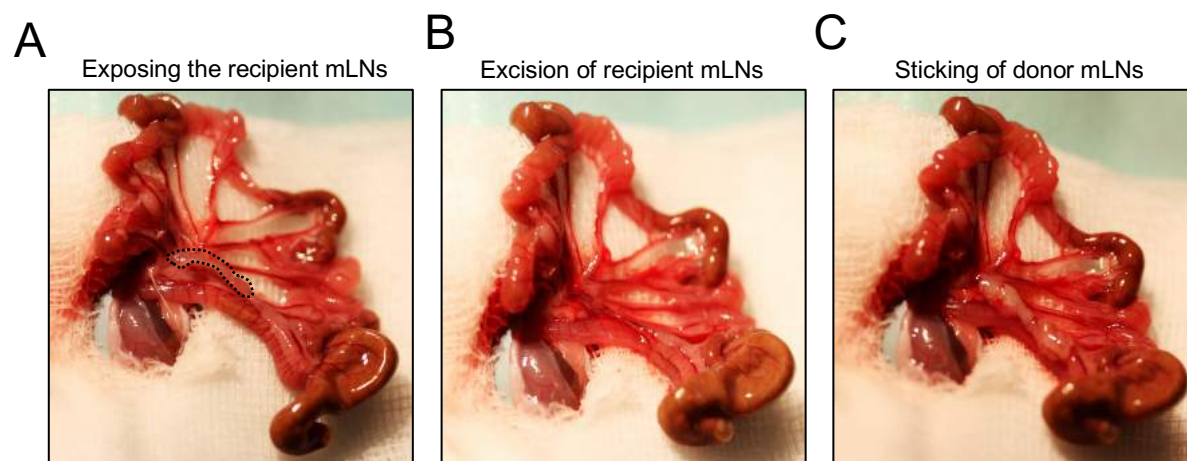


Figure 4.14 Procedure of mesenteric lymph node transplantation.

(A) The peritoneal cavity of the mice was carefully surgically opened and the small bowel along with the caecum taken out with cotton swabs and laid on DPBS wetted gauze to make all the mLNs visible. (B) All the recipient mLNs were carefully excised avoiding bleeding from the superior mesenteric artery lying just behind the mLNs (C) 20 μ l of fibronectin was pipetted on the scar, donor mLNs soaked in thrombin were carefully placed on the scar and incubated for 3-5 min before internalizing the complete bowel into the peritoneal cavity and subsequent suturing the peritoneal and skin incisions.

The surgically transplanted donor mLNs engrafted within few weeks of lymph node transplantation, which could be followed by transplanting a luc⁺ donor mLNs into an albino B6 mice (**Figure: 4.15a, b**). The transplanted mLNs retained vasculature (vessel length and diameter) which was comparable to that in an untreated mouse, however the density of blood vessels was slightly reduced (**Figure: 4.15c, d**). Importantly, the lymphatic vessels of donor mLNs conjoined with the lymphatic system of the GIT, which we assessed by 3D-LSFM staining of lymphatic vessels in the transplanted mLNs and drainage of injected Evan's blue from ileac Peyer's patches into the mLNs (**Figure: 4.16a, b**).

We further characterized the cellular composition of the donor mLNs after engraftment. To this end we utilized congenic markers of CD45 and transplanted mLNs from B6.CD45.1 mouse into a WT B6.CD45.2 mouse; 5 weeks after engraftment the donor lymph nodes were assessed for host and donor hematopoietic cells with flow cytometry (**Figure: 4.17a**). Here, we found that the transplanted mLNs were almost completely populated with the host hematopoietic cells (CD45.2⁺) with negligible number (<0,1%) of donor hematopoietic cells

(CD45.1⁺) comprising no myeloid cells and very few donor derived resident B and T cells (Figure: 4.17b).

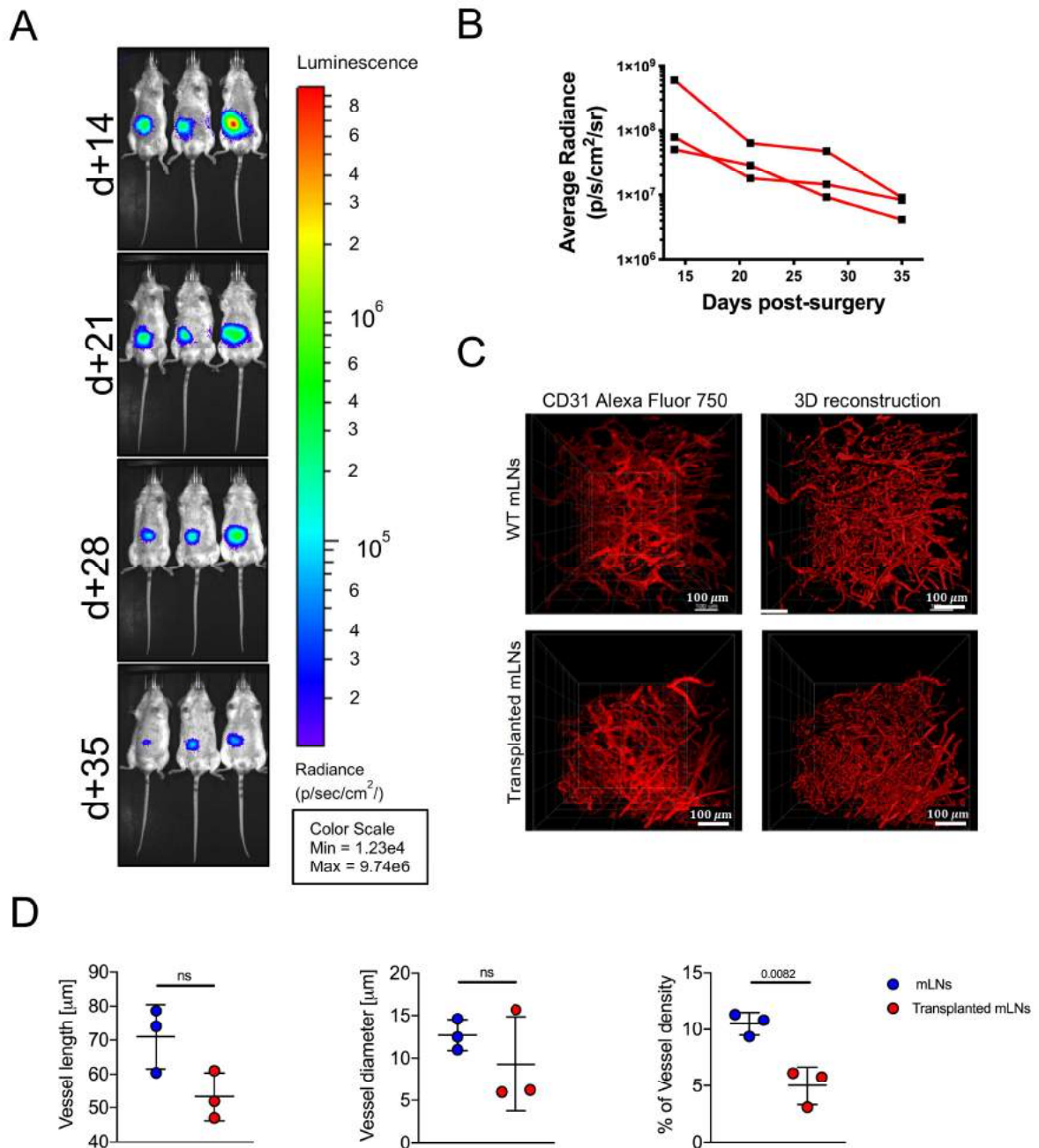
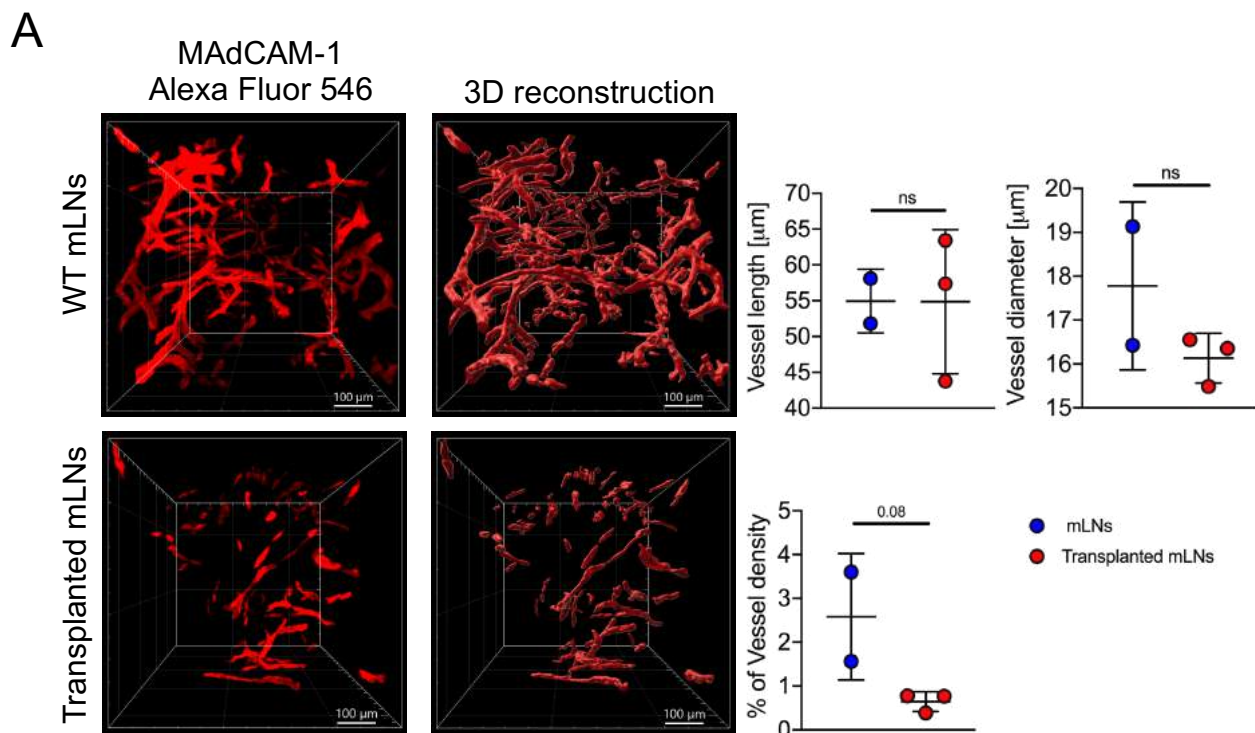


Figure 4.15 Donor mLN were engrafted in the recipient mice after lymph node transplantation.

(A) Sustainable bioluminescence was emitted from luc⁺ mLN from B6.L2G85 mice transplanted into a B6 albino recipient mouse. (B) Quantification of BLI signals (photons per second) from donor luc⁺ mLN. (C) Zoomed LSFM images depict 3D rendered CD31⁺ blood vessels (20x objective, scale bar = 100 µm). (D) Blood vessel length, diameter and density was analyzed from reconstructed LSFM images. Data pooled from different lobes of mLN from a single mouse. Two-tailed unpaired T test was applied (Mean ± SD); **p* < 0.05.



B

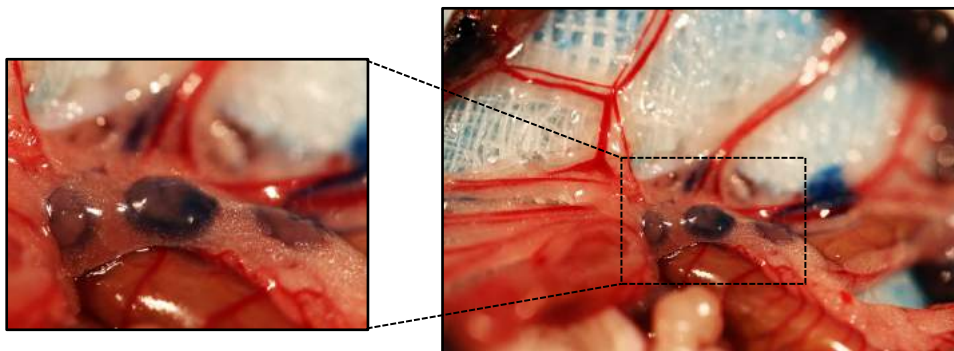


Figure 4.16 Donor mLN lymph vessels conjoin with recipient's intestinal lymphatic vasculature after LN transplantation. (A) Zoomed LSFM images of lymphatic vessels staining with anti-MAAdCAM-1 antibody and 3D reconstruction (20x objective, scale bar = 100 μ m). Lymphatic vessel length, diameter and density analysed from reconstructed images on Imaris software. (B) Evan's blue injected into the iliac Peyer's patches drains into the transplanted mLN. Data pooled from different lobes of mLN from a single mouse. Statistics are according to Two-tailed unpaired T test (Mean \pm SD); * $p < 0.05$.

Since non-hematopoietic cell composition cannot be identified by a congenic marker, we utilized fluorescent protein (dsRed) transgenic reporter mice to evaluate the non-hematopoietic host-donor composition of the transplanted mLN. The mLN transplanted from a B6.DsRed mouse into a WT mouse retained dsRed signal on all subsets of LNSCs after engraftment (**Figure: 4.17c**). Conclusively these experiments revealed that the surgically transplanted mLN retain the non-hematopoietic cells from the donor whereas the hematopoietic cells are replaced by the cells of host origin. Next, we asked if the transplanted mLN were capable of mounting an immune response. To this end we transplanted mLN from a B6.WT into a B6.WT mouse. 5 weeks post-surgery we transplanted these mice with allogeneic FVB/N BM and luciferase transgenic FVB.L2G85 T cells to induced aGvHD in these animals (**Figure: 4.18a**).

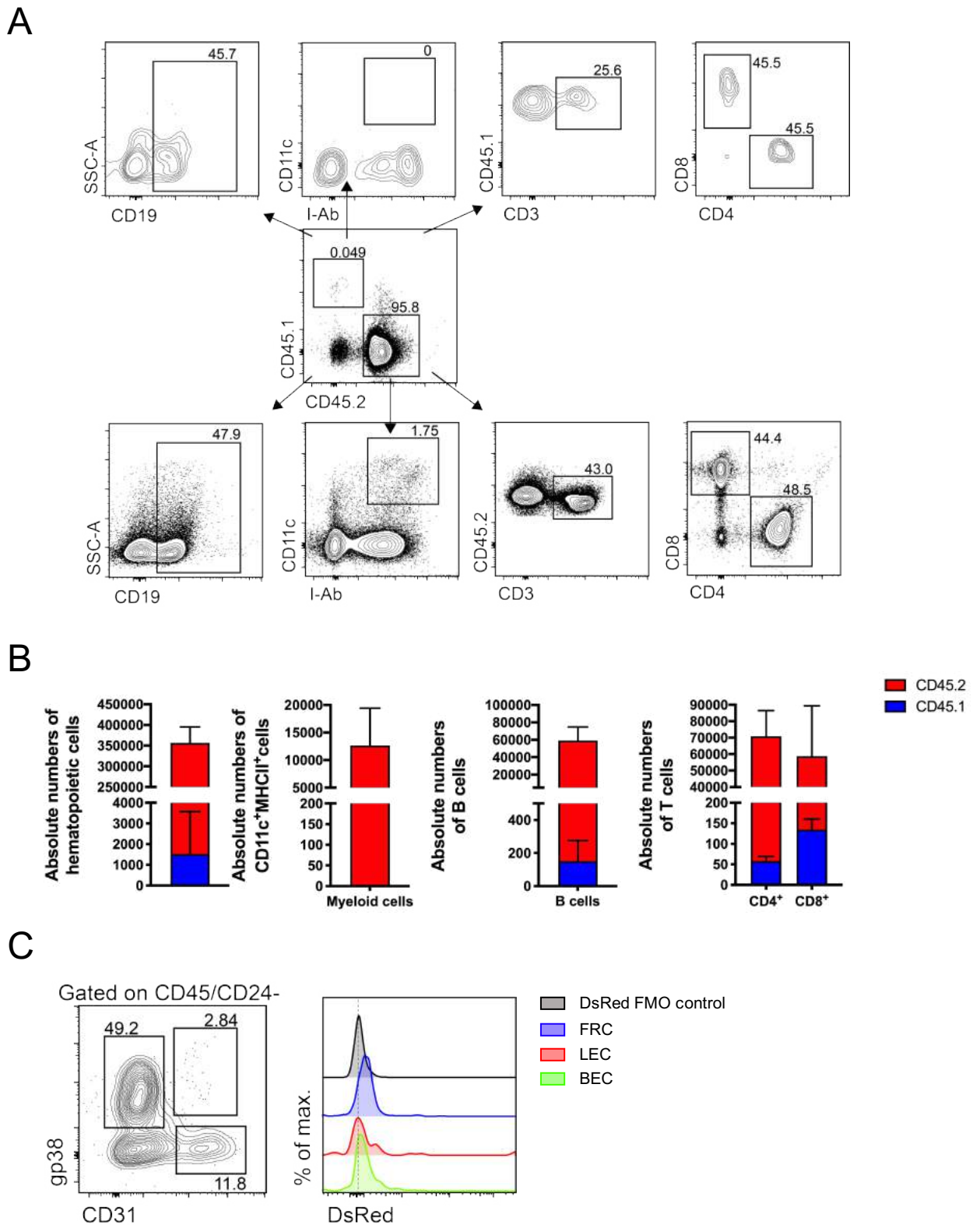
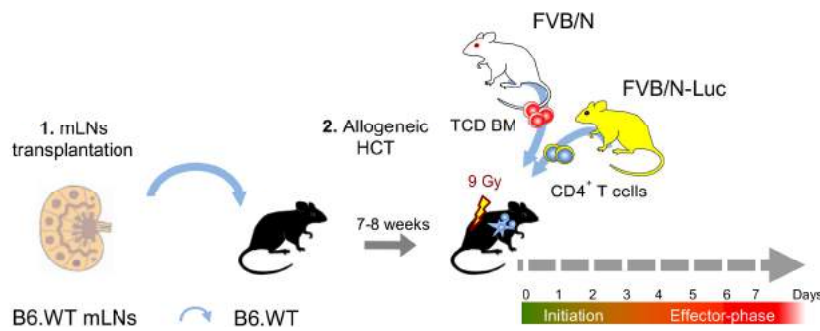


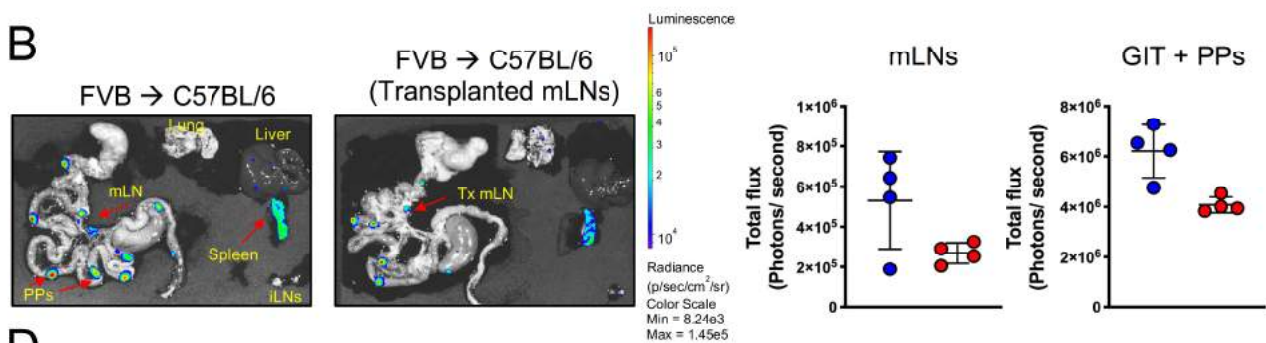
Figure 4.17 Donor mLNs are populated with recipient hematopoietic cells after surgically transplantation.
(A) Flow cytometry gating of hematopoietic cells in mLNs from B6.CD45.1 mouse transplanted in a B6.CD45.2 mouse. **(B)** Absolute numbers of hematopoietic cells, myeloid cell (dendritic cells and macrophages), B cells and CD3⁺ pre-gated CD4⁺ and CD8⁺ T cells in CD45.1⁺ and CD45.2⁺ sub-populations. Data pooled from five mice analysed in two experiments. **(C)** Flow cytometry gating of non-hematopoietic LNSCs and DsRed fluorescence signal from B6.DsRed mLNs transplanted in a B6.WT mouse. Error bars represent Mean \pm SD.

Bioluminescence signals from the transplanted mLNs revealed alloreactive CD4⁺ T cell activation (**Figure: 4.18b**) and flow cytometry revealed upregulation of T cell activation molecules CD44 and CD25 that was comparable to that in a WT mouse on day +3 of allo-HCT (**Figure: 4.18c**). Moreover, alloreactive donor CD4⁺ T cells upregulated the hallmark gut homing integrin $\alpha 4\beta 7$ as well as Ki67 indicating active proliferation in the transplanted mLN (**Figure: 4.18d, e**).

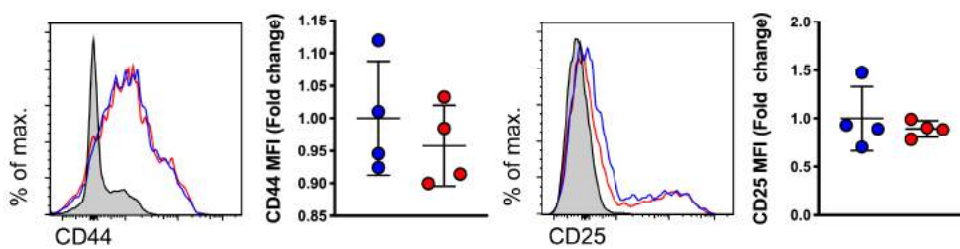
A



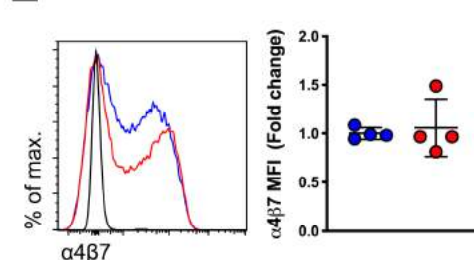
B



D



E



F

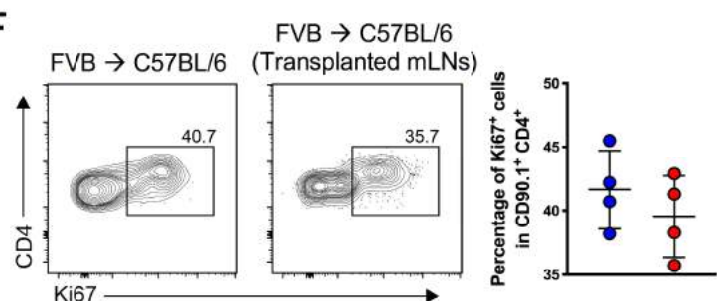


Figure 4.18 Alloreactive CD4⁺ T cells are robustly activated and proliferate in the transplanted mLNs in aGVHD after allo-HCT.

(A) Experimental strategy: mLNs from B6.WT mice were transplanted into B6.WT recipients; 5-6 weeks after surgery MHC major mismatch aGVHD was induced by myeloablative irradiation (9 Gy) and allo-HCT 5×10^6 TCD BM cells from FVB/N mice and 5×10^6 CD4⁺ T cells from FVB.L2G85 mice. (B) BLI signals from adoptively transplanted luc⁺ CD4⁺ T cells on d+3 of allo-HCT. (C) Mean fluorescence intensity (MFI) of CD44 and CD25 on donor CD4⁺ T cells at d+3 after allo-HCT. (D) MFI of $\alpha 4\beta 7$ on donor T cells d+3 after allo-HCT. (E) Proliferative capacity of donor CD4⁺ T cells analyzed by expression of Ki67 d+3 after allo-HCT. Data pooled from four mice analysed in two experiments). Error bars represent Mean \pm SD.

Taken together these experiments prove that lymph node transplantation is a robust technique that can be used to test antigen presentation by non-hematopoietic cells.

4.4.3 Alloreactive CD4⁺ T cells show effector phenotype in the B6.MHCII^Δ mice transplanted with mesenteric LNs of CD11c.DOG mice

To integrate the lymph node transplantation technique in our experimental setup of aGvHD, we surgically removed mLNs from MHCII^Δ mice and transplanted donor mLNs from a CD11c.DOG mice (depleted of CD11c⁺ cells by the administration of diphtheria toxin pre-surgery). After the successful engraftment of the donor mLNs, aGvHD was induced in these animals by allo-HCT of 5×10^6 TCD BM and 5×10^6 CD4⁺ T cells from FVB.L2G85 mice or in B6.MHCII^Δ mice as controls, respectively (**Figure: 4.19a**). At day +13 the absolute numbers of alloreactive CD4⁺ T cells in the spleen of MHCII^Δ (without LN transplants) were significantly lower compared to the MHCII^Δ mice with syngeneically transplanted CD11c.DOG mLNs (**Figure (Figure: 4.19b)**).

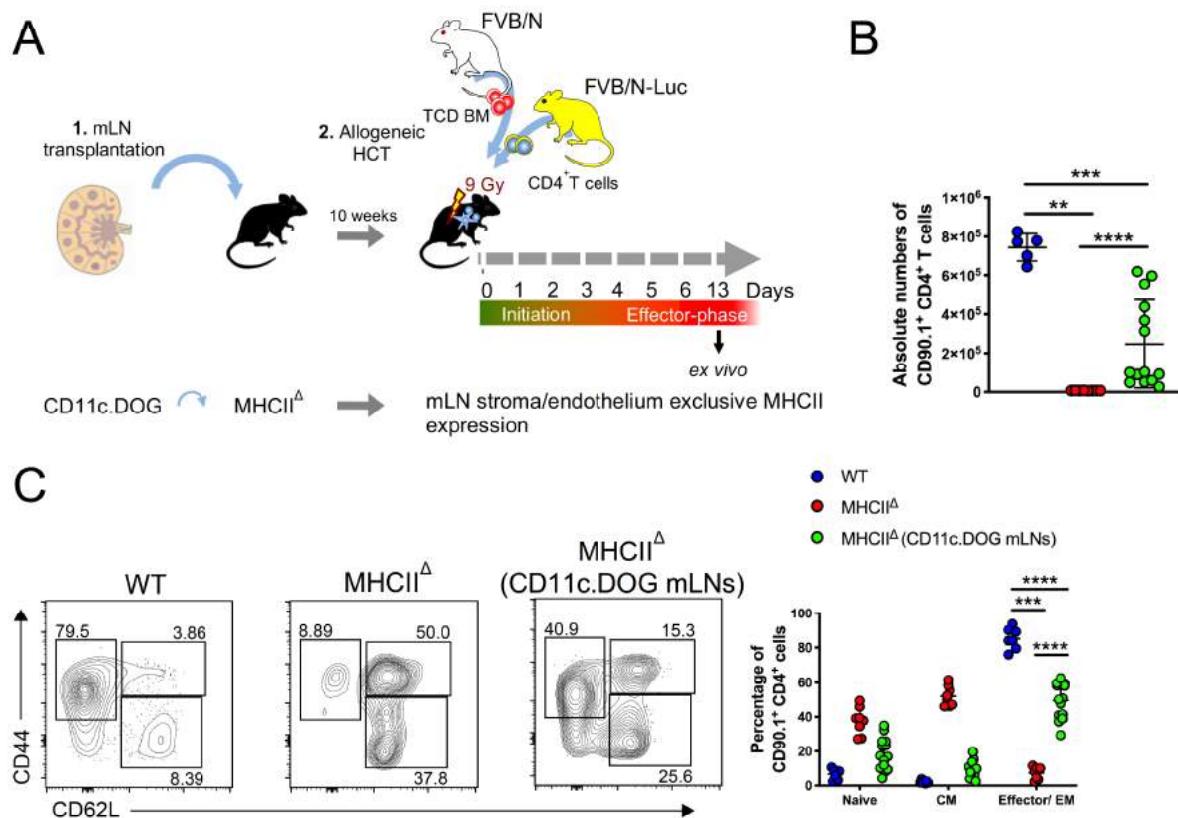


Figure 4.19 Alloreactive CD4⁺ T cells activate in MHCII^Δ mouse transplanted with mLNs of CD11c.DOG mouse.

(A) Experimental strategy: mLNs of B6.MHCII^Δ mouse were surgically removed and transplanted with donor mLNs from B6.CD11c.DOG mice that had been depleted of CD11c⁺ cells by i.p. administration with diphtheria toxin 20 ng/gram body weight day -5 until the day of surgery. 10 weeks post-surgery MHCII^Δ (CD11c.DOG mLNs), untreated B6.WT and MHCII^Δ mice were myeloablatively irradiated with 9 Gy and i.v. transplanted with 5×10^6 T cell-depleted (TCD) BM and 5×10^6 CD4⁺ T cells from MHCII^Δ and FVB.L2G85 mice respectively and analyzed on day +13 of allo-HCT. (B) Absolute numbers of donor CD90.1⁺ CD4⁺ in the spleen. (C) CD44 and CD62L expression profile of alloreactive CD4⁺ T cells to differentiate EM/effector, CM and naive cells and their quantification. Each data point represents one mouse analyzed in three experiments. Unpaired non-parametric Mann-Whitney test, (Mean \pm SD); ***p* < 0.01, ****p* < 0.001 and *****p* < 0.0001.

Furthermore CD4⁺ T cells in the MHCII^Δ recipients showed a naïve phenotype (CD62L^{high}CD44^{low}) and the MHCII^Δ with CD11c.DOG mLNs showed effector phenotype (CD62L^{low}CD44^{high}) (**Figure: 4.19c**). Collectively these results clearly indicated that a subset of LNSCs has the capacity to prime alloreactive CD4⁺ T cells in aGvHD inflammatory setting.

4.5 MHC class II on reticular stromal cells

4.5.1 FRCs moderately prime CD4⁺ T cells in the initiation phase of aGvHD

LNSCs have been shown to regulate MHCII expression via IFN γ [22]. We treated B6.WT mouse subcutaneously (s.c.) with PBS or 3 μ g of IFN γ for 6 days and measured the expression of MHCII on LNSCs. Here we could clearly see that IFN γ administration induced MHCII expression on LNSCs (**Figure: 4.20a, b**).

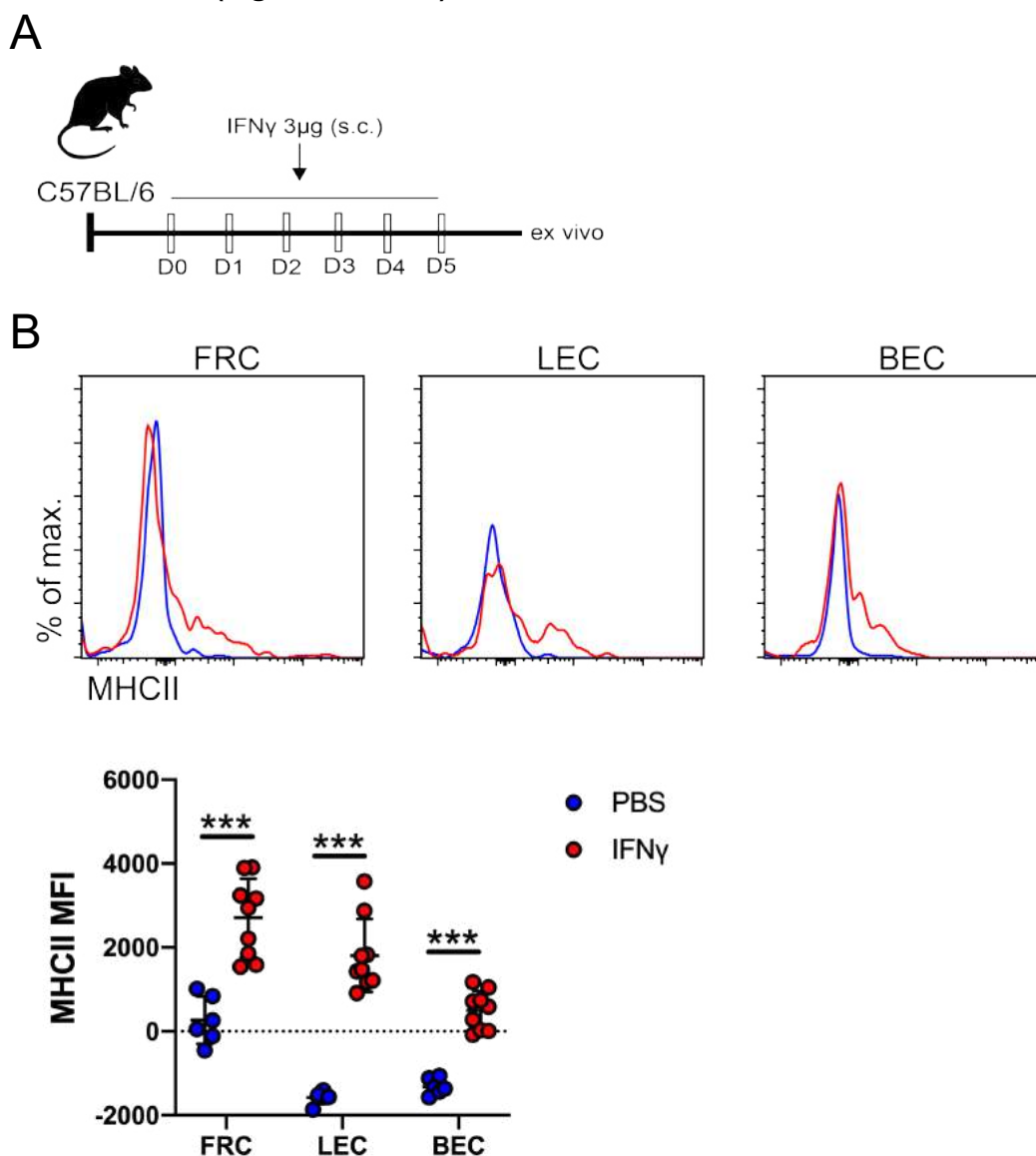


Figure 4.20 LNSCs upregulate MHC class II upon treatment with IFN γ .

(**A**) Experimental strategy: B6 mice were either treated with PBS or 3 μ g of IFN γ for 6 days subcutaneously (s.c.). (**B**) Expression of MHCII on FRC, LEC and BEC upon treatment with IFN γ and quantification. Each data point represents one mouse analyzed in two experiments. Statistics are according to unpaired non-parametric Mann-Whitney test, (Mean \pm SD); *** p < 0.001.

To study MHCII class II antigen presentation by FRCs in aGvHD, first, we performed mixed lymphocyte reaction (MLR). In these experiments, we FACS sorted $\text{Pdpn}^+\text{CD31}^-$ FRCs from B6 mice that were pre-treated with $\text{IFN}\gamma$ for 6 days prior to cell sorting to boost MHCII expression and cultured them with allogeneic naïve CD4^+ T cells from BALB/c mice for 5 days. FRCs from BALB/c mice served as a syngeneic control (**Figure 4.21a**).

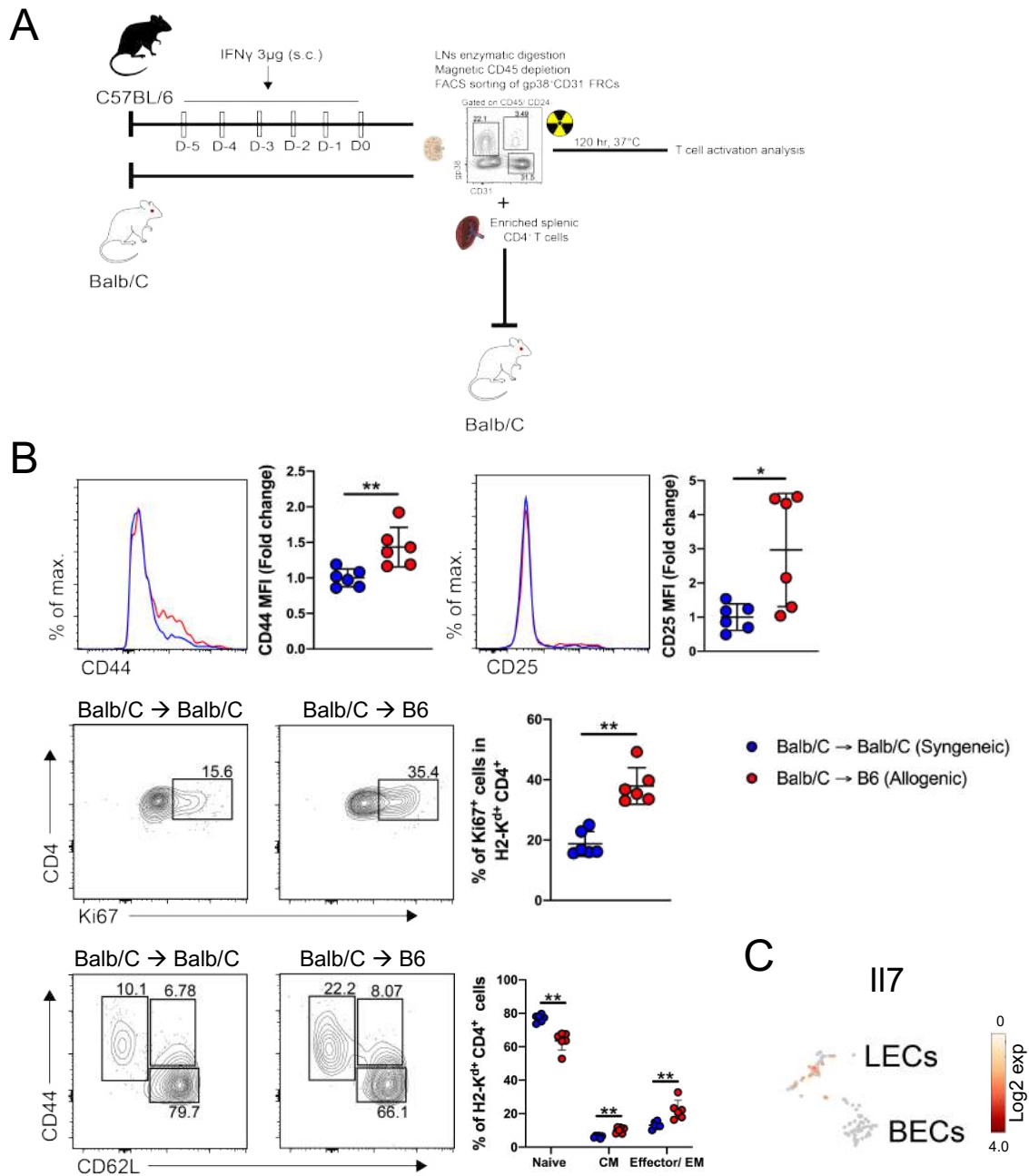


Figure 4.21 Alloreactive CD4^+ T cells are activated by allogeneic FRCs in a mixed lymphocyte reaction.

(A) Experimental strategy: B6 mice were s.c. injected with $\text{IFN}\gamma$ from day -5 until day -1. Lymph nodes from $\text{IFN}\gamma$ treated B6 and untreated BALB/c mice were pooled, isolated and magnetically depleted of CD45 cells and FACS sorted for $\text{gp38}^+\text{CD31}^-\text{CD45}^-$ CD24^- followed by irradiation. FRCs were cultured with alloreactive CD4^+ T cells from BALB/c mouse at 1:1 ratio of 1×10^4 cells for 5 days at 37°C . (B) Flow cytometry analysis of alloreactive CD4^+ T cells gated on CD4^+ and H2-K^{d} population for T cell activation (CD25 , CD44) and proliferation (Ki67) markers. (C) Expression of IL7 on LECs and BECs on scRNA sequencing dataset. Unpaired non-parametric Mann-Whitney test, (Mean \pm SD); * $p < 0.05$ and ** $p < 0.01$.

We observed dramatic upregulation of the T cell activation markers CD25 and CD44, this upregulation led to proliferation of CD4⁺ T cells and differentiation into effector cells (CD44^{hi}CD62L⁻), which was significantly higher compared to CD4⁺ T cells cultured with BALB/c FRCs (syngeneic control) (**Figure 4.21b**). These experiments were further performed with FACS sorted LECs, BECs and DNCs, however in these cultures CD4⁺ T cells failed to survive and proliferate, possibly because of the absence of IL-7 that is secreted majorly by FRCs minimally by LECs and not at all by BECs (**Figure 4.21c**).

To elucidate the role of MHC class II on FRCs in relation to alloreactive CD4⁺ T cells we generated MHCII^{ΔCcl19} mice. A Ccl19-intrinsic deletion of MHC class II on all *Ccl19* expressing stromal and stromal reticular cells was possible by crossing mice with floxed *H2-Ab1* gene (*H2-Ab1^{fl}*) with mice expressing Cre recombinase under the control of *Ccl19* promoter (*Ccl19^{Cre}*).

During initiation phase of aGvHD (day 3 after allo-HCT) we could not see significant differences of alloreactive CD4⁺ T cell activation between MHCII^{ΔCcl19} and WT recipient mice utilizing the FVB→B6 allo-HCT model (**Figure 4.22a**). Absolute numbers of donor CD4⁺ T cells in the spleen (**Figure 4.22b**), activation molecules CD44 and CD25 (**Figure 4.22c**) as well as proliferation marker Ki67 (**Figure 4.22d**) were marginally reduced in the MHCII^{ΔCcl19} mice as compared to WT littermates: *H2-Ab1^{fl}*.

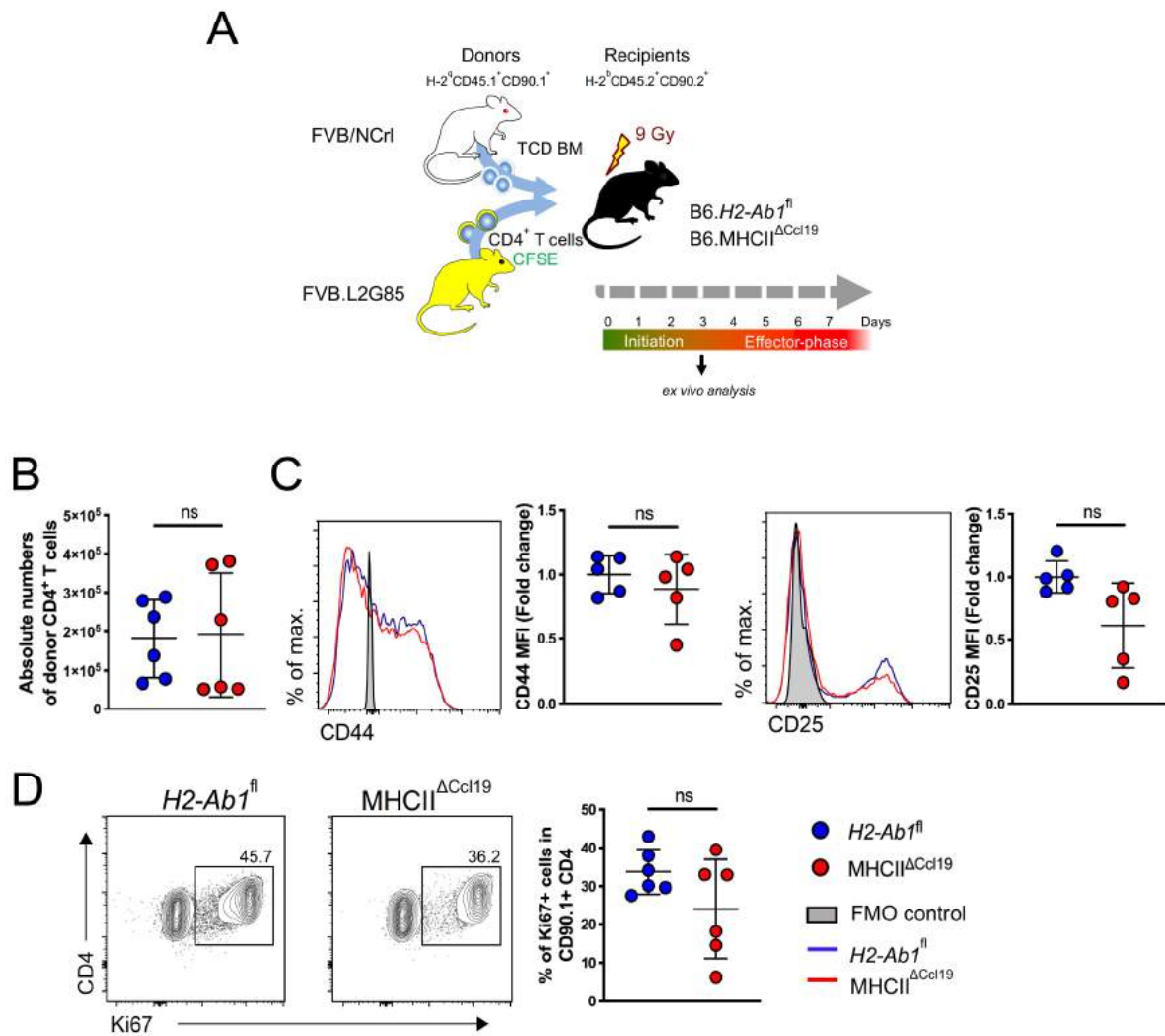


Figure 4.22 Alloreactive CD4⁺ T cells proliferation is slightly decreased in MHCII^{ΔCcl19} mice during aGvHD initiation. (A) Experimental strategy: B6.H2-Ab1^{fl} (WT littermates) or B6.MHCII^{ΔCcl19} recipients were myeloablatively irradiated with 9 Gy and i.v. transplanted with 5x10⁶ T cell-depleted (TCD) BM and 5x10⁶ CD4⁺ T cells from FVB/N and FVB.L2G85 mice respectively and analyzed day+3 of allo-HCT. (B) Absolute numbers of CD4⁺CD90.1⁺ T cells in spleen day+3 of allo-HCT. (C) Expression of CD44 and CD25 on donor T cells (CD90.1⁺ and CD4⁺). (D) Proliferative capacity of donor CD4⁺ T cells analyzed by expression of Ki67 on day+3 after allo-HCT. Each data point represents one mouse analyzed in two experiments. Unpaired non-parametric Mann-Whitney test, (Mean± SD).

Moreover, to further study direct antigen presentation by FRCs to alloreactive CD4⁺ T cells, we employed an OVA transgenic model of iFABP-tOVA mice [144] (**Figure 4.23a**), which express a truncated OVA on intestinal epithelial cells and ectopically on FRCs (**Figure 4.23b**). When OTII specific CD4⁺ T cells from B6.Rag^Δ.OTII.L2G85 mice were adoptively transferred into myeloablatively irradiated B6.CD11c.DOG mice expressing OVA on CD11c⁺ cells, they excessively proliferated in the mLNs within 72 hours, however OT-II T cells failed to proliferate in the mLNs of B6.iFABP-tOVA mice (**Figure 4.23c, d**), indicating that FRCs could process antigens via MHC class II machinery but they were unable to directly activate alloreactive OT-II CD4⁺ T cells in this model.

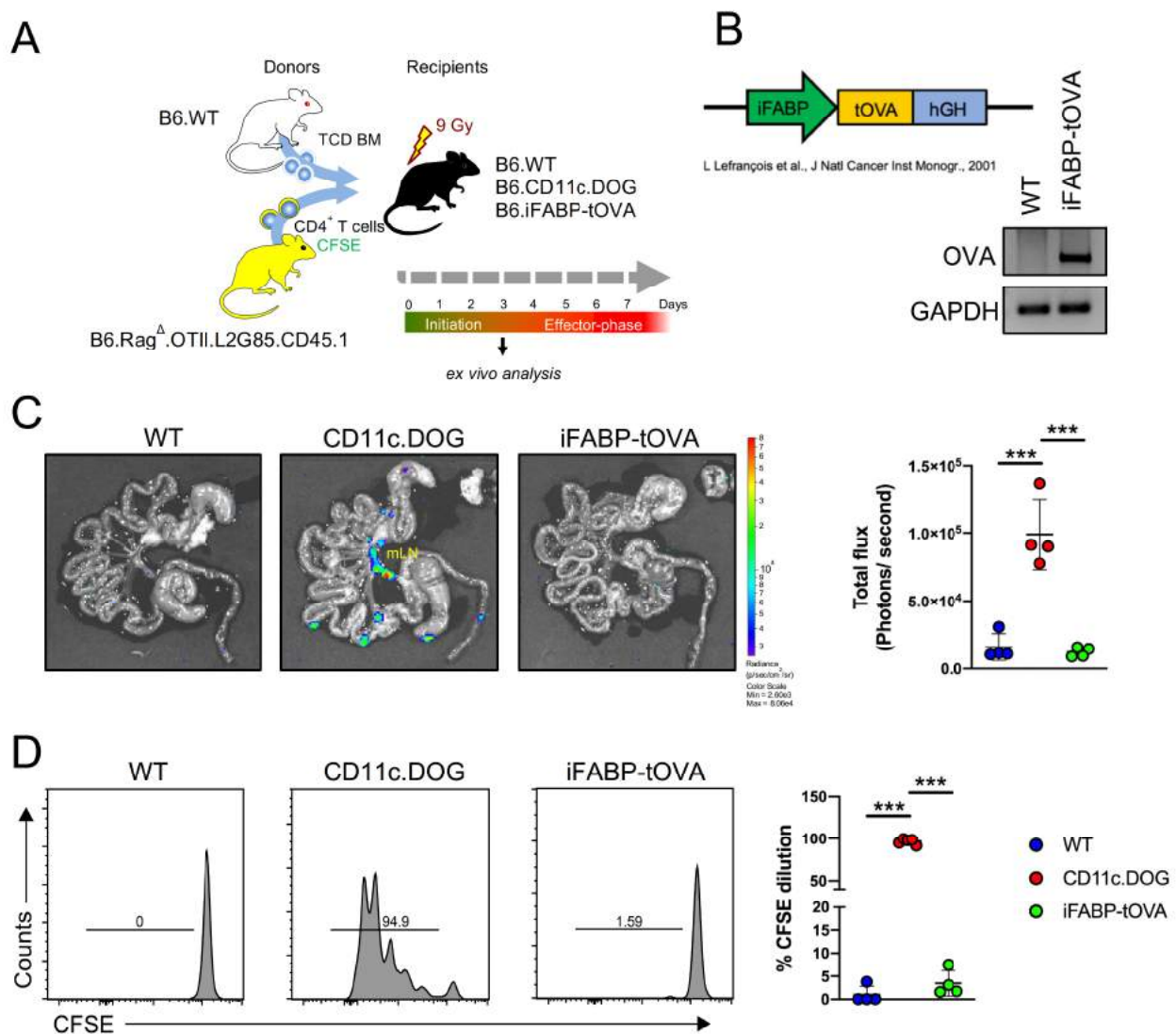


Figure 4.23 Naïve OT-II T cells do not proliferate in the SLOs of iFABP-tOVA mouse.

(**A**) Experimental strategy: B6.WT, B6.CD11c.DOG and B6.iFABP-tOVA recipients were myeloablatively irradiated with 9 Gy and transplanted i.v. with 5×10^6 T cell-depleted (TCD) BM and 1×10^6 OT-II CD4⁺ T cells from B6.WT or B6.Rag^Δ.OTII.L2G85 mice, respectively and analyzed day+3 of allo-HCT. (**B**) Transgene layout of B6.iFABP-tOVA mice and RT-PCR of OVA and GAPDH as house-keeping gene from FACS sorted FRCs from B6.WT and iFABP-tOVA mouse. (**C**) BLI signal from adoptively transplanted OT-II T cells and quantification from mLN on day+3 of allo-HCT. (**D**) Proliferative capacity of donor OT-II CD4⁺ T cells analyzed by CFSE dilution and quantification at day+3 after allo-HCT. Each data point represents one mouse analyzed in two experiments. Unpaired non-parametric Mann-Whitney test, (Mean \pm SD); *** $p < 0.001$.

4.5.2 MHC class II on FRCs plays an immune-modulatory role during the effector phase of aGvHD

As FRCs did not strongly influence alloreactive CD4⁺ T cell activation *in vivo* during the initiation phase of aGvHD, we further assessed the role of FRCs MHC class II during the effector/ symptomatic phase of aGvHD (day 30 of allo-HCT). RNA sequencing of alloreactive CD4⁺ T cells at this time-point revealed significant enrichment of genes involved in mitosis (*Cdkn1a*, *Cks1b*, *Pclaf*, *Dnase1l3*, *Cenpf*, *Cenpe* and *Cdkn3*) active chromatin (*H2Az1*, *H2Az2*, *Hmgn2*, *H1f0*, *Kn11*, *Smc2*, *Tacc3*, *Topa2* and *Nusap1*), growth and cellular differentiation (*Lif*, *Nr2c2*, *Sgms2*, *Iqsec1*, *Brca2* and *Zbtb20*) suggesting that CD4⁺ T cells in MHCII^{ΔCcl19} were in higher activation state comparatively to WT littermates. On the contrary allogeneic CD4⁺ T cells in MHCII^{ΔCcl19} mice down-regulated genes involved in: glucose metabolism (*Shpk*, *Ust*, *Slc2a2*, *Galm*, *Tktl2*, *Tnfrsf1b*, *Lfng*, *Runx2*) – suggesting T cell utilizing alternate metabolic pathway to support biosynthesis, anti-proliferative proteins (*Btg2*, *S1pr5* and *Ifitm1*), gene involved in cell adhesion and extracellular matrix (*Ccdc80*, *P4ha1*, *Ifitm1*, *Galnt6* and *Tmprss6*) as well gene signature for invariant natural killer T (iNKT) cells (*Klrd1*, *Klrk1*, *Klrc1*, *Klrc2* and *Klri2*) – suggesting loss of iNKT cells in MHCII^{ΔCcl19} mice (**Figure: 4.24a, b**).

At this time-point allogeneic CD4⁺ T cells in the MHCII^{ΔCcl19} mice up-regulated effector molecules such as CD44, CD127 and more CD4⁺ T cells cells were proliferating (Ki67 expression), however at this time-point the T cell exhaustion marker (PD-1 and Lag3) as well as the expression of Th1 cytokines (TNF α and IFN γ) did not differ in MHCII^{ΔCcl19} mouse from the WT littermates: *H2-Ab1^{fl}* (**Figure: 4.25a, b, c, f**). Notably, in MHCII^{ΔCcl19} allo-HCT recipients Treg frequencies were reduced (**Figure: 4.25d**).

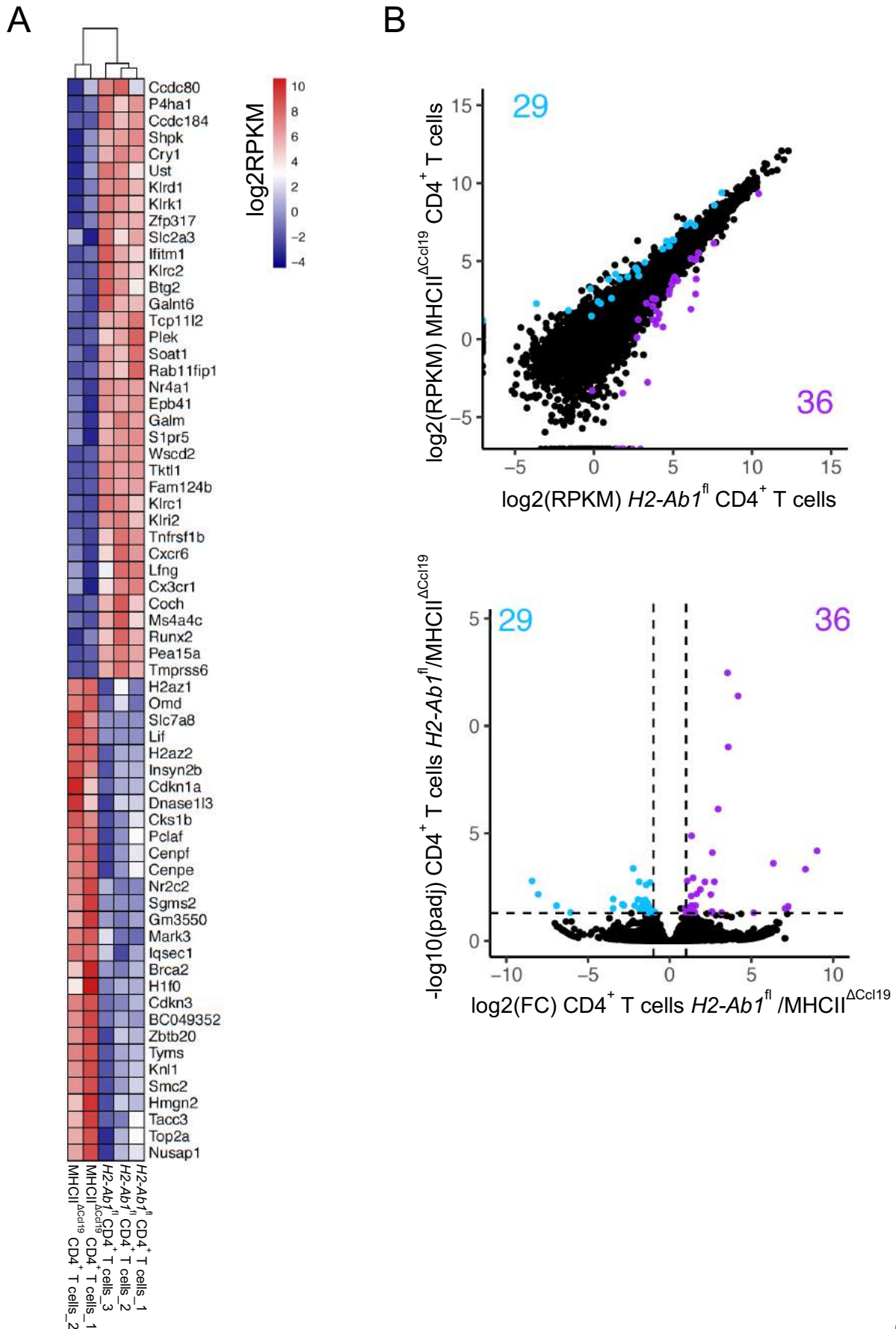
When we assessed the phenotype in the later stages of aGvHD (day 60 of allo-HCT), MHCII^{ΔCcl19} mice showed exacerbated aGvHD with significantly higher expression of activation markers (CD44 and CD127), T cell proliferation (Ki67⁺ donor T cells) and down-regulated T cell exhaustion molecules (PD-1 and Lag3) (**Figure: 4.26a, b**). This corresponded with overall poor survival of MHCII^{ΔCcl19} mice as compared to the *H2-Ab1^{fl}* littermates (**Figure: 4.26c**).

4.5.3 FRCs MHC class II regulate donor Tregs during aGvHD effector phase

To further dissect the role of FRCs MHCII in maintenance of donor Tregs, we performed allo-HCT experiments transplanting TCD BM, Tregs (CD25^{hi}, CD4⁺) along with CD4⁺ T cells from FVB/NCrl and FVB.L2G85 mice, respectively (**Figure: 4.27a**). Survival experiments revealed long-term protection against GvHD in *H2-Ab1^{fl}* mice that received Tregs. However, MHCII^{ΔCcl19} recipients despite receiving donor Tregs succumbed to aGvHD mice similar to *H2-Ab1^{fl}* controls that had not received Tregs (**Figure: 4.27b**). Furthermore, in MHCII^{ΔCcl19} recipients, non-invasive *in vivo* BLI imaging revealed stronger alloreactive CD4⁺ T cell proliferation during the initial 30 days of allo-HCT (**Figure: 4.28a**). This was accompanied by higher levels of the proinflammatory cytokine TNFα (**Figure: 4.28b**) as well as the expression of CD44, effector/EM cells (CD44^{hi}CD62L⁻) and Ki67 expression in MHCII^{ΔCcl19} mice on day +60 of allo-HCT (**Figure: 4.28c**), promoting GvHD-related tissue damage and eventually poor survival (**Figure: 4.27b**). To further test, whether MHC class II expression of FRCs maintains donor Tregs after allo-HCT we transplanted splenocytes and BM from an OT-II mouse into myeloablatively irradiated CD11c.DOG mice to activate OT-II T cells *in vivo* in antigen specific conditions, yet allo-HCT-like inflammatory conditions. 14 days after syn-HCT, antigen-specific CD4⁺ OT-II T cells were enriched from SLOs and adoptively transferred into a WT or iFABP-tOVA mouse (**Figure: 4.29a**). Day +6 after this second cell transfer, we clearly observed higher expression of Ki67 on Tregs (CD45.1⁺CD4⁺FoxP3⁺) and to some extent on Tcons (CD45.1⁺CD4⁺) spleen (**Figure: 4.29d**) and LNs (**Figure: 4.29e**). Thus, indicating that indeed MHC class II on FRCs plays a role in maintenance of Tregs on the effector phase of GvHD. Subsequently, we used a different approach to study FRCs and their direct role in GvHD. To this end, we generated Ccl19.iDTR mice. and to some extent on Tcons (CD45.1⁺CD4⁺) in lymph nodes (**Figure: 4.28b, c**) and spleen (not shown). Thus, indicating that indeed MHC class II on FRCs plays a role in maintenance of Tregs during the effector phase of aGvHD. Subsequently, we used a different approach to study FRCs and their direct role in aGvHD. To this end, we generated Ccl19.iDTR mice. A Ccl19-intrinsic expression of fl-STOP-fl-iDTR cassette that after recombination results in the deletion of STOP codon leading to cells susceptible to depletion by administration of DTx (**Figure: 4.30a**). In these experiments, FRCs were depleted prior to the induction of aGvHD at days -5 and -3 before allo-HCT (**Figure: 4.30b**). FRCs depletion in allo-HCT recipients resulted in fast onset of lethal aGvHD the DTR+Cre+ mice with drastically worse survival ($p=0.088$) compared to control recipients (**Figure: 4.30c**), further indicating the crucial role of FRCs in maintaining the lymphoid organs niches.

Figure 4.24 RNA sequencing revealed genes involved in mitosis were enriched whereas glucose pathways were down-regulated in MHCII^{ΔCcl19} mice at the effector phase of allo-HCT.

(A) Heat-map of highly differentially expressed genes (DEGs). **(B)** DEGs are highlighted in scatter and in volcano plot. Few DEGs at lenient cutoff of $|\log_2FC| = 0.75$ & $p_{adj} < 0.05$. Gene Ontology analysis was not insightful due to low number of DEGs.



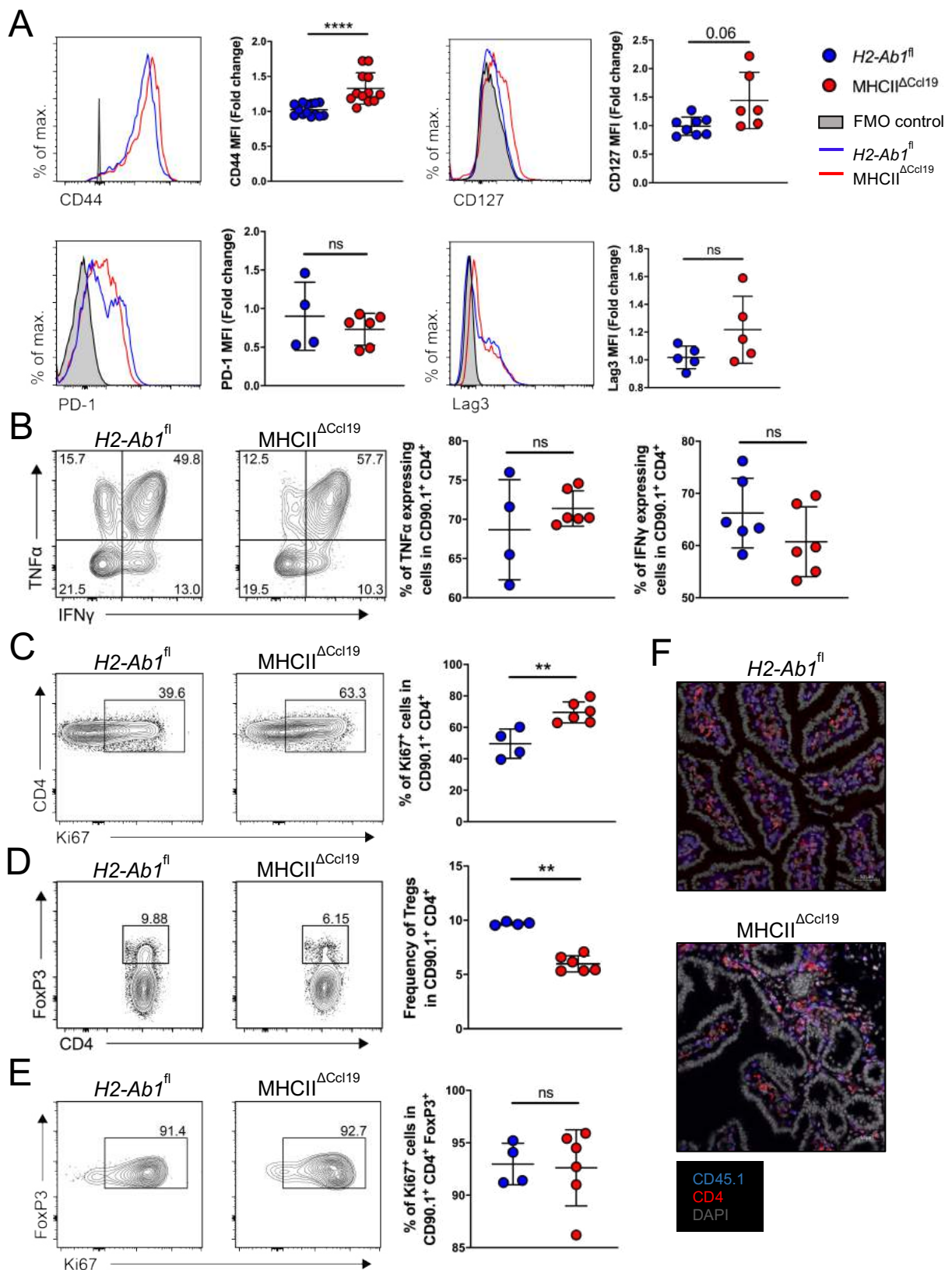


Figure 4.25 Alloreactive CD4 $^{+}$ T cells upregulate effector molecules whereas FoxP3 $^{+}$ CD4 $^{+}$ Tregs are reduced during the GvHD effector phase in MHCII $\Delta Ccl19$ recipient mice.

(A) Expression of effector molecules (CD44, CD127) and exhaustion molecules (PD-1, Lag3) on day +30 after allo-HCT on CD4 $^{+}$ CD90.1 $^{+}$ T cells in spleen of $H2-Ab1^{fl}$ and MHCII $\Delta Ccl19$ mice. (B) Expression of effector cytokines TNF α and IFN γ . (C) Expression of Ki67. (D) Frequency of FoxP3 $^{+}$ CD4 $^{+}$ CD90.1 $^{+}$ donor Tregs in total donor CD4 $^{+}$ CD90.1 $^{+}$ in spleen. (E) Expression of Ki67 in FoxP3 $^{+}$ CD4 $^{+}$ CD90.1 $^{+}$ cells. (F) Confocal immunofluorescence imaging of CD45.1 and CD4 of the small intestines (SI) at day +30 after allo-HCT. Each data point represents one mouse analyzed in two experiments. Unpaired non-parametric Mann-Whitney test, (Mean \pm SD); ** p < 0.01 and **** p < 0.0001.

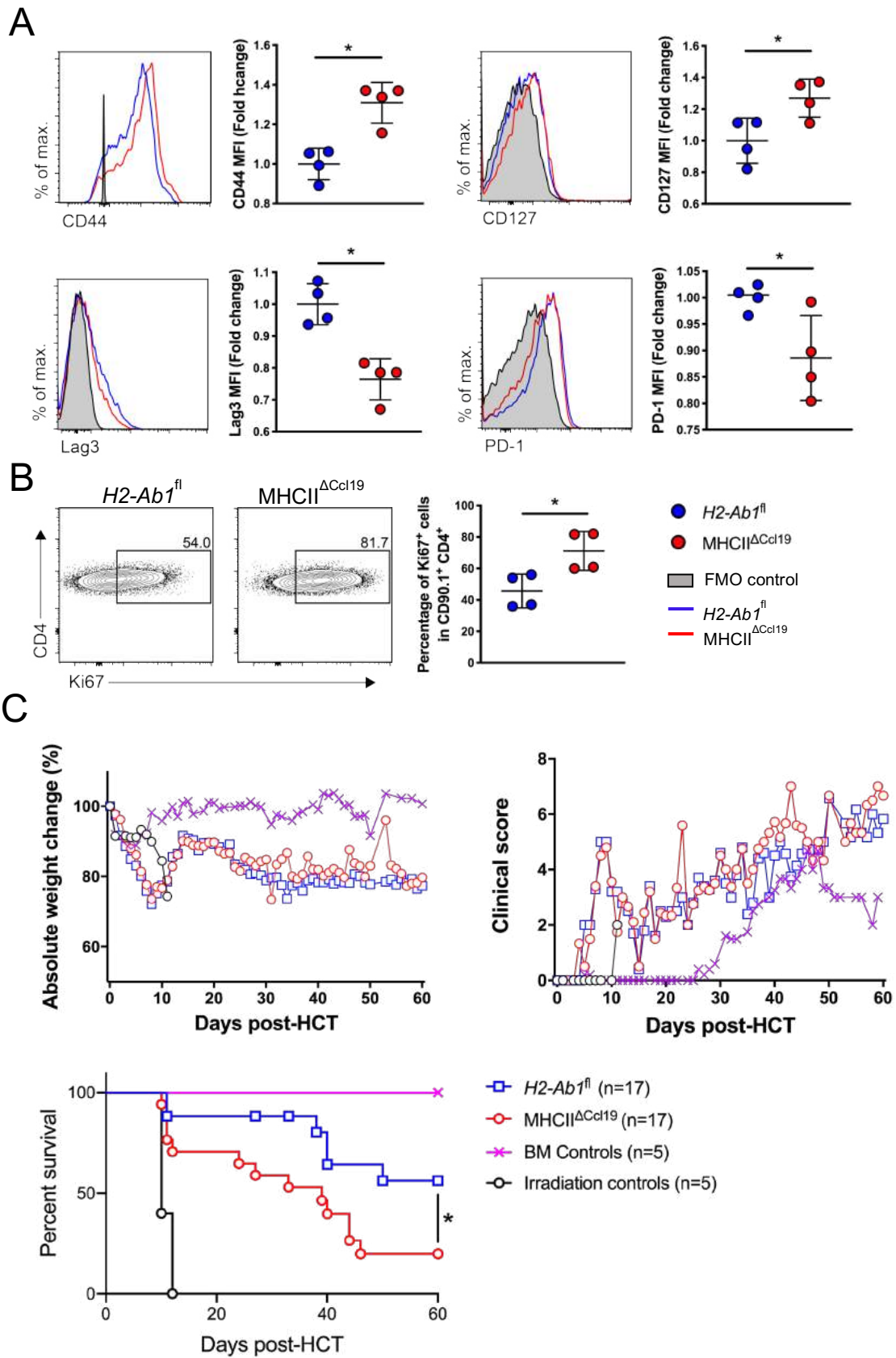


Figure 4.26 Exacerbated aGvHD in MHCII $\Delta Ccl19$ mice displaying enhanced effector molecule expression and poor survival. (A) Expression of effector molecules (CD44, CD127) and exhaustion molecules (PD-1, Lag3) on day +60 after allo-HCT on CD4⁺CD90.1⁺ T cells in spleens of $H2-Ab1^{fl}$ and MHCII $\Delta Ccl19$ recipient mice. (B) Expression of Ki67 in donor CD4⁺CD90.1⁺ T cells. Unpaired non-parametric Mann-Whitney test, (Mean \pm SD); * p < 0.05. (C) Survival, clinical score and weight of myeloablatively irradiated (9 Gy) B6. $H2-Ab1^{fl}$ and B6.MHCII $\Delta Ccl19$ mice transplanted with 5×10^6 allogeneic T cell-depleted (TCD) BM and 6×10^5 enriched CD4⁺ T cells from FVB/N mice.

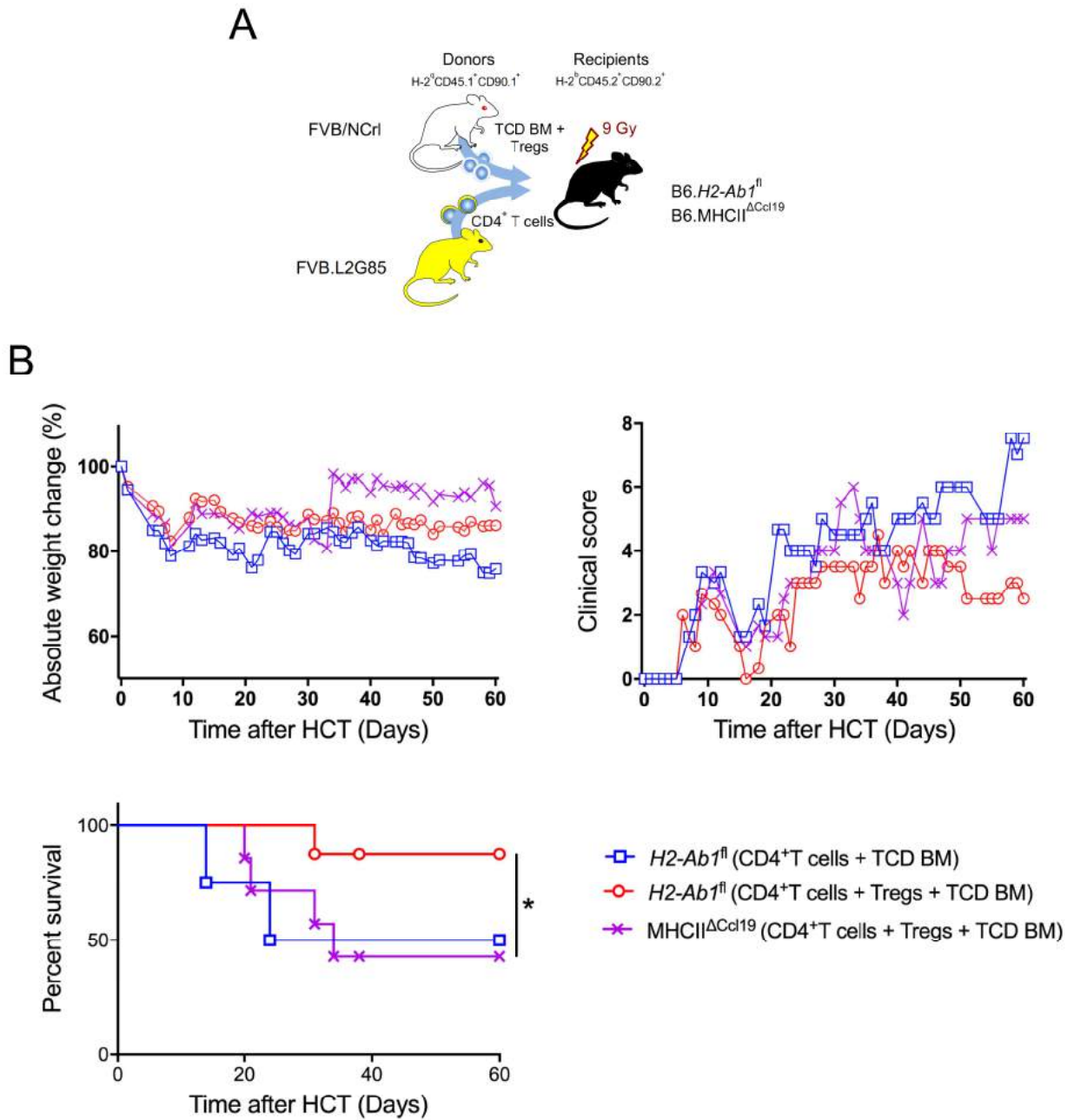


Figure 4.27 Tregs fail to protect $MHCII^{\Delta Ccl19}$ mice against GvHD.

(A) Experimental strategy: $B6.H2\text{-}Ab1^{fl}$ and $B6.MHCII^{\Delta Ccl19}$ recipients were myeloablatively irradiated with 9 Gy and i.v. transplanted with 5×10^6 TCD BM $\pm 0.3 \times 10^5$ regulatory T cells from FVB/N mice and 0.6×10^5 $\text{CD}4^+$ T cells from FVB.L2G85 mice. (B) Survival, clinical score and weight of myeloablatively irradiated (9 Gy) $B6.H2\text{-}Ab1^{fl}$ and $B6.MHCII^{\Delta Ccl19}$ mice ($n = 7$).

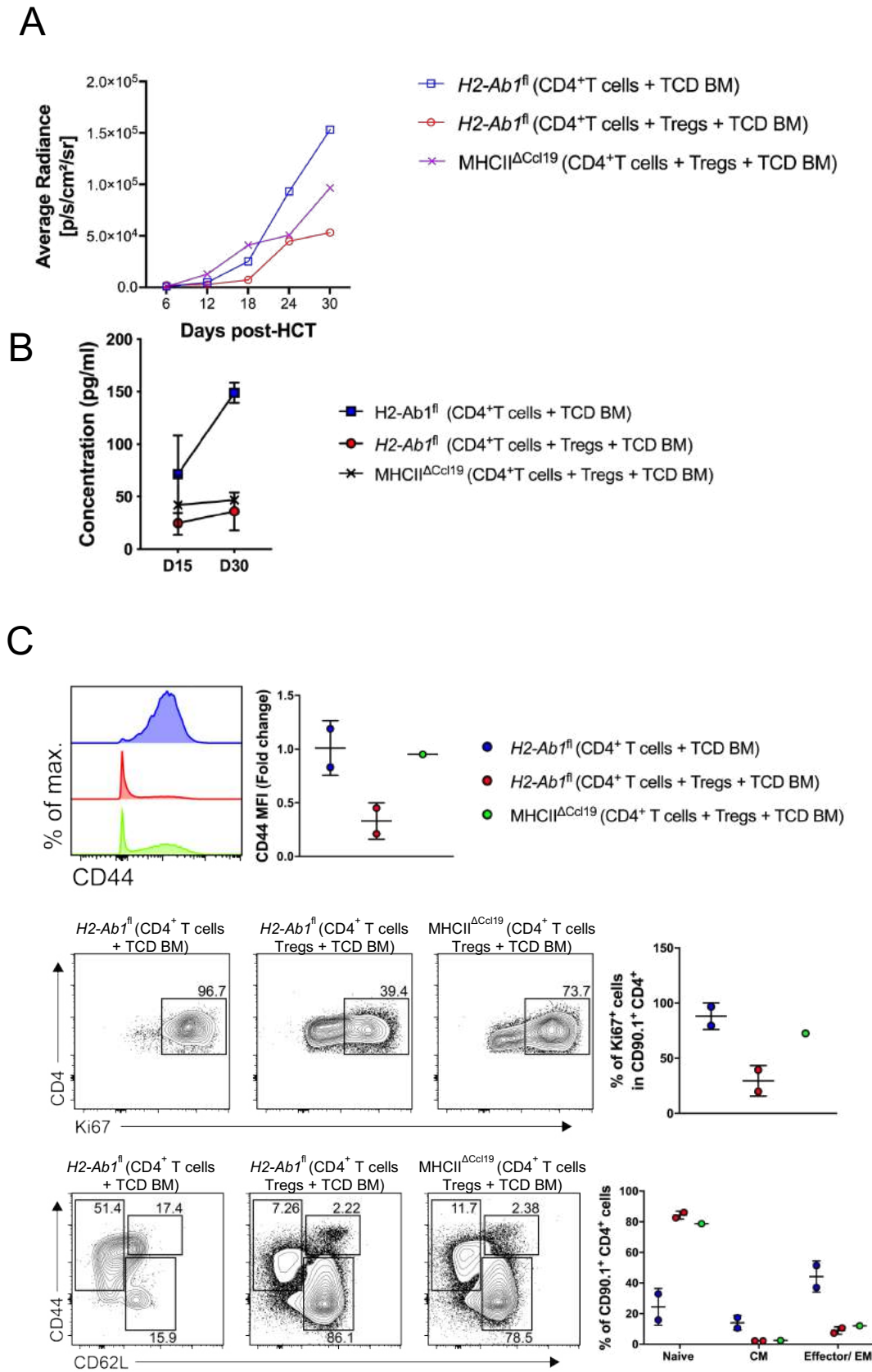


Figure 4.28 Alloreactive CD4⁺ T cells express higher levels of effector molecules in MHCII^{ΔCcl19} recipients that had been (A) *in vivo* bioluminescent imaging of shaved B6.*H2-Ab1^{fl}* ±Tregs and B6.MHCII^{ΔCcl19} Tregs recipients on day +6, +12, +24 and +30 of allo-HCT. (B) Concentration of TNFα in serum at day +15 and +30 of allo-HCT, measured by CBA. (C) Flow cytometry analysis of alloreactive CD4⁺ T cells gated on CD4⁺CD90.1⁺ population for T cell activation and proliferation markers on day +60 of allo-HCT in lymph nodes. Data analyzed from surviving mice on day +60 of allo-HCT.

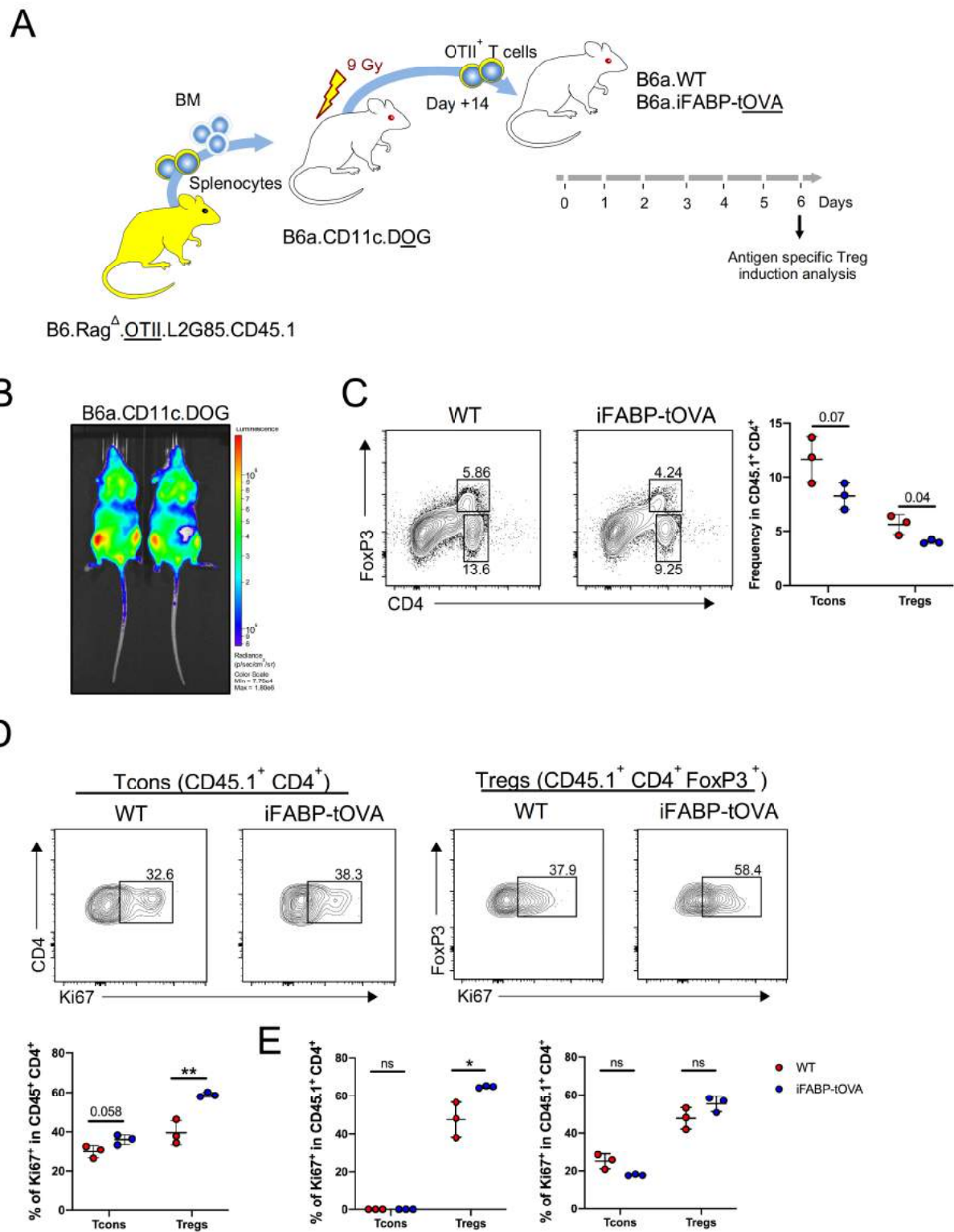
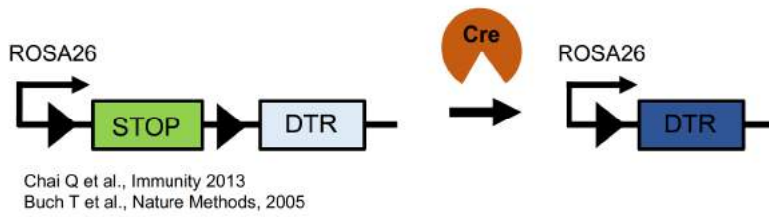


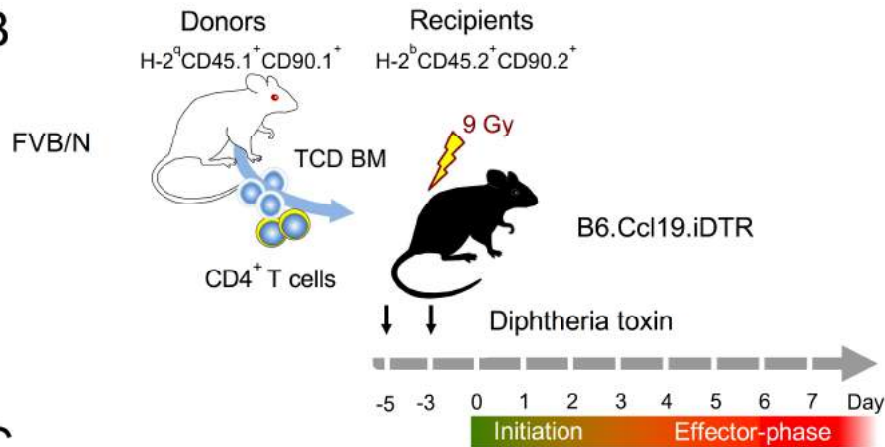
Figure 4.29 MHCII on FRCs supports the proliferation of pre-activated OT-II Tregs and moderately of Tcons in aGvHD like inflammatory conditions in iFABP-tOVA transgenic mice.

(A) Experimental strategy: B6.CD11c.DOG recipients were myeloablatively with 9 Gy and i.v. transplanted with 5×10^6 splenocytes and 5×10^6 BM cells from B6.Rag Δ .OTII.L2G85.CD45.1 mouse. At day +14 after syn-HCT mice were euthanized and CD4⁺ T cells were enriched from the spleen and LNs. Subsequently 1×10^7 enriched CD4⁺ T cells were transplanted into B6.WT or B6.iFABP-tOVA mice. (B) In vivo bioluminescent imaging of OT-II T cells in B6.CD11c.DOG mice at day +14 of syn-HCT. (C) Frequency of Tcons (CD45.1⁺CD4⁺) and Tregs (CD45.1⁺CD4⁺FoxP3⁺) in B6.WT and B6.iFABP-tOVA mice. (D) Expression of Ki67 on Tcons and Tregs at day +6 of adoptive transfer of OT-II CD4⁺ T cells in B6.WT and B6.iFABP-tOVA mice in spleen and in (E) mLNs and pLNs. Each data point represents one mouse. Unpaired parametric, 2-tailed Student's t test, (Mean \pm SD); **p < 0.01.

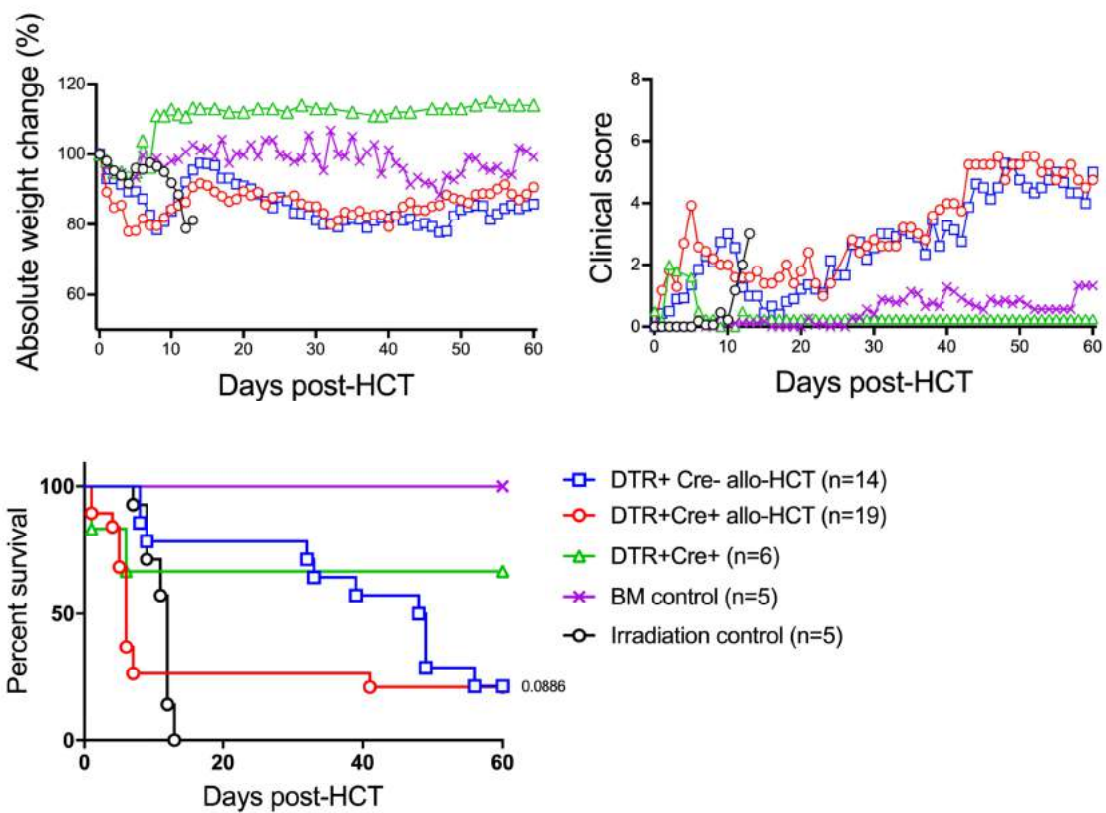
A



B



C



4.6 MHC class II on endothelial cells

4.6.1 Knock-out of MHC class II on endothelial cells results in improved clinical score and survival following GvHD

To study the role of MHC class II on LECs and BECs, the endothelial cells of the lymphoid organs in relation to alloreactive CD4⁺ T cells we generated MHCII^{ΔVE-Cadherin} mice. A VE-Cadherin-driven deletion of MHC class II on all VE-Cadherin-expressing endothelial cells resulted from crossing mice with floxed *H2-Ab1* gene (*H2-Ab1^{fl}*) with mice expressing Cre recombinase under the control of VE-Cadherin promoter (*VE-Cadherin^{Cre}*).

In the initiation aGvHD phase (day +3) (**Figure: 4.31a**), in the SLO of MHCII^{ΔVE-Cadherin} donor CD4⁺ T cells activation (CD44, CD25 MFI and effector/ EM, CM to naïve T cell ratio) and proliferation (Ki67 expression) was slightly decreased (**Figure: 4.31b**). However, knock-out of MHC class II on endothelial cells resulted in overall improved survival and a sub-clinical GvHD score following allo-HCT (**Figure: 4.32**) suggesting that VE-Cadherin expressing endothelial cells actively participate in CD4⁺ specific antigen presentation.

To further characterize MHC class II antigen presentation by LN endothelial cells we crossed MHCII^{ΔVE-Cadherin} mice with MHCII^{ΔVav1} mice. The resulting MHCII^{ΔVav1 ΔVE-Cadherin} mice lacked the capacity to present antigen via MHC class II by endothelial as well as by hematopoietic cells. Allogeneic CD4⁺ T cells from BALB/c mice when cultured with LNSC from MHCII^{ΔVav1 ΔVE-Cadherin} (**Figure: 4.33a**) did not upregulate activation markers in a preliminary experiment (**Figure: 4.33b**). Taken together these preliminary data support that VE-Cadherin expressing endothelial cells actively participate in specific antigen presentation to alloreactive CD4⁺ T cells.

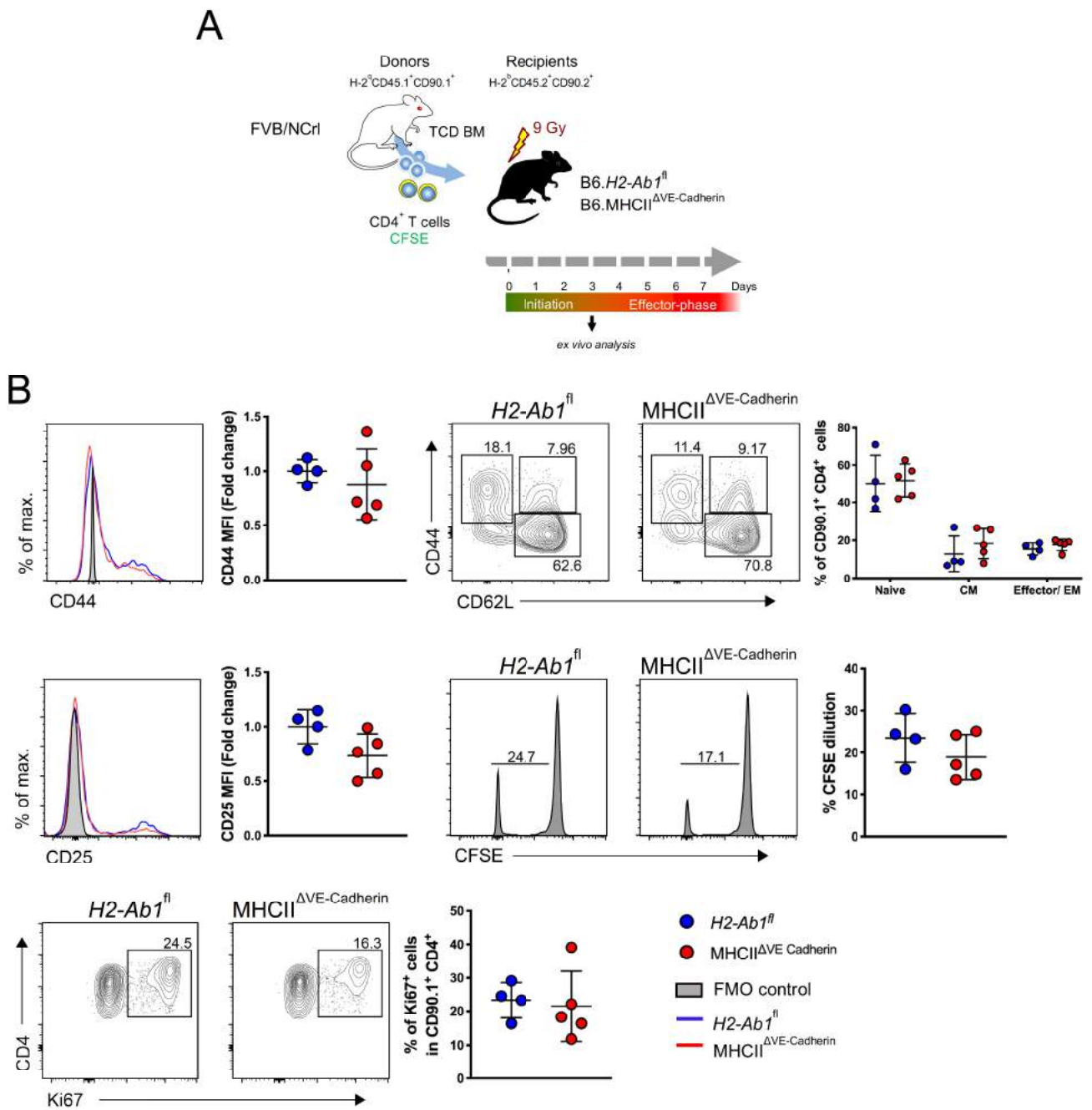


Figure 4.31 Alloreactive CD4⁺ T cell proliferation is moderately decreased in MHCII^{ΔVE-Cadherin} mouse in the initiation phase of aGvHD.

(A) Experimental strategy: B6.H2-Ab1^{fl} and B6.MHCII^{ΔVE-Cadherin} recipients were myeloablatively irradiated with 9 Gy and i.v. transplanted with 5x10⁶ T cell-depleted (TCD) BM and CFSE stained 5x10⁶ CD4⁺ T cells from FVB/NCr (B) Absolute numbers of CD4⁺CD90.1⁺ T cells in spleen day+3 of allo-HCT. (C) Expression of CD44 and CD25 on donor T cells (CD90.1⁺ and CD4⁺). (D) Proliferative capacity of donor CD4⁺ T cells analysed by expression of Ki67 and CFSE dilution day+3 of allo-HCT. One data point represents one mouse analysed in two experiments. Statistics are according to unpaired non-parametric Mann-Whitney test, (Mean± SD).

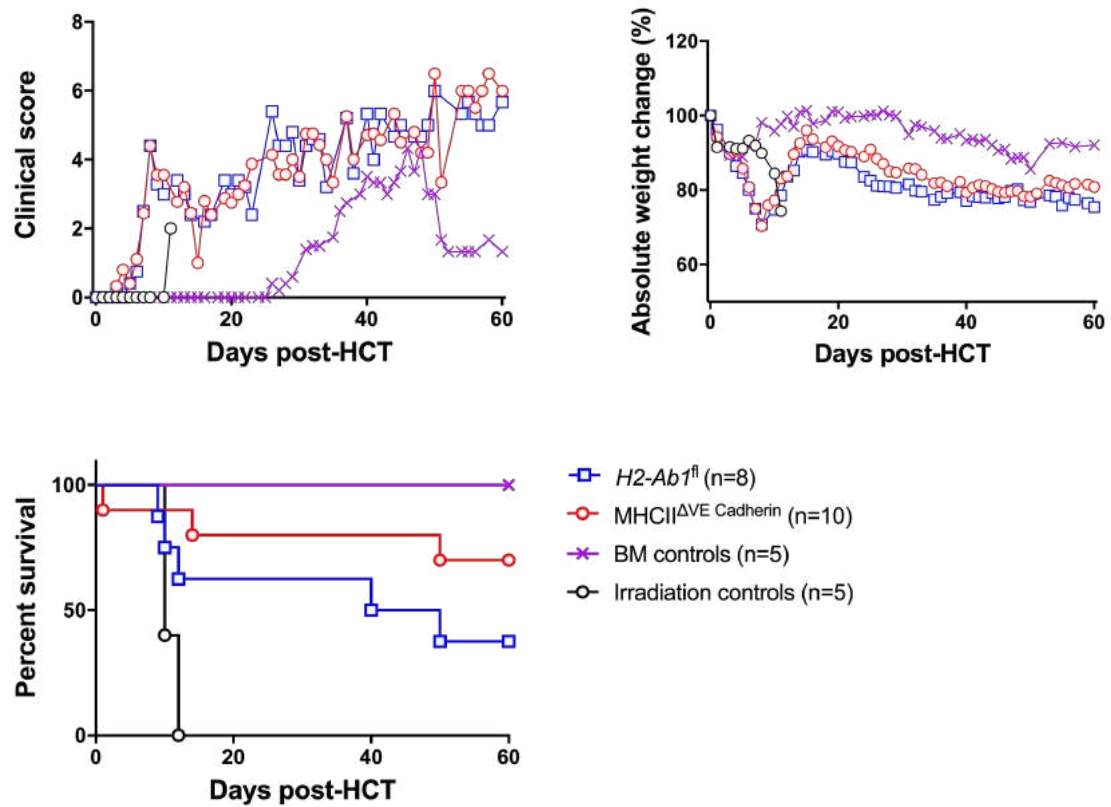
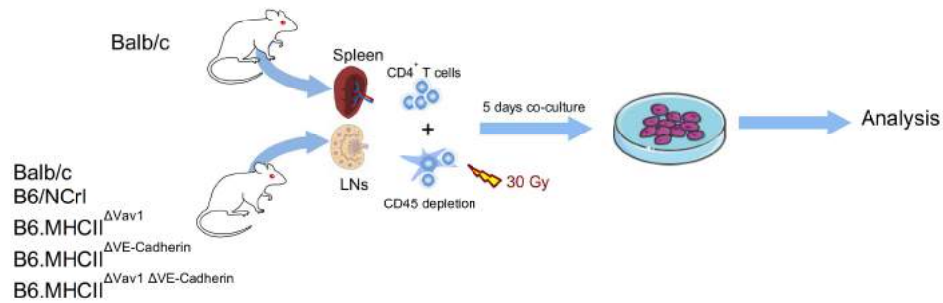


Figure 4.32 *MHCII^{ΔVE}Cadherin* mice trend toward improved survival subsequent to GvHD.

Survival, clinical score and weight of myeloablatively irradiated (9 Gy) B6.*H2-Ab1^{fl}* and B6.*MHCII^{ΔVE}Cadherin* mice.

A



B

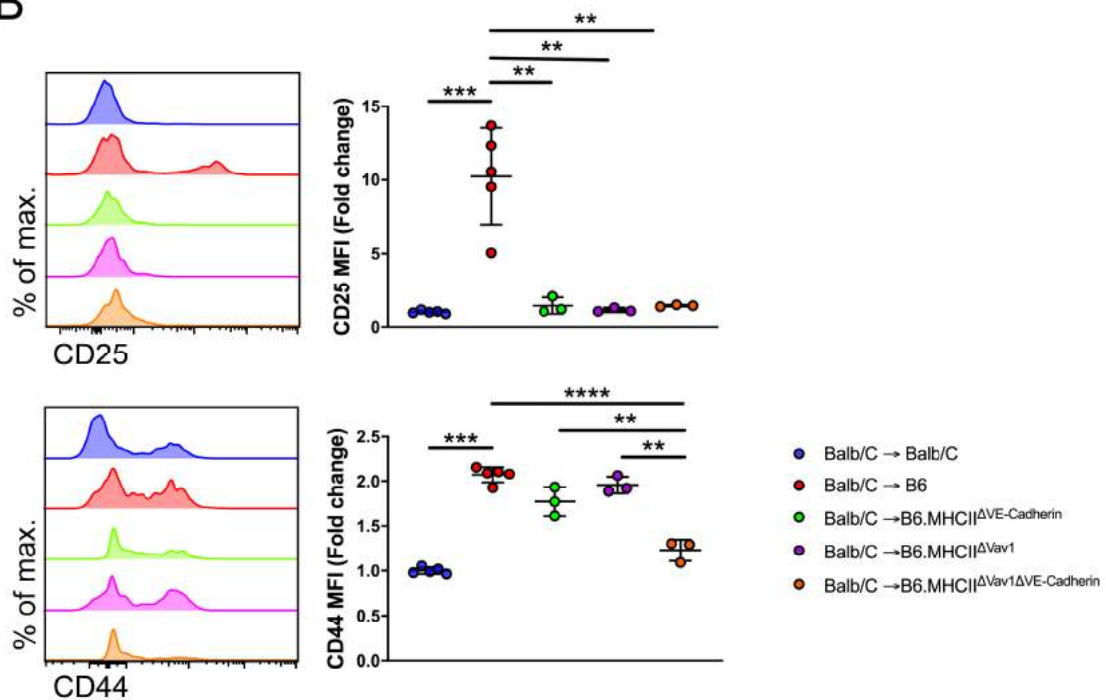


Figure 4.33 Allogeneic CD4⁺ are not activated by the LNSCs of MHCII^{ΔVav1ΔVE-Cadherin} mice in a mixed lymphocyte reaction. (A) Experimental strategy: Magnetically enriched CD4⁺ T cells (H-2^d) from BALB/c mice were cultured with the enzymatically digested, pooled lymph nodes and depleted of CD45 cells followed by irradiation from BALB/c, B6, B6.MHCII^{ΔVE-Cadherin}, MHCII^{ΔVav1} and MHCII^{ΔVav1 ΔVE-Cadherin} for 5 days at 37°C. (B) Flow cytometric analysis of alloreactive CD4⁺ T cells gated on CD4⁺ and H-2K^d population for T cell activation markers. Unpaired parametric, 2-tailed Student's t test, (Mean± SD); **p* < 0.05, ***p* < 0.01, ****p* < 0.001, *****p* < 0.0001.

5 Discussion

5.1 LNSCs process exogenous antigen and upregulate co-stimulatory receptors under inflammatory conditions

The role of LNSCs in regulating the innate and adaptive immune system has been well studied over the past few years [23, 145-147]. In the context of MHC class II antigen presentation, LNSCs particularly FRC and LEC have been shown to present self-antigen to CD4⁺ T cells leading to regulation of the immune response [15, 16, 20, 22, 111, 120, 121]. Here we asked how LNSCs respond to irradiation as a prototypic allo-HCT conditioning regimen. As FRCs are the most abundant LNSCs subset, first, we irradiated an immortalized FRC cell line (iFRCs) with 30Gy of irradiation and clearly observed an upregulation in the expression MHC class II (I-Ab, CD74), co-stimulatory molecules (CD40, CD80) as well as adhesion molecule (CD104) after 24 h that became further prominent after 72 h post-irradiation.

We further evaluated the influence of myeloablative irradiation on LNSCs *in vivo*. CD80 and CD86 were up-regulated within 24 h post lethal irradiation (9Gy) in B6.WT mice, however, we observed a sharp decrease in surface expression of MHCII by all subsets of LNSCs subsequent to irradiation. Others have shown that LNSCs express endogenous MHCII via MHC class II transactivator (CIITA) type IV and additionally acquire MHCII from dendritic cells by endocytosis [22, 120]. Indeed, we observed sharp loss/depletion of DCs from spleen and mLNs within 24 h after irradiation, implying that DCs are radiosensitive cells and their depletion results in the downregulation of MHC class II on FRC, LEC and BEC post-irradiation.

As LNSCs could express and upregulate co-stimulatory receptors we further probed whether LNSCs have the MHC class II machinery in place to degrade and present exogenous antigens. Indeed, FACS sorted FRCs, LECs and BECs could process DQ-OVA at 37°C. The antigen degradation and processing capability of LNSCs was comparable to that of splenic DCs (CD45⁺CD11c⁺MHCII⁺F4/80⁺CD64⁻). Taken together these experiments indicated that FRCs, LECs and/or BECs could serve as non-hematopoietic APCs in aGvHD inflammatory settings.

5.2 Alloreactive T cells home to and are activated in secondary lymphoid organs at the initiation phase of aGvHD

Acute GvHD is a life-threatening complication of hematopoietic stem cell transplantation (HCT), which is why it is crucial to study and identify the early events of aGvHD in pre-clinical animal models. Previously our group showed that SLOs are crucial for the induction of aGvHD as blocking T cell entry into specific SLOs, or ablating some of them was not sufficient to prevent aGvHD in mouse models and only by preventing alloreactive T cell entry to all SLOs

could completely abrogate the initiation of aGvHD [110]. These observations are key in the understanding of aGvHD pathophysiology. However, recently it has been proposed that naïve alloreactive CD4⁺ T cells can be primed by the intestinal epithelial cells (IELs) of the ileum [107]. To test our hypothesis that SLO are the primary sites of alloreactive T cell homing and activation, we performed allo-HCT utilizing (FVB → B6) major-mismatch GvHD model. Bioluminescence imaging at day 3, 4 and 6 of allo-HCT revealed that alloreactive T cells primarily home to the SLOs (spleen, lymph nodes and Peyer's patches) and are activated at these sites until day 3 of allo-HCT. Subsequently after activation, at days +3.5 to +4 day after allo-HCT, these T cells down-regulate CD62L and upregulate target organ specific homing receptors (CCR9, αEβ7, α4β7) and egress to target organs [110], which became visible by the distribution of bioluminescent signals of luc⁺ donor T cells in the *lamina propria*. Already by day +6 after allo-HCT the alloreactive T cells had entered the effector phase of aGvHD and had invaded the target organs: lung, liver and GIT followed by skin (not shown). When CFSE-stained alloreactive T cells were transferred into myeloablatively irradiated recipients we could clearly visualize a typical CFSE dilution curve of continuously proliferating cells in the SLOs (spleen and mLNs), whereas in the GIT we could only find few alloreactive T cells with a terminally diluted CFSE pattern at day +3 of allo-HCT indicating that these cells had not proliferated at these sites but rather had migrated to the GIT from SLOs. These observations further corresponded with 3D-LSFM imaging where we could only detect CD45.1⁺ alloreactive T cells in the Peyer's patches and at their direct borders at day 3 after allo-HCT. Collectively, these experiments suggest that during the initiation phase of aGvHD naïve alloreactive T cells home to SLOs and not to the gastrointestinal tract.

5.3 Allo-reactive CD4⁺ T cells are activated within the SLOs in the absence of professional MHC class II antigen presentation

Utilizing transgenic mouse models is a robust genetic approach and has several advantages over the use of antibodies [148] and other conventional methods [149] to study cellular and physiological functions of a certain molecule. To dissect the MHC class II antigen presentation by non-hematopoietic cells inflammatory settings of allo-HCT to induce CD4⁺ T cell mediated aGvHD, we employed *H2-Ab1*^{fl} mice [150], which possess a *loxP*-flanked neo cassette upstream of exon 1 and a single *loxP* site downstream of exon 1 of *H2-Ab1* locus. These mice when crossed with a Cre-expressing mouse under the control of a defined promoter will result in MHC class II knock-out on the respective cell types. Consequently, we crossed *H2-Ab1*^{fl} mice with *CD11c*-Cre mice [151] that resulted in the loss of MHCII antigen presentation by cells of the myeloid lineage in MHCII^{ΔCD11c} mice. Upon induction of aGvHD in these animals, alloreactive CD4⁺ T cells homed normally to the SLOs until day +3 after allo-HCT and showed

signs of activation and proliferation. However, the activation signal was significantly weaker than that of *Cre⁻ H2-Ab1^{fl}* littermates that presented a WT phenotype. Yet remarkably depletion of *CD11c⁺* prior to allo-HCT resulted in hyperactivation of alloreactive *CD4⁺* T cells in *CD11c.DOG* (diphtheria toxin, OVA, GFP) recipients. Furthermore, *MHCII^{ΔCD11c}* were initially protected but succumbed to aGvHD in the later stages, whereas due to hyperactivation of alloreactive *CD4⁺* T cells, *CD11c⁺* cell-depleted *CD11c.DOG* mice readily died within 10 days of aGvHD induction. Manipulating MHCII antigen presentation in *CD11c* cells resulted in apparently contradicting phenotypes in *MHCII^{ΔCD11c}* and *CD11c.DOG* mice. In *MHCII^{ΔCD11c}* mice, *CD11c* cells retain all other cellular functions, however, in *CD11c.DOG* mice diphtheria toxin kills the *CD11c^{hi}* cells, which also results in the loss of anti-inflammatory signals provided by these *CD11c* cells in an aGvHD inflammatory settings. Additionally, host DCs (*CD11c⁺*) have been shown to induce a high degree of donor alloreactive T cell death in SLOs [93] as we have found from a subset of host myeloid cells capable of suppressing T cell effector functions via PD-L1 in the GIT (Le DD *et al.*, unpublished data). As, *MHCII^{ΔCD11c}* mice did not provide comprehensive insights into non-hematopoietic antigen presentation of LNSCs due to the limitations of this model in which only a certain subset of myeloid cells is targeted, we next opted to employ BM chimeras. BM chimeras are a powerful tool and are routinely used in immunology as well as in other fields of biology, since they allow to explore the role of genes in distinct cell populations such as hematopoietic versus non-hematopoietic cells [152]. To further dissect the role of non-hematopoietic antigen presentation we generated *MHCII^Δ* chimeras by syngeneically transplanting 1×10^7 TCD BM cells from a B6.*MHCII^Δ* mouse into myeloablatively irradiated B6.WT mice whereas syngeneic B6.WT into B6.WT HCT recipients served as controls. However, to our surprise a B6.*MHCII^Δ* → B6.WT chimeras started to lose weight within 30 days after syn-HCT, displayed signs of autoimmune disease and developed a severe wasting disease. Huang and colleagues described that in MHC class II knock-out chimeras there is defective development of innate memory phenotype (IMP, *CD44^{hi}/CD62L^{low}*) *CD4⁺* T cells [135]. The functional development of IMP *CD4⁺* requires hematopoietic but not thymic MHC class II. In these *MHCII^Δ* → WT BM chimeras conventional Tregs are unable to suppress pathogenesis, whereas IMP *CD4⁺* T cells, which include conventional Tregs can suppress pathogenesis. Nevertheless, recent studies have utilized *MHCII^Δ* BM chimeras [107], [153] to study MHC II antigen presentation. We administered Gentamycin sulphate (1 mg/ml) in acidified water (pH 2.5 – 3) to delay the disease symptoms in these chimeras. However, while taking these precautionary measures it was not possible to perform long-term survival experiments with humane endpoints in these chimeras. Therefore, we could only analyze *CD4⁺* T cell activation during the initiation phase following allo-HCT. In these *MHCII^Δ* → WT BM chimeras, in complete absence of MHC class II antigen presentation from hematopoietic cells we were able to measure slight extent of alloreactive *CD4⁺* T cells activation and proliferation,

which was significantly reduced compared to WT → WT BM chimeras, nevertheless suggesting that the activation cues are given by non-hematopoietic APCs of the SLOs during the initiation phase of aGVHD.

5.4 Genetic targeting of lymph node stroma and endothelium

Stromal immunity is an emerging branch of immunology and seminal work has been done on characterization of lymph node stromal and endothelial cells in homeostasis and disease [146]. In the past two years several studies have characterized the LNSCs from spleen, LNs and PPs utilizing single cell RNA sequencing (scRNA sequencing) [136-138, 140]. To effectively target LNSCs we performed scRNA sequencing on steady-state FACS sorted LNSCs. Upon analysis on Loupe browser, we identified 9 clusters based on differentially expressed genes (DEGs) in each cluster on t-SNE distribution. At first glance, we could recognize known major LNSCs subpopulation, including BEC: $\text{Pdpn}^- \text{Pecam1}^+$, LEC: $\text{Pdpn}^+ \text{Pecam1}^+$ and non-endothelial cells stromal cells by $\text{Pdpn}^+ \text{Pecam1}^- \text{Ackr4}^-$. The PvCs (DNCs) were identified by their high expression of *Acta2*. TRCs being the prominent subset of LNSCs that are in direct contact and crosstalk with the T cells we utilized *Ccl19-Cre* [48] mice. One can also use *Ccl21-Cre* mice, however since *Ccl21* is also expressed by LEC, *Ccl19-Cre* mice is a far superior model to target the TRCs of LNs. *Ccl19-Cre* specifically targets the TRCs of SLOs and has been successful used to study FRCs biology [38, 124, 154, 155]. However, endothelial cells are difficult to target as certain genes are shared by hematopoietic and endothelial cell precursors during development stages [156]. In our scRNA analysis we could clearly distinguish cluster number 9 accumulating the endothelial cells: LEC and BEC. We could underpin LEC by their expression of $\text{Pecam1}^+ \text{Lyve1}^+ \text{Prox1}^+ \text{Ackr4}^+$ and Pdpn^+ , whereas BEC were identified by their expression profile of Esm1^+ and Igta1^+ . *Tie2* is a molecule that is shared by the cells of hematopoietic and endothelial lineages during development. *Tie2-Cre* mice [157] have been extensively used to target and study the vascular endothelium and recently they were used to investigate the MHCII-mediated antigen presentation by endothelial cells [107] However due to leakiness in cells of the hematopoietic system [158, 159], targeting the endothelium via VE-Cadherin (*Cdh5*) deemed to be a more suitable option to us. VE Cadherin is exclusively expressed on endothelial cells and not on cells of hematopoietic or stromal lineages, *Cdh5-Cre* [142] mouse can be safely used to specifically target the cells of endothelium. Moreover, to overcome the technical and biological difficulty that hinders the use of MHCII^{Δ} BM chimeras to study the non-hematopoietic MHCII antigen presentation, *Vav1-iCre* mice [143] can be used to target all hematopoietic cells, as we could not detect *Vav1* expression in our scRNA dataset ensuring its specificity to be exclusively expressed in cells of hematopoietic lineage.

5.5 Alloreactive CD4⁺ T cells receive activation cues from LNSCs within SLOs

The VAV1 gene is a member of VAV gene family and the Vav protein belongs to the guanine nucleotide exchange factors (GEFs) for Rho family GTPases that regulate pathways leading to actin cytoskeletal rearrangement [160, 161] and transcriptional alterations [162, 163]. It is a 95kDa proto-oncogene product expressed specifically in hematopoietic cells [164]. The Vav1 protein has an important function in hematopoiesis, playing a crucial role in T- [165, 166] and B cell [167, 168] development and activation. The *Vav1*-Cre mouse was originally generated by De Boer J and colleagues in 2003 [143] and since then has been successfully used to target all cells of hematopoietic lineage [169, 170]. In line with our scRNA data and to effectively target the complete hematopoietic system as well as to overcome the limitation that hinders the use of MHCII^Δ BM chimeras to study non-hematopoietic antigen presentation, we crossed the *Vav1*-Cre mice with *H2-Ab1^{fl}* to have PAN MHC class II knock-out on all cells of hematopoietic origin.

The MHCII^{ΔVav1} mice were viable and did not display any gross physical or behavioral abnormalities. These mice lacked the expression of MHC class II on all cells of hematopoietic origin (CD45⁺) in the lymphoid organs, whereas retained the expression of MHCII on LNSCs. The expression of MHCII on LNSCs was comparatively low in MHCII^{ΔVav1} mice to that of WT littermate as they lacked MHCII transfer from the DCs [22, 120]. Upon induction of CD4⁺ T cell specific GvHD, MHCII^{ΔVav1} succumbed to aGvHD suggesting that non-hematopoietic MHCII antigen presentation in these mice was sufficient to induce lethal aGvHD.

In MLRs the CD4⁺ T cells from the BALB/c mouse were activated and showed significant proliferation when cultured with enzymatically digested LNs from MHCII^{ΔVav1} compared to that of MHCII^Δ revealing that non-hematopoietic antigen presentation by a subset(s) of LNSCs could activate alloreactive CD4⁺ T cells.

On a similar line, we performed mLNs surgical transplantation from CD11c.DOG donor mice after surgical removal of mLNs in MHCII^Δ recipients. Before surgery, we depleted CD11c⁺ cells in CD11c.DOG mLN donor mice by i.p. administration of DTx prior. Once the transplanted mLNs were engrafted, only the non-hematopoietic cell compartment of transplanted mLNs had the MHCII antigen presentation capacity. Upon induction of aGvHD by alloreactive CD4⁺ T cells, in MHCII^Δ (CD11c.DOG mLNs) mice we observed significantly higher expression of T cell activation markers as well as effector/EM ratio compared to that of MHCII^Δ mouse in spleen.

Over the last few years, the identity of the non-hematopoietic cells that can provide MHCII signal to alloreactive CD4⁺ T cells in GvHD has been contested. Others have shown that alloreactive CD4⁺ can get activated by the hepatic endothelial cells [100] and intestinal

epithelial cells [93, 100, 107]. Nevertheless, naïve alloreactive CD4⁺ T cells express high levels of CCR7 that leads them to home to SLOs towards *Ccl19*, *Ccl21* gradient and binds to endothelial cell of the HEVs receptors GlyCAM-1 and CD34 via CD62L. Furthermore, alloreactive naïve CD4⁺ T cells essentially require upregulation of homing receptors CCR9, $\alpha 4\beta 7$ [171] and CD44, VLA4 [172] to migrate to the GvHD organs: GIT and liver respectively. Taken together in light of these experiments we show for the first time that in absence of antigen presentation by hematopoietic cells, the non-hematopoietic cells (stromal and/or endothelial cells) can activate CD4⁺ T cells via MHC class II in SLOs.

In these experiments, we employed a novel yet complex method of mesenteric lymph node transplantation to study non-hematopoietic antigen presentation by the LNSCs. The lymphadenectomy has been used in the past to study GvHD in rats [173, 174]. Our surgical method resulted in the successful engraftment of the donor mLNs, which we could monitor by *in vivo* bioluminescent imaging over time upon transplantation of luc⁺ mLNs into an albino B6 mouse. Moreover, transplanted mLNs successfully conjoined with the existing blood and lymphatic vessel of the mesenteric tissue, which we visualized and analyzed by 3D-LSFM for blood vessels and Evan's blue drainage from the PPs into the transplanted mLNs for lymphatic vessels is similar line to [175]. Upon successful engraftment we could identify that around ± 99 % hematopoietic cells in the transplanted mLNs were of the host origin (CD45.2⁺) with negligible numbers of donor (CD45.1⁺) hematopoietic cells when mLNs from B6.CD45.1⁺ were transplanted into a B6.WT (CD45.2⁺) mice. While the hematopoietic cells in the transplanted mLNs were replaced with the host cells, mLNs stroma retained the donor FRCs, LECs and BECs, which we could determine by transplanting mLNs from B6.DsRed into a B6.WT mouse, similar to the findings by Hammerschmidt and colleagues [176]. Furthermore, transplanted mLNs could trigger an alloreactive T cells response after allo-HCT, confirming that transplanted donor mLNs were viable and functional.

5.6 MHC class II on FRCs activate alloreactive CD4⁺ T cells in the initiation phase of GvHD

MHC class II on FRCs has been shown to present self-antigen to induce peripheral tolerance [20, 22, 120] and it is regulated by IFN γ [22, 177]. In our hands, s.c. *in vivo* treatment with IFN γ in mice, induced strong MHCII upregulation on the cell surface of FRC as well as LEC and BEC. Considering IFN γ increases the antigen presentation capacity of LNSCs, we FACS sorted FRCs from B6 mouse treated with IFN γ and FRCs from untreated BALB/c mouse as syngeneic controls. Culturing of FRCs with allogeneic CD4⁺ T cells resulted in upregulation of T cell activation markers as well as expression of Ki67 in the allogeneic setting compared to syngeneic controls, revealing that FRCs can potentially serve as antigen presenting cells in

aGvHD inflammatory conditions. Furthermore, we utilized the MHCII^{ΔCcl19} mice, which we made by crossing the *Ccl19-Cre* mouse with *H2-Ab1^{fl}* mouse to generate selective FRC restricted MHCII knock-outs. *In vivo* allo-HCT experiments revealed during the aGvHD initiation phase only a moderate decrease in alloreactive CD4⁺ T cell activation that deemed not significant. This could be explained by the overwhelming antigen presentation by hematopoietic cells. Remaining MHCII competent host-type DCs and macrophages [91] in the initiation phase of aGvHD likely obscured differences in CD4⁺ T cell activation in MHCII deficient FRC recipients. To further probe FRCs antigen presentation to CD4⁺ T cells we utilized OVA as a model antigen and transplanted CD4⁺ T cells OT-II into myeloablatively irradiated iFABP-tOVA mice [11, 144]. However, 72 h after the cell transfer, we could not detect substantial OT-II T cell activation in the SLOs indicating that OVA-expressing FRCs were unable to directly active alloreactive OT-II CD4⁺ T cells in this particular mouse model.

5.7 MHC class II presentation on FRCs regulates Tregs in the effector phase of GvHD

Self-antigen presentation by FRCs via MHC class I and II to T cells in the effector phase of aGvHD, helps with the modulation of autoimmunity and delaying subsequent transition to cGvHD. Recently it was shown that GvHD leads to selective elimination of FRC that results in the loss of PTA presentation, resulting in the activation of auto-aggressive T cells [123]. On similar line we asked the possible role of MHC class II knock-out on *Ccl19*-expressing FRCs in the effector phase of aGvHD. RNA sequencing at day +30 post allo-HCT revealed significant enrichment of genes directly involved in cell cycle/ mitosis, DNA binding proteins - implicating transcriptionally active chromatin and cellular proliferation and differentiation genes. These observations coincided with a drastic phenotype of GvHD exacerbation in the MHCII^{ΔCcl19} resulting in the increased expression of T cell activation molecules (CD44, CD127 and Ki67) in the SLOs. Furthermore, allogeneic CD4⁺ T cells in MHCII^{ΔCcl19} mice downregulated genes involved in aerobic glycolysis compared to that in *H2-Ab1^{fl}*, suggesting that indeed CD4⁺ T cells in MHCII^{ΔCcl19} have transitioned into the memory phase in which alloreactive T cells biosynthesis is primarily maintained by fatty acid oxidation (FAO), whereas CD4⁺ T cells in *H2-Ab1^{fl}* were still in the expansion, effector phase of GvHD and primarily consuming glutamine and aerobic glycolysis as metabolic source [178]. Furthermore, RNA sequencing dataset revealed loss of expression of well-known signature genes for invariant natural killer T (iNKT) cells (*Klrd1*, *Klrk1*, *Klrc1*, *Klrc2* and *Klri2*) in CD4⁺ T cells in MHCII^{ΔCcl19} mice, suggesting potential loss of CD4⁺ iNKT cells in these mice. CD4⁺ iNKT cells have been shown to regulate GvHD through expansion of donor Tregs [179] and their dysregulation in MHCII^{ΔCcl19} mice could influence GvHD outcome. To our surprise sequencing dataset corresponded with flow

cytometric analysis as we observed reduced numbers of regulatory T cells (Tregs) frequency in the SLOs of MHCII^{ΔCcl19} mice. Day +60 is already considered as a late of aGvHD, at this time-point an exacerbated aGvHD phenotype in MHCII^{ΔCcl19} mice became more prominent with increased expression of effector molecules and down-regulated expression of T cell exhaustion markers on alloreactive CD4⁺ T cells leading to overall poor survival.

To further dissect the impact of defective FRCs MHC class II presentation on alloreactive donor Tregs we adoptively transferred FVB Tregs along with alloreactive conventional CD4⁺ T cells and BM in MHCII^{ΔCcl19} and *H2-Ab1*^{fl} recipients. We observed that Tregs failed to protect MHCII^{ΔCcl19} mice in survival experiments, whereas the protection provided by Tregs [180] was retained in the *H2-Ab1*^{fl} recipients. This was further confirmed as donor CD4⁺ T cells expressed higher levels of effector molecules and Ki67 in MHCII^{ΔCcl19} on day +60 after allo-HCT (data analyzed from the few surviving animals on day +60 after allo-HCT). Our hypothesis that MHCII antigen presentation by FRCs may be essential for proper donor Treg function was further confirmed when we utilized an ovalbumin TCR restricted transgenic model in iFAPB-tOVA in these experiments. When transferred OT-II CD4⁺ T cells that had been activated in the myeloablatively irradiated CD11c.DOG mouse into iFABP-tOVA mice, these secondarily transferred OT-II specific Tregs proliferated significantly more than in controls (and to some extent also OT-II specific Tcons) indicating that indeed MHC class II on lymph node FRCs promote/support Treg and Tcon proliferation in GvHD-like inflammatory conditions. Our observations correspond with recent studies where FRCs have been shown to promote Tregs and reduce autoimmunity under inflammatory conditions [120, 121]. Moreover, depletion of FRCs prior to allo-HCT resulted in the induction of a severe phenotype in DTR⁺Cre⁺ mice that resulted in overall poor survival of mice. Taken together these results reveal that MHC class II on FRCs plays a role in priming of alloreactive CD4⁺ T cells during the initiation phase of aGvHD along with providing the crucial notch ligands (DLL1/4) [124] whereas in the effector phase of aGvHD the role of MHC class II on FRCs upends as immunoregulatory via the maintenance of Tregs and dampening aGvHD.

5.8 Endothelium MHC class II antigen presentation in GvHD

In recent years, a dysfunctional endothelium [181, 182] has emerged as a predictive marker of GvHD severity [183] as well as a target in GvHD [184, 185]. Similar to FRCs, LECs have been shown to present PTA via MHC class II [15, 111] resulting in the tolerance induction of CD4⁺ T cells. On the contrary, BECs have been shown to activate alloreactive CD4⁺ T cells *in vitro* [186]. Recently in an elaborative study, Vokali and colleagues showed that LECs prime naïve CD8⁺ T cells into memory cells under steady-state conditions [187]. Taken together these previous studies support an emerging role of antigen presentation by endothelial cells

in steady-state and inflammatory conditions. To study MHC class II mediated antigen presentation in GvHD, we generated MHCII^{ΔVE-Cadherin} mice with restricted depletion MHCII presentation on all VE Cadherin-expressing endothelial cells. Upon induction of aGvHD in these mice we observed only a moderate decrease in alloreactive CD4⁺ T cell activation and proliferation at day +3 after allo-HCT, which could be due to excessive activation signal provided by the hematopoietic antigen presenting cells in the SLOs [91]. However, this intrinsic MHCII knock-out on endothelium resulted in a relative protection against aGvHD in survival experiments. Next, to rule out hematopoietic antigen presentation in MHCII^{ΔVE-Cadherin} mice we crossed these mice MHCII^{ΔVav1} to obtain mice deficient for MHC class II on both, cells of endothelial and hematopoietic lineages. Preliminary data revealed that LNSCs from MHCII^{ΔVav1 ΔVE-Cadherin} were unable to upregulate T cells activation molecules on allogeneic CD4⁺ T cells from BALB/c donors, thus indicating a crucial role of endothelial cells in MHCII antigen presentation in GvHD inflammatory settings.

5.9 Conclusion

Allogeneic T cell homing and priming are critical steps that define aGvHD severity in human and in mice. Naïve allogeneic T cells express CD62L and CCR7 that lead them to SLOs subsequent to allo-HCT, however in recent years this notion has been challenged and others have postulated that naïve allogeneic T cells might migrate directly to GvHD target organ(s) particularly small bowel resulting in the initiation of GvHD [107]. Here utilizing MHC major-mismatch model (FVB → B6) we show that allogeneic T cells home to SLOs and not to GvHD target organs (small bowel, liver, lung and skin) in the initiation phase of aGvHD (**Figure 5.1**). Absence of MHC class II antigen presentation from professional APCs in different genetic models (MHCII^Δ BM chimeras, MHCII^{ΔCD11c} and MHCII^{ΔVav1}) does not influence CD4⁺ T cells homing in the initiation phase of GvHD. Here we identified endothelial cells (BECs and/or LECs) of SLOs as the non-hematopoietic APCs involved in the antigen presentation, thereby explaining the inability of approaches that delete/ deplete hematopoietic professional recipient APCs to prevent aGvHD in preclinical models [96, 97, 188, 189]. DCs and other hematopoietic APCs do potently present alloantigen, but as an effect of this function can also result in activation-induced cell death and/or phagocytosis of donor CD4⁺ T cells, which paradoxically attenuates GvHD [93, 96, 190]. Thus, approaches to delete recipient hematopoietic APCs appear general deleterious and instead amplify GvHD (Le DD *et al.*, unpublished data). Our data support that indeed LNSCs: BECs and/or LECs play a synergistic role in allogeneic CD4⁺ T cells priming during aGvHD initiation. Conversely, FRCs, which provide crucial delta-like notch ligands to allogeneic T cells in aGvHD initiation [124], utilize their MHC class II to regulate aGvHD severity via regulatory T cells during the late effector phase of GvHD (**Figure 5.2**). In

conclusion, the findings of this thesis highlight the importance of LNSCs MHC class II antigen presentation in aGvHD and broaden our understanding of pathomechanisms involved. In future it would be interesting to investigate the potential role of non-hematopoietic antigen presentation in bone marrow and its influence on anti-tumor-specific allogeneic T cells in countering leukemic cells.

The involvement of LNSCs in active antigen presentation in aGvHD has potential clinical implications. As endothelial cells of the LNs serve in a synergistic manner in allogeneic CD4⁺ T cells activation it would be potentially interesting to block this mode of antigen presentation via masking the MHC class II on endothelial cells. This could be achieved by targeted blocking of MHCII on endothelial cells through a fusion protein, having a targeting domain to block MHC class II and guiding domain towards CD31. On the other hand, modulating the expression of MHC class II on FRCs could result in maintaining or even enhancing Treg function to reduce GvHD severity, however this will require further studies.

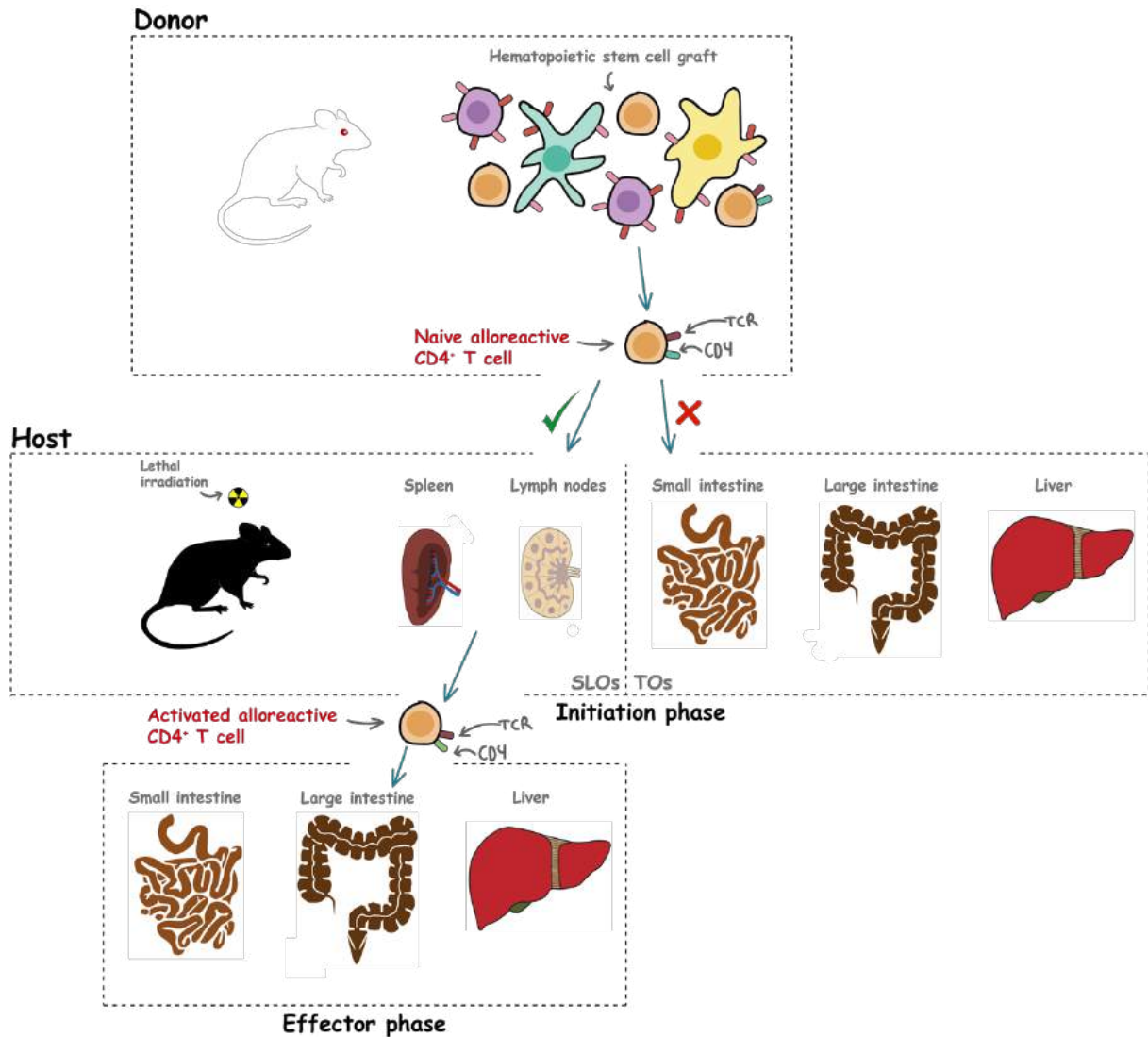
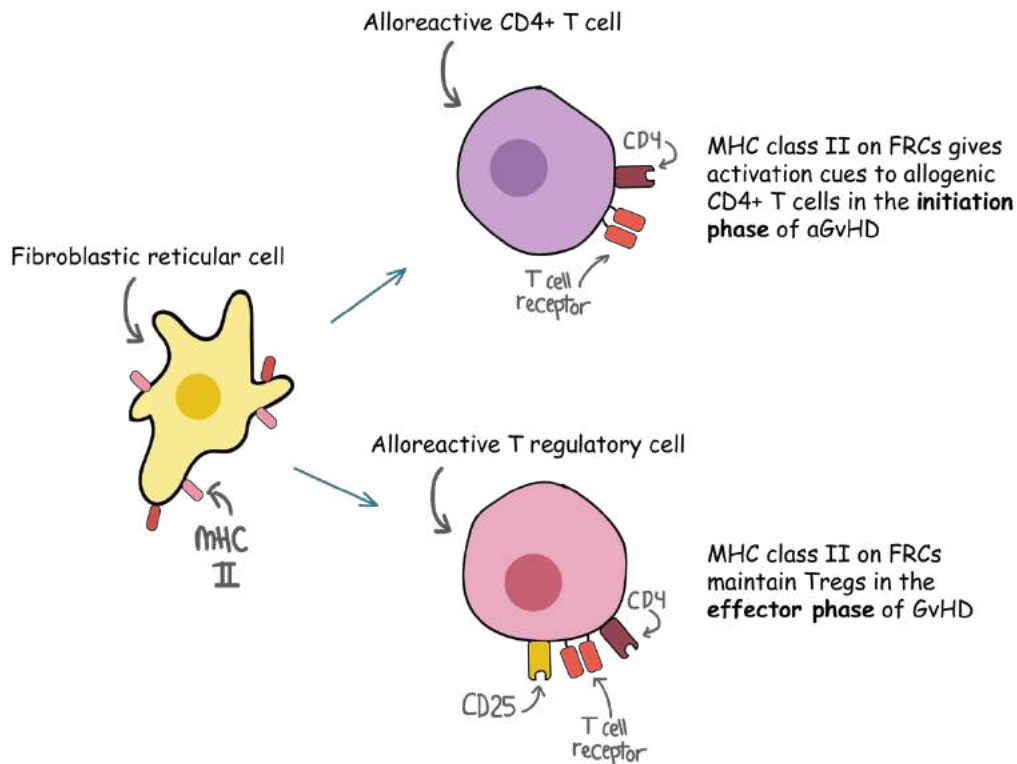


Figure 5.1 Alloreactive naïve CD4⁺ T cells home to SLOs and not to the target organs during the initiation phase of aGVHD.

Over the past few years, it has been contested whether naïve alloreactive T cells home to SLOs and/or to the GvHD target organs subsequent to allo-HCT. In light of our data, we propose a model in which naïve allogeneic T cells exclusively home to the SLOs (spleen, lymph nodes and Peyer's patches) in the initiation phase of aGVHD. After getting activation cues in SLOs, only activated T cells migrate to the target organs during the effector phase of aGVHD.

A



B

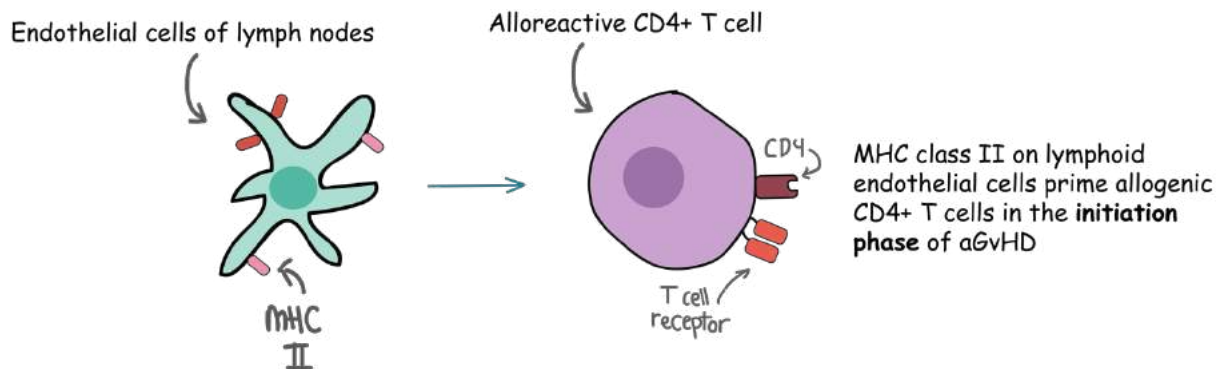


Figure 5.2 MHC class II on lymph node stromal cells modulate allogeneic CD4⁺ T cells in graft-versus-host-disease.

(A) Here we show MHC class II on Ccl19⁺ fibroblastic stromal cells (FRCs) prime allogeneic CD4⁺ T cells during the initiation phase of aGvHD. However, MHCII expression on Ccl19⁺ FRCs also regulates the severity of aGvHD by maintaining regulatory T cells. (B) In a mixed lymphocyte reaction of lymph node endothelial cells, lymph node endothelial cells prime alloreactive CD4⁺ T cells.

6 References

1. Hoorweg, K. and T. Cupedo, *Development of human lymph nodes and Peyer's patches*. *Semin Immunol*, 2008. **20**(3): p. 164-70.
2. Trepel, F., *Number and distribution of lymphocytes in man. A critical analysis*. *Klin Wochenschr*, 1974. **52**(11): p. 511-5.
3. Van den Broeck, W., A. Derore, and P. Simoens, *Anatomy and nomenclature of murine lymph nodes: Descriptive study and nomenclatory standardization in BALB/cAnNCrI mice*. *J Immunol Methods*, 2006. **312**(1-2): p. 12-9.
4. Buettner, M. and U. Bode, *Lymph node dissection--understanding the immunological function of lymph nodes*. *Clin Exp Immunol*, 2012. **169**(3): p. 205-12.
5. Bazemore, A.W. and D.R. Smucker, *Lymphadenopathy and malignancy*. *Am Fam Physician*, 2002. **66**(11): p. 2103-10.
6. Girard, J.P., C. Mousson, and R. Forster, *HEVs, lymphatics and homeostatic immune cell trafficking in lymph nodes*. *Nat Rev Immunol*, 2012. **12**(11): p. 762-73.
7. Willard-Mack, C.L., *Normal structure, function, and histology of lymph nodes*. *Toxicol Pathol*, 2006. **34**(5): p. 409-24.
8. Ahrendt, M., et al., *Stromal cells confer lymph node-specific properties by shaping a unique microenvironment influencing local immune responses*. *J Immunol*, 2008. **181**(3): p. 1898-907.
9. Luther, S.A., et al., *Coexpression of the chemokines ELC and SLC by T zone stromal cells and deletion of the ELC gene in the plt/plt mouse*. *Proc Natl Acad Sci U S A*, 2000. **97**(23): p. 12694-9.
10. Rakhimov, K., *[On the effect of the functional condition of the digestive system on the enzyme activity of the intestinal surface]*. *Fiziol Zh SSSR Im I M Sechenova*, 1968. **54**(1): p. 103-8.
11. Lee, J.W., et al., *Peripheral antigen display by lymph node stroma promotes T cell tolerance to intestinal self*. *Nat Immunol*, 2007. **8**(2): p. 181-90.
12. Link, A., et al., *Fibroblastic reticular cells in lymph nodes regulate the homeostasis of naive T cells*. *Nat Immunol*, 2007. **8**(11): p. 1255-65.
13. Magnusson, F.C., et al., *Direct presentation of antigen by lymph node stromal cells protects against CD8 T-cell-mediated intestinal autoimmunity*. *Gastroenterology*, 2008. **134**(4): p. 1028-37.
14. Molenaar, R., et al., *Lymph node stromal cells support dendritic cell-induced gut-homing of T cells*. *J Immunol*, 2009. **183**(10): p. 6395-402.
15. Cohen, J.N., et al., *Lymph node-resident lymphatic endothelial cells mediate peripheral tolerance via Aire-independent direct antigen presentation*. *J Exp Med*, 2010. **207**(4): p. 681-8.
16. Fletcher, A.L., et al., *Lymph node fibroblastic reticular cells directly present peripheral tissue antigen under steady-state and inflammatory conditions*. *J Exp Med*, 2010. **207**(4): p. 689-97.
17. Khan, O., et al., *Regulation of T cell priming by lymphoid stroma*. *PLoS One*, 2011. **6**(11): p. e26138.
18. Lukacs-Kornek, V., et al., *Regulated release of nitric oxide by nonhematopoietic stroma controls expansion of the activated T cell pool in lymph nodes*. *Nat Immunol*, 2011. **12**(11): p. 1096-104.
19. Malhotra, D., et al., *Transcriptional profiling of stroma from inflamed and resting lymph nodes defines immunological hallmarks*. *Nat Immunol*, 2012. **13**(5): p. 499-510.
20. Baptista, A.P., et al., *Lymph node stromal cells constrain immunity via MHC class II self-antigen presentation*. *Elife*, 2014. **3**.
21. Denton, A.E., et al., *Fibroblastic reticular cells of the lymph node are required for retention of resting but not activated CD8+ T cells*. *Proc Natl Acad Sci U S A*, 2014. **111**(33): p. 12139-44.

22. Dubrot, J., et al., *Lymph node stromal cells acquire peptide-MHCII complexes from dendritic cells and induce antigen-specific CD4(+) T cell tolerance*. *J Exp Med*, 2014. **211**(6): p. 1153-66.
23. Fletcher, A.L., S.E. Acton, and K. Knoblich, *Lymph node fibroblastic reticular cells in health and disease*. *Nat Rev Immunol*, 2015. **15**(6): p. 350-61.
24. Mionnet, C., et al., *High endothelial venules as traffic control points maintaining lymphocyte population homeostasis in lymph nodes*. *Blood*, 2011. **118**(23): p. 6115-22.
25. Luther, S.A., et al., *Differing activities of homeostatic chemokines CCL19, CCL21, and CXCL12 in lymphocyte and dendritic cell recruitment and lymphoid neogenesis*. *J Immunol*, 2002. **169**(1): p. 424-33.
26. Roozendaal, R., et al., *Conduits mediate transport of low-molecular-weight antigen to lymph node follicles*. *Immunity*, 2009. **30**(2): p. 264-76.
27. Gretz, J.E., et al., *Lymph-borne chemokines and other low molecular weight molecules reach high endothelial venules via specialized conduits while a functional barrier limits access to the lymphocyte microenvironments in lymph node cortex*. *J Exp Med*, 2000. **192**(10): p. 1425-40.
28. Katakai, T., et al., *Lymph node fibroblastic reticular cells construct the stromal reticulum via contact with lymphocytes*. *J Exp Med*, 2004. **200**(6): p. 783-95.
29. Katakai, T., et al., *Organizer-like reticular stromal cell layer common to adult secondary lymphoid organs*. *J Immunol*, 2008. **181**(9): p. 6189-200.
30. Katakai, T., *Marginal reticular cells: a stromal subset directly descended from the lymphoid tissue organizer*. *Front Immunol*, 2012. **3**: p. 200.
31. Jarjour, M., et al., *Fate mapping reveals origin and dynamics of lymph node follicular dendritic cells*. *J Exp Med*, 2014. **211**(6): p. 1109-22.
32. Heesters, B.A., R.C. Myers, and M.C. Carroll, *Follicular dendritic cells: dynamic antigen libraries*. *Nat Rev Immunol*, 2014. **14**(7): p. 495-504.
33. Cremasco, V., et al., *B cell homeostasis and follicle confines are governed by fibroblastic reticular cells*. *Nat Immunol*, 2014. **15**(10): p. 973-81.
34. Mionnet, C., et al., *Identification of a new stromal cell type involved in the regulation of inflamed B cell follicles*. *PLoS Biol*, 2013. **11**(10): p. e1001672.
35. Fasnacht, N., et al., *Specific fibroblastic niches in secondary lymphoid organs orchestrate distinct Notch-regulated immune responses*. *J Exp Med*, 2014. **211**(11): p. 2265-79.
36. Herzog, B.H., et al., *Podoplanin maintains high endothelial venule integrity by interacting with platelet CLEC-2*. *Nature*, 2013. **502**(7469): p. 105-9.
37. Bajenoff, M., et al., *Stromal cell networks regulate lymphocyte entry, migration, and territoriality in lymph nodes*. *Immunity*, 2006. **25**(6): p. 989-1001.
38. Astarita, J.L., et al., *The CLEC-2-podoplanin axis controls the contractility of fibroblastic reticular cells and lymph node microarchitecture*. *Nat Immunol*, 2015. **16**(1): p. 75-84.
39. Lammermann, T., et al., *Rapid leukocyte migration by integrin-independent flowing and squeezing*. *Nature*, 2008. **453**(7191): p. 51-5.
40. Sixt, M., et al., *The conduit system transports soluble antigens from the afferent lymph to resident dendritic cells in the T cell area of the lymph node*. *Immunity*, 2005. **22**(1): p. 19-29.
41. Acton, S.E., et al., *Dendritic cells control fibroblastic reticular network tension and lymph node expansion*. *Nature*, 2014. **514**(7523): p. 498-502.
42. Ansel, K.M., et al., *A chemokine-driven positive feedback loop organizes lymphoid follicles*. *Nature*, 2000. **406**(6793): p. 309-14.
43. Asperti-Boursin, F., et al., *CCR7 ligands control basal T cell motility within lymph node slices in a phosphoinositide 3-kinase-independent manner*. *J Exp Med*, 2007. **204**(5): p. 1167-79.
44. Majumder, S., et al., *IL-17 metabolically reprograms activated fibroblastic reticular cells for proliferation and survival*. *Nat Immunol*, 2019. **20**(5): p. 534-545.

45. Schaeuble, K., et al., *Attenuation of chronic antiviral T-cell responses through constitutive COX2-dependent prostanoid synthesis by lymph node fibroblasts*. PLoS Biol, 2019. **17**(7): p. e3000072.
46. Yu, M., et al., *Fibroblastic reticular cells of the lymphoid tissues modulate T cell activation threshold during homeostasis via hyperactive cyclooxygenase-2/prostaglandin E2 axis*. Sci Rep, 2017. **7**(1): p. 3350.
47. Yip, L., et al., *Deaf1 isoforms control the expression of genes encoding peripheral tissue antigens in the pancreatic lymph nodes during type 1 diabetes*. Nat Immunol, 2009. **10**(9): p. 1026-33.
48. Chai, Q., et al., *Maturation of lymph node fibroblastic reticular cells from myofibroblastic precursors is critical for antiviral immunity*. Immunity, 2013. **38**(5): p. 1013-24.
49. Novkovic, M., et al., *Topological Small-World Organization of the Fibroblastic Reticular Cell Network Determines Lymph Node Functionality*. PLoS Biol, 2016. **14**(7): p. e1002515.
50. Mackay, F. and P. Schneider, *Cracking the BAFF code*. Nat Rev Immunol, 2009. **9**(7): p. 491-502.
51. Saez de Guinoa, J., et al., *CXCL13/CXCR5 signaling enhances BCR-triggered B-cell activation by shaping cell dynamics*. Blood, 2011. **118**(6): p. 1560-9.
52. Acton, S.E., et al., *Podoplanin-rich stromal networks induce dendritic cell motility via activation of the C-type lectin receptor CLEC-2*. Immunity, 2012. **37**(2): p. 276-89.
53. Krautler, N.J., et al., *Follicular dendritic cells emerge from ubiquitous perivascular precursors*. Cell, 2012. **150**(1): p. 194-206.
54. Onder, L., et al., *IL-7-producing stromal cells are critical for lymph node remodeling*. Blood, 2012. **120**(24): p. 4675-83.
55. Scandella, E., et al., *Restoration of lymphoid organ integrity through the interaction of lymphoid tissue-inducer cells with stroma of the T cell zone*. Nat Immunol, 2008. **9**(6): p. 667-75.
56. Bajenoff, M. and R.N. Germain, *B-cell follicle development remodels the conduit system and allows soluble antigen delivery to follicular dendritic cells*. Blood, 2009. **114**(24): p. 4989-97.
57. Wu, Y., et al., *IL-6 produced by immune complex-activated follicular dendritic cells promotes germinal center reactions, IgG responses and somatic hypermutation*. Int Immunol, 2009. **21**(6): p. 745-56.
58. Wang, X., et al., *Follicular dendritic cells help establish follicle identity and promote B cell retention in germinal centers*. J Exp Med, 2011. **208**(12): p. 2497-510.
59. Matsumoto, M., et al., *Affinity maturation without germinal centres in lymphotoxin-alpha-deficient mice*. Nature, 1996. **382**(6590): p. 462-6.
60. Braun, A., et al., *Afferent lymph-derived T cells and DCs use different chemokine receptor CCR7-dependent routes for entry into the lymph node and intranodal migration*. Nat Immunol, 2011. **12**(9): p. 879-87.
61. Ulvmar, M.H., et al., *The atypical chemokine receptor CCRL1 shapes functional CCL21 gradients in lymph nodes*. Nat Immunol, 2014. **15**(7): p. 623-30.
62. Pham, T.H., et al., *Lymphatic endothelial cell sphingosine kinase activity is required for lymphocyte egress and lymphatic patterning*. J Exp Med, 2010. **207**(1): p. 17-27.
63. Cohen, J.N., et al., *Tolerogenic properties of lymphatic endothelial cells are controlled by the lymph node microenvironment*. PLoS One, 2014. **9**(2): p. e87740.
64. Miller, C.N., et al., *IL-7 production in murine lymphatic endothelial cells and induction in the setting of peripheral lymphopenia*. Int Immunol, 2013. **25**(8): p. 471-83.
65. Hirose, S., et al., *Steady-state antigen scavenging, cross-presentation, and CD8+ T cell priming: a new role for lymphatic endothelial cells*. J Immunol, 2014. **192**(11): p. 5002-11.
66. Muller, W.A., *The regulation of transendothelial migration: new knowledge and new questions*. Cardiovasc Res, 2015. **107**(3): p. 310-20.
67. Sage, P.T. and C.V. Carman, *Settings and mechanisms for trans-cellular diapedesis*. Front Biosci (Landmark Ed), 2009. **14**: p. 5066-83.

68. Chyou, S., et al., *Coordinated regulation of lymph node vascular-stromal growth first by CD11c+ cells and then by T and B cells*. J Immunol, 2011. **187**(11): p. 5558-67.
69. Warnock, R.A., et al., *Molecular mechanisms of lymphocyte homing to peripheral lymph nodes*. J Exp Med, 1998. **187**(2): p. 205-16.
70. Yang, C.Y., et al., *Trapping of naive lymphocytes triggers rapid growth and remodeling of the fibroblast network in reactive murine lymph nodes*. Proc Natl Acad Sci U S A, 2014. **111**(1): p. E109-18.
71. Lee, M., et al., *Transcriptional programs of lymphoid tissue capillary and high endothelium reveal control mechanisms for lymphocyte homing*. Nat Immunol, 2014. **15**(10): p. 982-95.
72. Chyou, S., et al., *Fibroblast-type reticular stromal cells regulate the lymph node vasculature*. J Immunol, 2008. **181**(6): p. 3887-96.
73. Benahmed, F., et al., *Multiple CD11c+ cells collaboratively express IL-1beta to modulate stromal vascular endothelial growth factor and lymph node vascular-stromal growth*. J Immunol, 2014. **192**(9): p. 4153-63.
74. Fletcher, A.L., et al., *Reproducible isolation of lymph node stromal cells reveals site-dependent differences in fibroblastic reticular cells*. Front Immunol, 2011. **2**: p. 35.
75. Gooley, T.A., et al., *Reduced mortality after allogeneic hematopoietic-cell transplantation*. N Engl J Med, 2010. **363**(22): p. 2091-101.
76. MacMillan, M.L., et al., *Response of 443 patients to steroids as primary therapy for acute graft-versus-host disease: comparison of grading systems*. Biol Blood Marrow Transplant, 2002. **8**(7): p. 387-94.
77. Ferrara, J.L., et al., *Graft-versus-host disease*. Lancet, 2009. **373**(9674): p. 1550-61.
78. Blazar, B.R., W.J. Murphy, and M. Abedi, *Advances in graft-versus-host disease biology and therapy*. Nat Rev Immunol, 2012. **12**(6): p. 443-58.
79. Glucksberg, H., et al., *Clinical manifestations of graft-versus-host disease in human recipients of marrow from HL-A-matched sibling donors*. Transplantation, 1974. **18**(4): p. 295-304.
80. Przepiorka, D., et al., *1994 Consensus Conference on Acute GVHD Grading*. Bone Marrow Transplant, 1995. **15**(6): p. 825-8.
81. Perrin, R.G. and M. Bernstein, *Iatrogenic seeding of anaplastic astrocytoma following stereotactic biopsy*. J Neurooncol, 1998. **36**(3): p. 243-6.
82. Floisand, Y., et al., *Safety and Effectiveness of Vedolizumab in Patients with Steroid-Refractory Gastrointestinal Acute Graft-versus-Host Disease: A Retrospective Record Review*. Biol Blood Marrow Transplant, 2019. **25**(4): p. 720-727.
83. Hill, L., et al., *New and emerging therapies for acute and chronic graft versus host disease*. Ther Adv Hematol, 2018. **9**(1): p. 21-46.
84. Carpenter, P.A., et al., *A phase II/III randomized, multicenter trial of prednisone/sirolimus versus prednisone/ sirolimus/calcineurin inhibitor for the treatment of chronic graft-versus-host disease: BMT CTN 0801*. Haematologica, 2018. **103**(11): p. 1915-1924.
85. Peled, J.U., A.M. Hanash, and R.R. Jenq, *Role of the intestinal mucosa in acute gastrointestinal GVHD*. Hematology Am Soc Hematol Educ Program, 2016. **2016**(1): p. 119-127.
86. Matsukuma, K.E., et al., *Diagnosis and differential diagnosis of hepatic graft versus host disease (GVHD)*. J Gastrointest Oncol, 2016. **7**(Suppl 1): p. S21-31.
87. Bleakley, M. and S.R. Riddell, *Molecules and mechanisms of the graft-versus-leukaemia effect*. Nat Rev Cancer, 2004. **4**(5): p. 371-80.
88. Markey, K.A., et al., *Cross-dressing by donor dendritic cells after allogeneic bone marrow transplantation contributes to formation of the immunological synapse and maximizes responses to indirectly presented antigen*. J Immunol, 2014. **192**(11): p. 5426-33.
89. Wang, X., et al., *Mechanisms of antigen presentation to T cells in murine graft-versus-host disease: cross-presentation and the appearance of cross-presentation*. Blood, 2011. **118**(24): p. 6426-37.

90. Nakayama, M., *Antigen Presentation by MHC-Dressed Cells*. Front Immunol, 2014. **5**: p. 672.
91. Duffner, U.A., et al., *Host dendritic cells alone are sufficient to initiate acute graft-versus-host disease*. J Immunol, 2004. **172**(12): p. 7393-8.
92. Zhang, Y., et al., *Preterminal host dendritic cells in irradiated mice prime CD8+ T cell-mediated acute graft-versus-host disease*. J Clin Invest, 2002. **109**(10): p. 1335-44.
93. Koyama, M., et al., *Recipient nonhematopoietic antigen-presenting cells are sufficient to induce lethal acute graft-versus-host disease*. Nat Med, 2011. **18**(1): p. 135-42.
94. Li, H., et al., *Profound depletion of host conventional dendritic cells, plasmacytoid dendritic cells, and B cells does not prevent graft-versus-host disease induction*. J Immunol, 2012. **188**(8): p. 3804-11.
95. Weber, M., et al., *Host-derived CD8(+) dendritic cells protect against acute graft-versus-host disease after experimental allogeneic bone marrow transplantation*. Biol Blood Marrow Transplant, 2014. **20**(11): p. 1696-704.
96. Hashimoto, D., et al., *Pretransplant CSF-1 therapy expands recipient macrophages and ameliorates GVHD after allogeneic hematopoietic cell transplantation*. J Exp Med, 2011. **208**(5): p. 1069-82.
97. MacDonald, K.P., et al., *An antibody against the colony-stimulating factor 1 receptor depletes the resident subset of monocytes and tissue- and tumor-associated macrophages but does not inhibit inflammation*. Blood, 2010. **116**(19): p. 3955-63.
98. Li, H., et al., *Langerhans cells are not required for graft-versus-host disease*. Blood, 2011. **117**(2): p. 697-707.
99. Matte-Martone, C., et al., *Recipient B cells are not required for graft-versus-host disease induction*. Biol Blood Marrow Transplant, 2010. **16**(9): p. 1222-30.
100. Toubai, T., et al., *Induction of acute GVHD by sex-mismatched H-Y antigens in the absence of functional radiosensitive host hematopoietic-derived antigen-presenting cells*. Blood, 2012. **119**(16): p. 3844-53.
101. Saada, J.I., et al., *Subepithelial myofibroblasts are novel nonprofessional APCs in the human colonic mucosa*. J Immunol, 2006. **177**(9): p. 5968-79.
102. Kundig, T.M., et al., *Fibroblasts as efficient antigen-presenting cells in lymphoid organs*. Science, 1995. **268**(5215): p. 1343-7.
103. Powell, D.W., et al., *Mesenchymal cells of the intestinal lamina propria*. Annu Rev Physiol, 2011. **73**: p. 213-37.
104. Hershberg, R.M., et al., *Intestinal epithelial cells use two distinct pathways for HLA class II antigen processing*. J Clin Invest, 1997. **100**(1): p. 204-15.
105. Hershberg, R.M., et al., *Highly polarized HLA class II antigen processing and presentation by human intestinal epithelial cells*. J Clin Invest, 1998. **102**(4): p. 792-803.
106. Beers, C., et al., *Cathepsin S controls MHC class II-mediated antigen presentation by epithelial cells in vivo*. J Immunol, 2005. **174**(3): p. 1205-12.
107. Koyama, M., et al., *MHC Class II Antigen Presentation by the Intestinal Epithelium Initiates Graft-versus-Host Disease and Is Influenced by the Microbiota*. Immunity, 2019. **51**(5): p. 885-898 e7.
108. Schroeder, M.A. and J.F. DiPersio, *Mouse models of graft-versus-host disease: advances and limitations*. Dis Model Mech, 2011. **4**(3): p. 318-33.
109. Beilhack, A., et al., *In vivo analyses of early events in acute graft-versus-host disease reveal sequential infiltration of T-cell subsets*. Blood, 2005. **106**(3): p. 1113-22.
110. Beilhack, A., et al., *Prevention of acute graft-versus-host disease by blocking T-cell entry to secondary lymphoid organs*. Blood, 2008. **111**(5): p. 2919-28.
111. Rouhani, S.J., et al., *Roles of lymphatic endothelial cells expressing peripheral tissue antigens in CD4 T-cell tolerance induction*. Nat Commun, 2015. **6**: p. 6771.
112. Mueller, S.N. and R.N. Germain, *Stromal cell contributions to the homeostasis and functionality of the immune system*. Nat Rev Immunol, 2009. **9**(9): p. 618-29.
113. El Shikh, M.E. and C. Pitzalis, *Follicular dendritic cells in health and disease*. Front Immunol, 2012. **3**: p. 292.

114. Reith, W., S. LeibundGut-Landmann, and J.M. Waldburger, *Regulation of MHC class II gene expression by the class II transactivator*. *Nat Rev Immunol*, 2005. **5**(10): p. 793-806.
115. Norder, M., et al., *Lymph node-derived lymphatic endothelial cells express functional costimulatory molecules and impair dendritic cell-induced allogenic T-cell proliferation*. *FASEB J*, 2012. **26**(7): p. 2835-46.
116. Gray, D., M. Kosco, and B. Stockinger, *Novel pathways of antigen presentation for the maintenance of memory*. *Int Immunol*, 1991. **3**(2): p. 141-8.
117. Schnizlein, C.T., et al., *Follicular dendritic cells in suspension: identification, enrichment, and initial characterization indicating immune complex trapping and lack of adherence and phagocytic activity*. *J Immunol*, 1985. **134**(3): p. 1360-8.
118. Denzer, K., et al., *Follicular dendritic cells carry MHC class II-expressing microvesicles at their surface*. *J Immunol*, 2000. **165**(3): p. 1259-65.
119. Ng, C.T., et al., *Immortalized clones of fibroblastic reticular cells activate virus-specific T cells during virus infection*. *Proc Natl Acad Sci U S A*, 2012. **109**(20): p. 7823-8.
120. Dubrot, J., et al., *Absence of MHC-II expression by lymph node stromal cells results in autoimmunity*. *Life Sci Alliance*, 2018. **1**(6): p. e201800164.
121. Nadafi, R., et al., *Lymph Node Stromal Cells Generate Antigen-Specific Regulatory T Cells and Control Autoreactive T and B Cell Responses*. *Cell Rep*, 2020. **30**(12): p. 4110-4123 e4.
122. Suenaga, F., et al., *Loss of lymph node fibroblastic reticular cells and high endothelial cells is associated with humoral immunodeficiency in mouse graft-versus-host disease*. *J Immunol*, 2015. **194**(1): p. 398-406.
123. Dertschnig, S., et al., *Graft-versus-host disease reduces lymph node display of tissue-restricted self-antigens and promotes autoimmunity*. *J Clin Invest*, 2020. **130**(4): p. 1896-1911.
124. Chung, J., et al., *Fibroblastic niches prime T cell alloimmunity through Delta-like Notch ligands*. *J Clin Invest*, 2017. **127**(4): p. 1574-1588.
125. Roche, P.A. and K. Furuta, *The ins and outs of MHC class II-mediated antigen processing and presentation*. *Nat Rev Immunol*, 2015. **15**(4): p. 203-16.
126. Thibodeau, J., M.C. Bourgeois-Daigneault, and R. Lapointe, *Targeting the MHC Class II antigen presentation pathway in cancer immunotherapy*. *Oncoimmunology*, 2012. **1**(6): p. 908-916.
127. Tsai, S. and P. Santamaria, *MHC Class II Polymorphisms, Autoreactive T-Cells, and Autoimmunity*. *Front Immunol*, 2013. **4**: p. 321.
128. Fernando, M.M., et al., *Defining the role of the MHC in autoimmunity: a review and pooled analysis*. *PLoS Genet*, 2008. **4**(4): p. e1000024.
129. Cao, Y.A., et al., *Shifting foci of hematopoiesis during reconstitution from single stem cells*. *Proc Natl Acad Sci U S A*, 2004. **101**(1): p. 221-6.
130. Tung, J.W., et al., *New approaches to fluorescence compensation and visualization of FACS data*. *Clin Immunol*, 2004. **110**(3): p. 277-83.
131. Herzenberg, L.A., et al., *Interpreting flow cytometry data: a guide for the perplexed*. *Nat Immunol*, 2006. **7**(7): p. 681-5.
132. Stegner, D., et al., *Thrombopoiesis is spatially regulated by the bone marrow vasculature*. *Nat Commun*, 2017. **8**(1): p. 127.
133. Arras, M., et al., *Optimization of intraperitoneal injection anesthesia in mice: drugs, dosages, adverse effects, and anesthesia depth*. *Comp Med*, 2001. **51**(5): p. 443-56.
134. Hochweller, K., et al., *A novel CD11c.DTR transgenic mouse for depletion of dendritic cells reveals their requirement for homeostatic proliferation of natural killer cells*. *Eur J Immunol*, 2008. **38**(10): p. 2776-83.
135. Huang, W., et al., *Dendritic cell-MHC class II and I κ k regulate functional development of regulatory innate memory CD4⁺ T cells in bone marrow transplantation*. *J Immunol*, 2014. **192**(7): p. 3435-3441.
136. Rodda, L.B., et al., *Single-Cell RNA Sequencing of Lymph Node Stromal Cells Reveals Niche-Associated Heterogeneity*. *Immunity*, 2018. **48**(5): p. 1014-1028 e6.

137. Cheng, H.W., et al., *Origin and differentiation trajectories of fibroblastic reticular cells in the splenic white pulp*. Nat Commun, 2019. **10**(1): p. 1739.
138. Xiang, M., et al., *A Single-Cell Transcriptional Roadmap of the Mouse and Human Lymph Node Lymphatic Vasculature*. Front Cardiovasc Med, 2020. **7**: p. 52.
139. Brulois, K., et al., *A molecular map of murine lymph node blood vascular endothelium at single cell resolution*. Nat Commun, 2020. **11**(1): p. 3798.
140. Pezoldt, J., et al., *Neonatally imprinted stromal cell subsets induce tolerogenic dendritic cells in mesenteric lymph nodes*. Nat Commun, 2018. **9**(1): p. 3903.
141. Sitnik, K.M., et al., *Context-Dependent Development of Lymphoid Stroma from Adult CD34(+) Adventitial Progenitors*. Cell Rep, 2016. **14**(10): p. 2375-88.
142. Alva, J.A., et al., *VE-Cadherin-Cre-recombinase transgenic mouse: a tool for lineage analysis and gene deletion in endothelial cells*. Dev Dyn, 2006. **235**(3): p. 759-67.
143. de Boer, J., et al., *Transgenic mice with hematopoietic and lymphoid specific expression of Cre*. Eur J Immunol, 2003. **33**(2): p. 314-25.
144. Lefrancois, L. and V. Vezys, *Transgenic mouse model of intestine-specific mucosal injury and repair*. J Natl Cancer Inst Monogr, 2001(29): p. 21-5.
145. Hirose, S. and J. Dubrot, *Modes of Antigen Presentation by Lymph Node Stromal Cells and Their Immunological Implications*. Front Immunol, 2015. **6**: p. 446.
146. Krishnamurty, A.T. and S.J. Turley, *Lymph node stromal cells: cartographers of the immune system*. Nat Immunol, 2020. **21**(4): p. 369-380.
147. Santambrogio, L., S.J. Berendam, and V.H. Engelhard, *The Antigen Processing and Presentation Machinery in Lymphatic Endothelial Cells*. Front Immunol, 2019. **10**: p. 1033.
148. Schonbrunn, A., *Editorial: Antibody can get it right: confronting problems of antibody specificity and irreproducibility*. Mol Endocrinol, 2014. **28**(9): p. 1403-7.
149. Ruedl, C. and S. Jung, *DTR-mediated conditional cell ablation-Progress and challenges*. Eur J Immunol, 2018. **48**(7): p. 1114-1119.
150. Hashimoto, K., S.K. Joshi, and P.A. Koni, *A conditional null allele of the major histocompatibility IA-beta chain gene*. Genesis, 2002. **32**(2): p. 152-3.
151. Caton, M.L., M.R. Smith-Raska, and B. Reizis, *Notch-RBP-J signaling controls the homeostasis of CD8- dendritic cells in the spleen*. J Exp Med, 2007. **204**(7): p. 1653-64.
152. Ferreira, F.M., et al., *Bone marrow chimeras-a vital tool in basic and translational research*. J Mol Med (Berl), 2019. **97**(7): p. 889-896.
153. Koyama, M. and G.R. Hill, *The primacy of gastrointestinal tract antigen-presenting cells in lethal graft-versus-host disease*. Blood, 2019. **134**(24): p. 2139-2148.
154. Gil-Cruz, C., et al., *Fibroblastic reticular cells regulate intestinal inflammation via IL-15-mediated control of group 1 ILCs*. Nat Immunol, 2016. **17**(12): p. 1388-1396.
155. Novkovic, M., et al., *Topological Structure and Robustness of the Lymph Node Conduit System*. Cell Rep, 2020. **30**(3): p. 893-904 e6.
156. Hou, S., et al., *Embryonic endothelial evolution towards first hematopoietic stem cells revealed by single-cell transcriptomic and functional analyses*. Cell Res, 2020. **30**(5): p. 376-392.
157. Kisanuki, Y.Y., et al., *Tie2-Cre transgenic mice: a new model for endothelial cell-lineage analysis in vivo*. Dev Biol, 2001. **230**(2): p. 230-42.
158. Tang, Y., et al., *The contribution of the Tie2+ lineage to primitive and definitive hematopoietic cells*. Genesis, 2010. **48**(9): p. 563-7.
159. Arai, F., et al., *Tie2/angiopoietin-1 signaling regulates hematopoietic stem cell quiescence in the bone marrow niche*. Cell, 2004. **118**(2): p. 149-61.
160. Villalba, M., et al., *Vav1/Rac-dependent actin cytoskeleton reorganization is required for lipid raft clustering in T cells*. J Cell Biol, 2001. **155**(3): p. 331-8.
161. Wulfig, C., et al., *The vav exchange factor is an essential regulator in actin-dependent receptor translocation to the lymphocyte-antigen-presenting cell interface*. Proc Natl Acad Sci U S A, 2000. **97**(18): p. 10150-5.

162. Houlard, M., et al., *Vav1 is a component of transcriptionally active complexes*. J Exp Med, 2002. **195**(9): p. 1115-27.
163. Katzav, S., *Vav1: an oncogene that regulates specific transcriptional activation of T cells*. Blood, 2004. **103**(7): p. 2443-51.
164. Bonnefoy-Berard, N., et al., *Vav: function and regulation in hematopoietic cell signaling*. Stem Cells, 1996. **14**(3): p. 250-68.
165. Reynolds, L.F., et al., *Vav1 transduces T cell receptor signals to the activation of phospholipase C-gamma1 via phosphoinositide 3-kinase-dependent and -independent pathways*. J Exp Med, 2002. **195**(9): p. 1103-14.
166. Helou, Y.A., A.P. Petrashen, and A.R. Salomon, *Vav1 Regulates T-Cell Activation through a Feedback Mechanism and Crosstalk between the T-Cell Receptor and CD28*. J Proteome Res, 2015. **14**(7): p. 2963-75.
167. Tedford, K., et al., *Compensation between Vav-1 and Vav-2 in B cell development and antigen receptor signaling*. Nat Immunol, 2001. **2**(6): p. 548-55.
168. Malhotra, S., et al., *Vav and Rac activation in B cell antigen receptor endocytosis involves Vav recruitment to the adapter protein LAB*. J Biol Chem, 2009. **284**(52): p. 36202-12.
169. Perez-Cunningham, J., et al., *Hematopoietic stem cell-specific GFP-expressing transgenic mice generated by genetic excision of a pan-hematopoietic reporter gene*. Exp Hematol, 2016. **44**(8): p. 755-764 e1.
170. Joseph, C., et al., *Deciphering hematopoietic stem cells in their niches: a critical appraisal of genetic models, lineage tracing, and imaging strategies*. Cell Stem Cell, 2013. **13**(5): p. 520-33.
171. Iwata, M., et al., *Retinoic acid imprints gut-homing specificity on T cells*. Immunity, 2004. **21**(4): p. 527-38.
172. Fu, H., E.J. Ward, and F.M. Marelli-Berg, *Mechanisms of T cell organotropism*. Cell Mol Life Sci, 2016. **73**(16): p. 3009-33.
173. Luck, R., J. Klempnauer, and B. Steiniger, *Abrogation of lethal graft-versus-host disease in MHC disparate small-bowel transplantation in the rat by mesenteric lymphadenectomy*. Transplant Proc, 1990. **22**(6): p. 2471.
174. Luck, R., J. Klempnauer, and B. Steiniger, *Immunogenetic investigations of graft-versus-host reactions after small bowel transplantation with mesenteric lymphadenectomy*. Transplant Proc, 1993. **25**(5): p. 2869.
175. Aschen, S.Z., et al., *Lymph node transplantation results in spontaneous lymphatic reconnection and restoration of lymphatic flow*. Plast Reconstr Surg, 2014. **133**(2): p. 301-10.
176. Hammerschmidt, S.I., et al., *Stromal mesenteric lymph node cells are essential for the generation of gut-homing T cells in vivo*. J Exp Med, 2008. **205**(11): p. 2483-90.
177. Waldburger, J.M., et al., *Selective abrogation of major histocompatibility complex class II expression on extrahematopoietic cells in mice lacking promoter IV of the class II transactivator gene*. J Exp Med, 2001. **194**(4): p. 393-406.
178. Nguyen, H.D., et al., *T-Cell Metabolism in Hematopoietic Cell Transplantation*. Front Immunol, 2018. **9**: p. 176.
179. Schneidawind, D., et al., *CD4+ invariant natural killer T cells protect from murine GVHD lethality through expansion of donor CD4+CD25+FoxP3+ regulatory T cells*. Blood, 2014. **124**(22): p. 3320-8.
180. Riegel, C., et al., *Efficient treatment of murine acute GvHD by in vitro expanded donor regulatory T cells*. Leukemia, 2020. **34**(3): p. 895-908.
181. Mir, E., et al., *Endothelial damage is aggravated in acute GvHD and could predict its development*. Bone Marrow Transplant, 2017. **52**(9): p. 1317-1325.
182. Cordes, S., et al., *Endothelial damage and dysfunction in acute graft-versus-host disease*. Haematologica, 2020.
183. Almici, C., et al., *Circulating endothelial cell count: a reliable marker of endothelial damage in patients undergoing hematopoietic stem cell transplantation*. Bone Marrow Transplant, 2017. **52**(12): p. 1637-1642.

184. Luft, T., et al., *Steroid-refractory GVHD: T-cell attack within a vulnerable endothelial system*. *Blood*, 2011. **118**(6): p. 1685-92.
185. Andrulis, M., et al., *Loss of endothelial thrombomodulin predicts response to steroid therapy and survival in acute intestinal graft-versus-host disease*. *Haematologica*, 2012. **97**(11): p. 1674-7.
186. Tigges, U., et al., *A novel and simple method for culturing pericytes from mouse brain*. *Microvasc Res*, 2012. **84**(1): p. 74-80.
187. Vokali, E., et al., *Lymphatic endothelial cells prime naive CD8(+) T cells into memory cells under steady-state conditions*. *Nat Commun*, 2020. **11**(1): p. 538.
188. Rowe, V., et al., *Host B cells produce IL-10 following TBI and attenuate acute GVHD after allogeneic bone marrow transplantation*. *Blood*, 2006. **108**(7): p. 2485-92.
189. Li, H., et al., *Graft-versus-host disease is independent of innate signaling pathways triggered by pathogens in host hematopoietic cells*. *J Immunol*, 2011. **186**(1): p. 230-41.
190. Markey, K.A., et al., *Flt-3L Expansion of Recipient CD8alpha(+) Dendritic Cells Deletes Alloreactive Donor T Cells and Represents an Alternative to Posttransplant Cyclophosphamide for the Prevention of GVHD*. *Clin Cancer Res*, 2018. **24**(7): p. 1604-1616.

7 Acknowledgements

I would like to take the opportunity to thank the people who helped me accomplish the completion of this thesis.

First of all, I would like to thank Prof. Andreas Beilhack for making me a part of his research group and to entrust me with this exciting project. Thank you for your insightful scientific and personal guidance, the freedom to take action and execute. The motivation, which always encouraged me to continue and think independently as well as in the team.

Thank you to Prof. Manfred Lutz and PD Dr. Niklas Beyersdorf for being on my thesis committee. The long and wise scientific discussion and input during the committee meetings was of great value for me and considerably contributed to achieving the objectives of this thesis. Special thanks to The European Regional Development Fund (EFRE) for funding this project.

I would also like to thank Prof. Jochen Hühn and Prof. Burkhard Ludewig for the fruitful discussion and ideas that led to the progress of this thesis. Thanks to Dr. Jörn Pezoldt for his assistance with the bioinformatic part of the thesis and Dr. Sophie Acton for her kind gift of iFRC cell line.

Big thanks to Juan Gamboa Vargas and Maria Ulbrich who greatly contributed to this project during their Master thesis. It was and is a pleasure to work with you, thank you for the friendship and the trust you have put in me.

Thank you Dr. Katja Jarick, Dr. Duc-Dung Le, Josefina Peña Mosca, Caroline Graf and Estibaliz Arellano for the great team atmosphere, the experimental group efforts and the fun times in and outside the lab. Thank you Dr. Julia Delgado-Tascón, Dr. Zeinab Mokhtari, Marlene Strobel, Sabine Stöckel-Eckard and all the members of the Beilhack laboratory for discussions and help. I would like to thank Juan Gamboa Vargas, Hadiqa Raees for their careful proofreading and feedback of the thesis and Marlene Strobel for German translation of the summary.

I would like to thank my parents M Aslam Shaikh (late) and Gulnaz Parveen, my brother M Usman Shaikh, my sister Sana Shaikh and my sister-in-law Ramsha Usman for their support, praise and spur my professional progress. I would also like to thank my friends; Tahira Zar, Dr. Asghar Nasir, Dr. Khalid Shaikh and Abdul Wahab, without their support this journey would not have been possible. Special thanks to my wife Urooj Salahuddin for always being there for me.

8 List of publications

Jarick KJ, Mokhtari Z, Scheller L, Hartweg J, Thusek S, Le DD, Ranecky M, **Shaikh H**, Qureischi M, Heinze KG, Beilhack A. Photoconversion of Alloreactive T Cells in Murine Peyer's Patches During Acute Graft-Versus-Host Disease: Tracking the Homing Route of Highly Proliferative Cells In Vivo. *Frontiers of Immunology* 2018 Jun 27;9:1468.

Ranjan, S, Gohl A, Kohli S, Gadi I, Pierau M, Shahzad K, Gupta D, Bock F, Wang H, **Shaikh H**, Kähne T, Reinhold D, Niemz J, Schnöder T, Brunner-Weinzierl M, Fischer T, Kalinski T, Schraven B, Luft T, Huehn J, Naumann M, Heidel F, Isermann B. Activated protein C protects from GvHD via PAR2/PAR3 signalling in regulatory T-cells. *Nature Communications* 2017 Aug 21;8(1):311.

9 Curriculum vitae

MUHAMMAD HAROON SHAIKH

University Hospital Würzburg
 Medicine Clinic II, Experimental stem cell transplantation
 Zinklesweg 10
 97078 Würzburg, Germany
 Telephone: +49 (0)931 201 44041
 Email: E_Shaikh_H@ukw.de

Place and date of Birth: Karachi, Pakistan, January 12th, 1991

Nationality: Pakistani

EDUCATION

- Since Feb 2017 PhD in Immunology
 Supervisor: Prof. Dr. Dr. Andreas Beilhack
 Thesis: Non-hematopoietic lymphoid stromal cells prime alloreactive CD4⁺ T cells in acute graft-versus-host disease
 Department of Internal Medicine II, University Hospital, Würzburg, Germany
- Jan 2012 – Dec 2012 Master of Science (MSc in Biotechnology)
 Department of Biotechnology, University of Karachi
 » Final Grade: 84%
 » Distinction with Third position
- Jan 2009 - Dec 2011 Bachelor of Science (BSc Honors in Biotechnology)
 Department of Biotechnology, University of Karachi
 » Final Grade: 77.5%

RESEARCH EXPERIENCE

- Jan – Nov 2019 Master thesis supervision
 Name: Juan Fernando Gamboa Vargas
 Title: The role of Ccl19+ stromal cells in intestinal integrity in aGvHD
- Mar – Nov 2018 Master thesis supervision
 Name: Maria Ulbrich
 Title: The impact of lymph node stromal cells on the induction of aGvHD
- Aug – Dec 2016 Qualification phase thesis
 Supervisor: Prof. Andreas Beilhack
 Thesis: Alloreactive T-cell activation in absence of host dendritic cells in acute graft versus host disease (aGvHD)
 Department of Internal Medicine II, University Hospital, Würzburg, Germany
- Mar 2015 – Feb 2016 Research Associate
 Supervisor: Prof. Berend Isermann
 Project: The regulation of T-cell activation by the serine protease activated protein C (aPC) and the protease activated receptor (PAR-3)
 Institute of Clinical Chemistry and Pathobiochemistry, Universitätsklinikum Magdeburg, Germany
- May 2013 – Feb 2015 Research Associate
 Office of Research and Graduate Studies
 Aga Khan University, Karachi, Pakistan
 Project 1: Investigating the correlation of Androgen Receptor (AR) and CD44 expression in prostatic cell line model

Project 2: Establishment and analysis of Hepatitis C genotype 3a Replicon system

CONFERENCES

62nd American Society of Hematology (ASH) annual meeting and exposition, 5 – 8 December 2020, virtual meeting (**Oral Presentation**)
MHC Class II on Ccl19⁺ Reticular Cells Mitigates Graft-*versus*-Host Disease via Maintenance of Regulatory T cells.

Keystone Symposia: Stromal Cells in Immunity and Disease (Q5), 19 – 23 February 2020, Victoria, BC, Canada (**Poster Presentation**)
Non-Hematopoietic Lymphoid Stromal Cells Prime Allo-Reactive CD4⁺ T cells in acute Graft-*versus*-host disease.

61st American Society of Hematology (ASH) annual meeting and exposition, 7 – 10 December 2019, Orlando, FL, USA (**Poster Presentation**)
Non-Hematopoietic Lymphoid Stromal Cells Prime Allo-reactive CD4⁺ T Cells in Acute Graft-*versus*-host Disease.

Harald von Boehmer Midwinter Conference 2019: Advances in Immunobiology, 19 – 23 January 2019, Seefeld in Tirol, Austria (**Oral presentation**)
Non-Hematopoietic Antigen Presenting Cells of the Lymphoid Organs in Acute Graft-*versus*-host Disease.

5th European Congress of Immunology (ECI), 2 – 5 September 2018, Amsterdam, The Netherlands (**Poster presentation**)
Non-Hematopoietic Antigen Presenting Cells in Lymphoid Organs.

AWARDS AND HONORS

ASH abstract achievement award at 62nd American Society of Hematology (ASH) Annual Meeting and Exposition – virtual meeting – Dec 2020

ASH abstract achievement award at 61st American Society of Hematology (ASH) Annual Meeting and Exposition – Orlando, FL, USA – Dec 2019

Scholarship awarded by GRK 2157, German Research Foundation (DFG) to conduct qualification phase thesis, Aug 2016 – Dec 2016

Secured Third Position in Master of Science (MSc Biotechnology) – 2012

LANGUAGES

- » Urdu – Native
- » English – Fluent (IELTS: 7 bands)
- » German – Basic (A1)

SPECIALIZED COURSES

21st-28th/09/2019 FEBS Advance Lecture Course
20th International Summer School on Immunology
Hvar, Croatia

2nd/09/2018 Advanced Cytometry Course
A Satellite symposium of the 5th European Congress of Immunology 2018 (ECI), Amsterdam, The Netherlands

18th-20th/07/2018 FELASA B animal handling course
Humboldt-Universität zu Berlin, Germany

- 18th-23rd/03/2018 14th Spring School of Immunology, organized by The German Society for Immunology (DGfI) in Ettal, Germany
- 10/2015 – 01/2016 Introduction to Laboratory handling and animal experimental methods
Universitätsklinikum Magdeburg, Germany
- 4th-9th/10/2015 7th Autumn School “Current Concepts in Immunology” organized by The German Society for Immunology (DGfI) in Merseburg, Germany

10 Affidavit

I hereby confirm that my thesis entitled 'Non-hematopoietic lymphoid stromal cells prime allo-reactive CD4⁺ T cells during acute Graft-versus-Host disease.' is the result of my own work. I do not receive any help or support from commercial consultants. All sources and/ or materials applied are listed and specified in the thesis.

Furthermore, I confirm that this thesis has not yet been submitted as part of another examination process neither in identical nor in similar form.

Place, date

Signature

Eidensstattliche Erklärung

Hiermit erkläre ich an Eides statt, die Dissertation „Nicht-hämatopoetische lymphoide Stromazellen aktivieren alloreaktive CD4⁺ T-Zellen in der Initiierung der akuten Graft-versus-Host Disease“ eigenständig, d.h. insbesondere selbständig und ohne Hilfe eines kommerziellen Promotionsberaters, angefertigt und keine anderen als die von mir angegebenen Quellen und Hilfsmittel verwendet zu haben.

Ich erkläre außerdem, dass die Dissertation weder in gleicher noch in ähnlicher Form bereits in einem anderen Prüfungsverfahren vorgelegen hat.

Ort, Datum

Unterschrift